SAPIENZA
UNIVERSITÀ DI ROMA

DIPARTIMENTO DI INGEGNERIA DELL'INFORMAZIONE,
ELETTRONICA E TELECOMUNICAZIONI

DOTTORATO IN ELETTROMAGNETISMO E MODELLI
MATEMATICI PER L'INGEGNERIA

SMART ANTENNAS FOR STRATEGIC ENVIRONMENT

Dottorando
Vincenzo Pascale

Relatore
Prof.Fabrizio Frezza

Coordinatore:

Prof. Daniele Andreucci

A mia Madre.

Acknowledgements

I would like to sincerely thank Prof. Fabrizio Frezza for having supervised my PhD activity along its path and having strongly supported me in such different ways, both technical and human point of view. Dr. Nicola Tedeschi, whose support and contribution to the activity were crucial along the way that lead to some of the results reported in this thesis.

I sincerely acknowledge Vincenzo Schena, (Telecommunication Satellite R&D Responsible at Thales Alenia Space Italia) for his continuous support and for the confidence he vested in me during the years we collaborate, together with his team at Thales Alenia Space Italia

And in the end, I would like to thank all the mates and colleagues, I collaborated with during this journey, I keep on learning from everyone of them and it has been an unparalleled occasion of growth and a great pleasure to work with such exceptional persons and extremely skilful engineers.

Contents

LIST OF FIGURES

LIST OF TABLES

OVERVIEW

The objective of this Thesis consists in presenting in a concise and effective way the results achieved during more than 3 years of researches and studies on satellite systems interference sources, advanced antenna arrays for satellite systems to mitigate the increasing anti-interference needs and on an innovative way to generates inhomogeneous wave in lossless media for contributing to the design of a novel type of antenna for deep penetrating lossy media.

The research activity concerning satellite interference analyses and mitigation has been developed with a collaboration with the R&D section of the Telecommunication Payload Domain of Thales Alenia Space Italia with finding in the fulfilment of actual industrial needs its essential goal. People involved in the activity were Vincenzo Schena (Telecommunication Satellite R&D Responsible at Thales Alenia Space Italia) and his team. The research team was in charge of identifying the actual needs in latest generation satellites, coordinating the research activity and assessing the results at system level as well as supervising and evaluating the quality of the results.

The research activity focused on the developing of a novel approach in generating inhomogeneous waves has been directly supervised by Prof. Fabrizio Frezza and Dr. Nicola Tedeschi, with contribution and inspiration of different members of Prof. Frezza Team.

Thesis structure consists of two Chapters, each one dedicated to a specific main research area. Chapter I regards the analysis of impacts of electromagnetic interference in satellite systems and the proposal an innovative approach in employing Beam-Forming Network architectures for Telecom commercial satellite. The most part of the present Thesis will be dedicated to this subject, being the core issue of the whole PhD activity. In Chapter II, the development of efficient analysis and synthesis strategies for generating inhomogeneous waves to meet a condition which can significantly decrease waves attenuation

in lossy media. Conclusions are summarised at the end of each Chapter Section to discuss and highlight the most relevant results achieved.

I. CHAPTER I

Low Cost Anti Interference Antenna Solution For Commercial Satellites

I.1 INTRODUCTION

In the context of commercial satellite communications, frequent interference (both unintentional or intentional) phenomena are generating concerns and are worrying the satellite operators, mainly for what concern the Broadcasting (and broadband) Satellite Services (BSS) and Fixed Satellite Services (FSS).

These phenomena are also a large risk for the emerging and growing Mobile Satellite Services typically operating in L band but, today, addressed towards other frequency ranges as the Ka band to expand the band capabilities. The main scope of the work that characterized the first part of my research activity so far is the Study, the dimensioning and the performance analysis of the low cost anti-interference system for commercial satellites.

Nowadays, some anti interference methodologies have been implemented in the military domain, so limited information is publicly available in literature, thus notwithstanding these abovementioned techniques may lead to a development costs which might exceed what satellite operators are willing to invest in order to protect their payloads against interferer.

I.1.1 Structure of the Work

This branch of my research activity has been modulated on different phases described, as follows:

In the first place a potential market analysis has been performed to correctly address the target cost related to the interference mitigation system. Since the aim of the study was the proposal of a low coast anti interference system at antenna level for commercial space system, it was crucial to assess what low cost means for a complex 15 years lifetime commercial GEO satellite. These analyses have been carried out by analysing market forecasts of satellite operators' revenues and satellites manufacturer orders within a 15 years' horizon. By studying the statistical distribution of interference events a preliminary assessment of the operator's revenues threatened by interferers were established.

In the second phase of the study an exhaustive and innovative survey on the interference phenomena affecting the commercial SATCOM were carried out. Every source of voluntary and involuntary interference was classified and physical characterised by the mean of a proper electromagnetic model by an exhaustive literature survey. For each interferer, a quantification of the market impact was also provided.

In the following phase, a reference satellite system has been defined and justified in order to provide the reference victim scenario in which interference phenomena might occur. The selected satellite system was implemented as a typical state- of - art satellite payload architecture in order to define a performance model with respect to which evaluate the impact of interference. This implementation lead to the development of a simulation tool based on a RF circuit CAD software of the whole end-to-end satellite system which has been carried on with the collaboration of J.Capolicchio during his thesis internship [R. 41] in the Telecommunication department of Thales Alenia Space Italia.

An exhaustive assessment of effects of unmitigated interferers against the selected satellite payload was the aim of the preliminary

assessment, which leaded to definition of the drivers of the choice of the anti-interference techniques. Every interferer was also modelled and analysed by a theoretical study and later implemented in MatLAB tool environment.

In order to correctly address the choice and the evaluation of the anti-interference techniques a set of justification and selection criteria has been defined. An extensive literature and patent survey was performed in order to identify the state of art of antenna level interference mitigation techniques and all the selected techniques are defined and analysed in terms of effectiveness, final implementation, and flexibility with respect to the satellite system. Antenna solution for mitigate interferer signals turns out to be the most effective one, thus the rest of the work has been developed by designing and providing an accurate design for Antenna with antenna nulling subsystem for standard commercial Ku satellite payload.

Starting from a reference coverage scenario antenna requirement has been carried out by link budget analyses. Afterwards a general description of the proposed Nulling sub-system and the possible technical solution at antenna level for its implementation has been described with the scope to provide a description and a justification of the proposed ant interference solution.

The conclusive phase leaded to a possible preliminary design of the system implementing the best two concurring solution to compare their performance.

I.2 REFERENCE SCENARIO

The considered reference scenario for the study and for the development of interferences countermeasures definition is defined is represented by a Ku band satellite commercial satellite with regional coverage for both user and feeder links in the Fixed-Satellite Service (FSS) or in the Broadcasting-Satellite Service (BSS) bands.

The main features and characteristics of this kind of satellite systems working in Ku band and used for BSS will be described as follows. In particular, it will be defined some kinds of possible performance and operational features through which the whole system will be analysed

. Among those will be defined examples of:

- Spacecraft Service Area;
- Spacecraft Uplink Performance (G/T);
- Spacecraft Uplink Performance (EIRP);
- Frequency Plan;
- Polarisation;
- Payload Main Characteristics;

Fig. I-1: Global Coverage of Ku-Band Satellite.

For this scenario, the satellite considered is a typical BSS Satellite system will be taken as reference. The chosen coverage will span over European, North African and partly Middle Easting by delivering mainly digital television and radio channel services [R. 2, R. 4].

I.2.1 Quantification of Market Potential and Low Cost Concept Definition

Growing satellite technologies and telecommunications in the commercial space industry and the ever-increasing revenues that are produced, today justify the necessity for the development of space security, already well developed in the Military Satellite Communication (MILSATCOM) context, also in the commercial and institutional one. At same time for what concerns COMSATCOM Operators, value for money has to be carefully thinking that possible

customised AI/AJ functions/solutions have to be an asset that is worth procuring and selling as an added feature, contributing in increasing their revenues. To approach this aim, for COMSATCOM applications the Operators have to assess the level of the risk (probability of interference per gravity of the effects) with respect to the costs of mitigating the impacts of interferences. Considering the two typologies of interferences experienced by the Operators, i.e. intentional and un-intentional, their experience is that: Intentional jamming (on a television program or critical communication link): while reduced, occurrences have been recorded, jamming has never ceased since the last decade. This is an issue for stakeholders in the value chain! Un-intentional interference: this is the case of more than 95% of the cases. [R. 10,R. 13,R. 14]These interferences can be due to bad settings of carrier frequency, polarisation etc. Training of the users of satellite capacity should contribute reducing the level of occurrences of these interferences. Network controlled operation of user terminals should also avoid emissions of user terminals if the signalling channel of the network cannot be received correctly. Satellites Manufacturers are involved from long time in developing effective and performing technologies finalising secure satellite control channels and traffic transponders through AI/AJ and encryption dedicated solutions (e.g. spread-spectrum approach for a Secure TT&C and nulling antijamming technology at satellite antenna level) mainly in the MILSATCOM field as done for military satellite System. This technological trend and capability gives the opportunity to propose these techniques also for COMSATCOM area. The opportunity to study and define suitable and effective solutions crossing the COMSATCOM Operators exigency and the technical experience and background of satellite manufacturers has been well acknowledged by European Space Agency (ESA) through the ARTES 1 Study titled "*Low Cost Anti-Interference Techniques for SATCOM Commercial Satellites*" (LoCATe Study). The Study at staring has provided a first understanding of the potential market of secured communication within civil institutional and commercial

satellite business, thus providing an evidence of the shift of secure technology from military customers to civilians too. When identifying the more relevant BSS, FSS and MSS satellite scenarios which could embark such a technology, performing market assessment and trend analysis to evaluate the room for these technological solutions, it has been provided an analysis highlighting the benefits for the secure communications towards the emerging markets requesting the solution studied in the Project. Despite the commercialisation of technologies securing satellite communications has not yet reached maturity, the need for secure communications is making progresses at a run. In all of violations mentioned in the paper it has been thrown light on the number of important issues such as absence of coercive measures despite a specific regulatory framework, the lack of bargaining power from public authorities (UN's ITU; EU) to make countries adhering at common standards and norms. The political willingness strategy is just hindering the commercialisation process of secure systems against jamming/blinding attacks on commercial satellites, apart from military ones. Thus, a potentially large market (over 120 satellites to be commissioned during the 2014-2018 period) has not yet fostered this level of technology as a new standard. In the hypothesis of an interference percentage of 5.3%, that seems to be consistent with operator provided interference monthly experienced events for such a number of transponder, we can assess total number of monthly affected transponders. This number represents the figure of interference events supposed to occur for a month for the band under test for the region we are considering. This procedure has been iterated for every region and every service, taking into account all the marginal costs due to interference attacks so that it was possible to assess the equivalent monthly total loss owed to interference event. The procedure has been repeated for every year from 2015 to 2020, under the hypothesis, anti-jamming technology might be ready to be embarked from 2015 onward. By this data, it has been possible to calculate even cumulative values of:

- Monthly and annual revenues threatened by interference events;
- Monthly and annual extra-costs for interference managing;
- Marginal monthly and Annual Revenues to be protected, which consider for every year only transponder which belongs to those same years launched Satellite;
- Cumulative revenues threatened plus Extra-Costs saved, that considered all the revenues and cost savings that can be protected by an AI/AJ technology from 2015 to year under test;
- Cumulative revenues threatened plus extra-costs saved in the 6 years' period: 2015-2020 has been considered.

This represents all the revenues that could be protected by a low-cost anti interference technique. It has to be noticed that even though revenues assessment refers to a 6 years' period, due to satellite market forecasts data are related to that period, a transponder equipped with a low- cost interference technique is reasonably capable to defend its payload revenues during most of its useful lifetime in service, make protected revenues even greater than the amount reported. Following reports cumulative data for the survey on 6 years' period. In addition, it might be useful to underline that during a modern satellite lifetime, about 15 years, savings and revenue protection owed to a proper AI/AJ technology implemented by the satellite communication systems might grant a loss reduction of hundreds of euros per transponder per years.

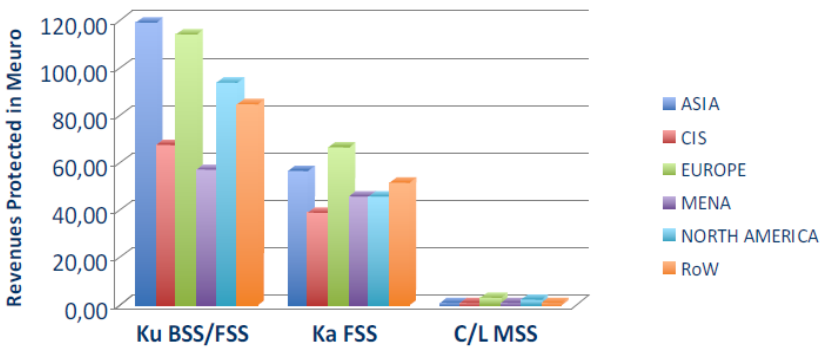

Fig. I-2 : Cumulative revenues and costs savings that could be protected by low-cost anti-interference techniques between 2015 and 2020. Data are in millions of Euro

I.3 CLASSIFICATION OF INTERFERENCES

"As above introduced, the Commercial Telecommunications Satellite Interference Scenario description has been carried out with the analysis of interference events as reported in literature and as experienced by several SATCOM Operators covering the following items:

- Definition of the nature of the interferences (voluntary, or involuntary);
- Collection of the orbital location(s) and coverage(s) of satellites that were interfered with during the last ten years (total number and statistics for involuntary interferences, events for voluntary ones);
- Characterisation of the nature of the networks that were interfered (broadcasting, mobile etc.);

For voluntary interferences, definition of the root cause of the interferences (political and so on).

A SATCOM system is an open communication system, which always suffers from intentional or unintentional interferences. Once the satellite system is interfered by radio frequency interference (RFI), the normal communication traffic performance might be degraded.

Interference is originated by a source external to a signal path and produces undesired artefacts in the signal. There are a very large number of situations where interference can occur, intentionally or otherwise. Thus, sources of radio frequency interference fall into two broad categories:

Unintentional: when interference occur mainly as result of defective equipment, operator error or propagation effects.

Intentional: when we refer to on purpose generated signals as defensive or offensive interference.

The most common form of defensive/offensive interference is often referred as “Jamming”. At radio level jamming phenomenon come from the RADAR world and for the telecommunications it can generally be related to TV and radio transmission, as a means of political censorship of information or can affect GPS signals for whatever purpose.

Once the simulator has been validated with the standard, the chain has been enhanced with the insertion of all the other blocks. The whole simulator has been then compared with the results found in literature and the ones carried out by the link budget analysis, to verify the output accordance with the theoretical

expected results. In the Thales Alenia Space - Italia laboratory the simulator results have been validated by comparison with the ones obtained using of a satellite E2E radiofrequency emulator.

Electronic Warfare (EW) consists in the use of electromagnetic energy to perform or prevent an attack toward the sensitive electronic devices or systems. Usually the Electronic Warfare is subdivided into three classes:

- Electronic Warfare Support (ES)
- Electronic Attack (EA)
- Electronic Protection (EP)

ES deals with detection of enemy signal activity, classification of signal features and determination of emitter location. EA deals with use of weapon (laser, microwave and particle beams), or anti-radiation missiles or electromagnetic pulses, to destruct enemy's equipment. Finally, EP deals with use of counter techniques for reducing the effectiveness of enemy attacks [5].

The aim of this work belongs to Electronic Protection class, where the enemy's activity is the jamming. Jamming is the intentional will of anyone who wants to impair the adversary's use of electronic devices, equipment or systems; this can be made in several ways such as radiation, re-radiation or reflection of electromagnetic energy through systems called *Jammers*. Since the jammers want to disrupt the communication system, they should know:

What is the best jamming waveform and strategy to make blind that kind of communication system;

How effective will be the jamming on that communication system.

These conditions are linked to many factors whose are in part the following:

- Coding and modulation methods;
- Frequencies;
- Transmitted power;
- System efficiency;
- Pattern of antennas;
- Environment;
- Self-interference.

Each satellite has several vulnerabilities through which is possible to interrupt the communication with ground segment (in satellite receiving phase) or with user segment (in satellite transmitting phase). During a communication between the earth stations and satellites or between users and satellites, information is exchanged via antennas both in reception and transmission. These antennas are the main access points to satellites. After that, in case of bent pipe satellites the information is amplified and then down-converted. In case of regenerative satellites the information is amplified, processed and then down-converted [3]. Starting from these considerations, the vulnerabilities of satellites are at:

Antennas level;

Transponder at radiofrequency level;

Transponder amplifiers.

Satellite system is a communication system that always suffers from intentional or unintentional interferences:

- **Unintentional** when interference occurs mainly as result of defective equipment, operator error or propagation effects.
- **Intentional** when there is the will of generate signals as defensive or offensive interference

I.3.1 Unintentional Interference

Unintentional interferences are due to many source of interference and are in percentage the 90% of the total interferences.

These sources of interference can be gathered in the following sections:

- Adjacent Satellite;

- Mismatching Polarization;
- Environment (like solar radiation, space debris and so on);
- Ground Stations;
- Others;

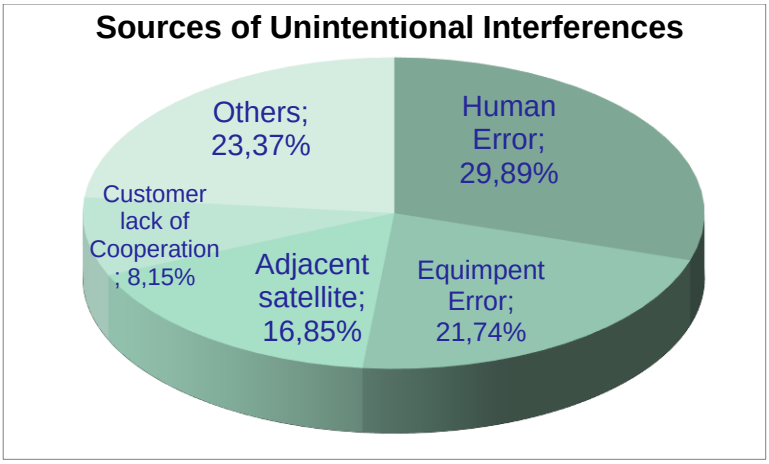

Fig. I-3 : Sources of Unintentional Interferences.

The causes of interferences are, as it is possible to see in Fig. I-3, due to human error, equipment error, adjacent satellite, customer lack of cooperation or other kinds of causes. For example, human operator errors (like pointing errors or misalignment errors) may cause an increasing of gains of the adjacent antennas and so a worsening quality of receiving information.

Let's now consider the types of interferences where will be highlighted the occurrence of these phenomena, their sources, their causes and the possible preventions.

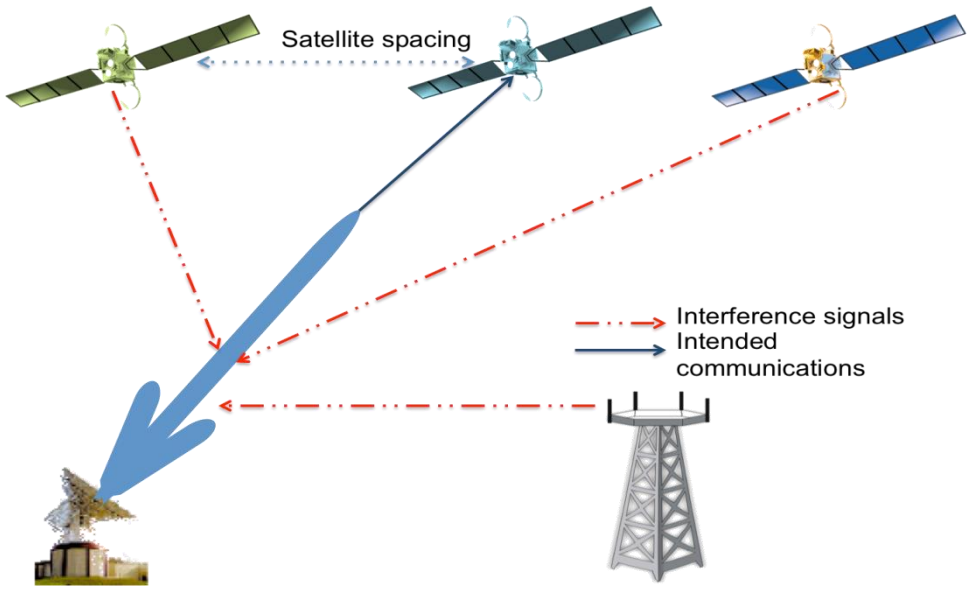

Fig. I-4 : Typical Interference Topology where are Involved Terrestrial Sources of Interference and Satellite's Ones, like Adjacent Satellite Interferences and Co-Channel Interference

I.3.1.1 *FM Interference*

The FM interference occurs when a terrestrial radio broadcast enters ground station or earth station antenna system with an FM (87-107 MHz) carrier, introducing spurious frequency at IF level, which could be re-transmitted towards Satellite with the intended signals.

The source of this phenomenon is given by FM radio towers and may happen when there is:

- Poor electrical shielding between baseband and RF transmission line;
- Poor equipment between baseband and RF in terms of electromagnetic compatibility;
- Poor grounding system FM interference.

Some preventions are possible and might be:

- The use of accessories with standard compliant specifications;
- The coordination with communication networks to perform User Acceptance Test (UAT)
- The measurement campaign with interference checking when a new station is installed
- The goodness of the grounding system

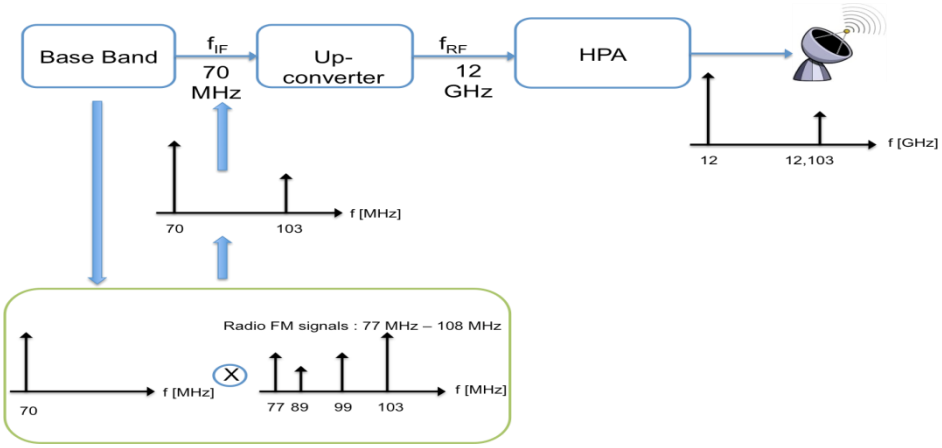

Fig. I-5 : Radio Interference between Commercial FM Radio Stations and Baseband Equipment.

I.3.1.2 *Cross Polarization Interference*

The Cross-Polarization Interference occurs when user or provider transmits towards satellite with a specific polarization, that doesn't exactly match the polarization accepted by the satellite antenna feed for that communication. If satellite antenna implements one polarization: the result is a power loss in direct ratio to polarization impurity. If the satellite antenna realizes double polarization cross-talk interference due to the opposite polarization on the same transponder will be present.

This phenomenon has its source in the uplink antenna when its XPD (Cross-Polarization Discrimination) is less than $30\ dB$. The causes that generate this kind of interference are:

- The poor antenna pointing;
- The poor Cross Polarization Isolation;
- The sudden changes in antenna pointing due to human mistakes or solar storm;
- The carrier uplink assignation without a proper UAT with Satellite-Personal Communication Network Satellite (S-PCNS) Cross-Polarization Interference.

Some preventions are possible and might be:

- Do not uplink the carrier without performing UAT with S-PCNS;
- Perform regular preventive maintenance.

I.3.1.3 *Un-authorized Digital Overriding*

The un-authorized digital overriding occurs when the transmitter equipment uses an un-authorized carrier to uplink towards satellite.

The source of this interference is the earth station equipment or the ground station one and is due to:

- The transmission of wrong carrier frequency by the user;
- Equipment malfunction.

Some preventions are possible and might be:

- Verify uplink frequency before transponder access;
- Perform UAT;
- S-PCNS can assign to customers, if needed, new carriers at some vacant slots;

- Perform preventive maintenance periodically.

I.3.1.4 *Intermodulation Interference*

The intermodulation interference happens when more than one carrier are transmitted by a single HPA. When Intermodulation (IM) occurs, other carriers are displayed at multiples of the difference between carrier frequencies. The power level of the intermodulation products is depending on the relative power level of the carrier and the purity of linearity of the amplifier. It can increase the noise floor at some frequency slots, so reducing E_b/N_0 over that frequency and increasing the power consumption of the equipment.

The sources of this interference are at the ground station and are caused by:

- The non-linear equipment that generates spurious frequencies due to intermodulation products at:
  - $f_{IM_1} = 2f_1 - f_2$
  - $f_{IM_2} = 2f_2 - f_1$

Where f_1 is the frequency of the carrier number 1, while f_2 is the frequency of the carrier number 2.

- The more relevance of the superior order of the modulation products, if the power amplification increases.

Some preventions are possible and might be:

- To avoid that the amplifier works in saturation zone, if it is not specifically needed;
- The correct setting of Input Back-Off (IBO) power in order to force amplifier to work in linear regime.

I.3.1.5 *Raised Noise Floor Interference*

The Raised Noise Floor Interference happens when some kinds of energy sources, some oscillations across the entire spectrum under test or even just in specific spectral areas are present. It is shown with noise floor the bottom of the radio spectrum of interest in Fig. I-2.

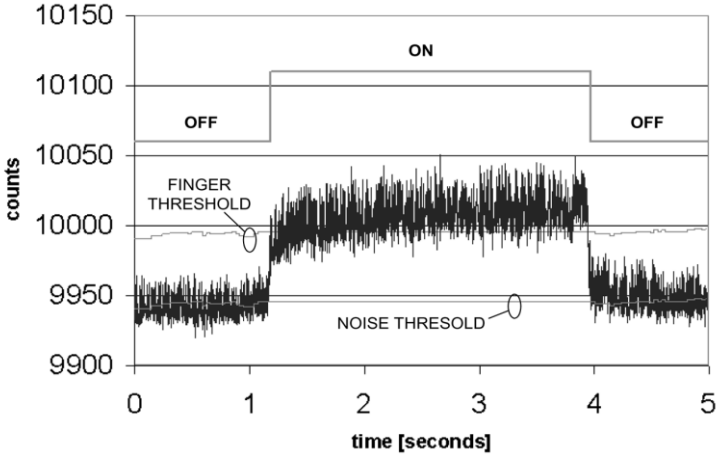

Fig. I-6 : Raised Noise Floor whether the Noise is Raised or Not.

The sources of the Raised Noise Floor Interference are either the ground station equipment or the satellite. These sources may be caused by:

- Wrong earth station equipment configuration;
- Not suitable set of HPA or gain of up-converter;
- Excess in uplink power;
- Wrong or not performed UAT, especially for coding division multiple access (CDMA) strategies.

Prevention for this source of interference may be:

- Right setup of earth station;
- Set suitable gain of earth station equipment;

- Do not increase the uplink power without informing S-PCNS;
- Verify uplink noise level at the output of HPA before transponder access.

I.3.1.6 *Radar Interference*

In the last years, it has been noted an increasing number of reported cases of interference to fixed-satellite service earth stations and terrestrial point-to-point microwave links in C-band (due to meteorological radar) as well as Ka and Ku Band. The increasing of interferences has been attributed to the rapid growth of the number of TeleVision Receive Only (TVRO) and Audio Receive Only (ARO) earth stations. Interference from radar may happen towards an earth station or satellite. The effect of this interference is a coupling of radar energy with the receiver system. Typically, the coupling is from the radar main beam to a side lobe of the receiver antenna, although other coupling combinations can also occur (e.g. main beam-to-main beam coupling or side lobe-to-side lobe coupling). This kind of interference may be caused by:

- Radar emissions:
  - Chirp pulses;
  - Harmonics of the fundamental frequency;
  - Spurious intermodulation products.

Some preventions are possible:

- Robust Filtering Spurious Frequency;
- Avoiding amplifier to work in saturation zone, if it's not specifically needed;
- Correct setting of Input Back-off power in order to force amplifier to work in linear zone.

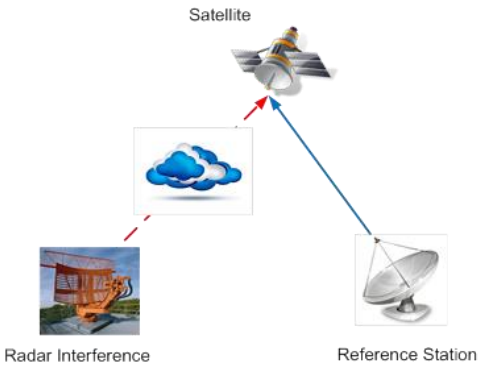

Fig. I-7 : Radar Interference Scenario

I.3.1.7 *Spike Interference*

The Spike Interference occurs when on the Receiving or Transmitting chain there are electronic equipment performing switching operations. The switch is due to the turning on or off of the diode when the current overcomes the Schottky barrier. When current overcomes the Schottky barrier of the diode, reverse current flows immediately for a very short time. This transient current is the cause of spike noise. The spike sources are at the earth station and at the satellite, while the causes might be an uplink equipment error (both baseband and RF equipment) with unpredictable frequency, bandwidth and time duration.

Some preventions may be performed:

- Periodically preventive maintenance;
- Run all uplink equipment under suitable conditions as directed by operational manual of the equipment;
- Find out root cause if the spike interference disappeared with unknown reason or equipment reset, in order to perform prevention.

I.3.1.8 *Ionospheric Solar Scintillation*

Ionospheric interference during a solar maximum activity is a phenomenon that happens when the sun crosses the equator and passes directly behind the geostationary satellite. This condition is verified every spring and autumn, as it is possible to see in Fig. I-8. This alignment causes the main beam of ground segment station receive antenna to be direct in the line-of-sight with the Sun, causing sun outage. That effect lasts for about 10 minutes and might overwhelm the intended signals, disturbing the correct signal reception. The source of this scintillation is an outer one and the cause is clearly the sun alignment with the link plane. Since the effect of this interference has duration of 10 minutes for only two seasons at year, prevention may be considered negligible.

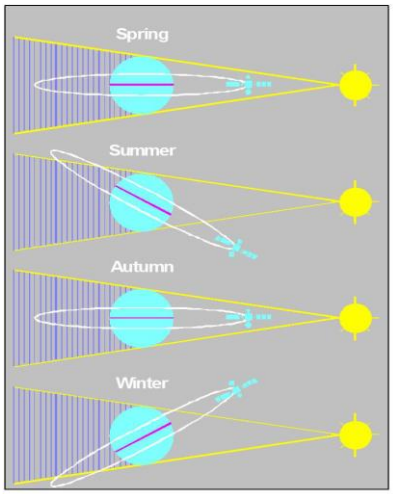

Fig. I-8 Solar Interaction with GEO Satellite Belt during 4 Seasons.

I.3.1.9 *Co-Channel Interference*

The Co-Channel interference occurs when simultaneous transmissions from different satellites (or earth stations) using adjacent carriers provided too narrow guard bands token place. The sources of this phenomenon may be on satellite and on earth stations, while the causes may be:

- Insufficient channel spacing, which can generate frequency sidebands overlapping;
- Congestion of the frequency spectrum that occurs because on one hand the bandwidth is largely required but on the other hand the spectrum is limited;
- Un-authorized carriers;
- Lack of correct frequency planning performed;
- Ionospheric reflections and then phase shifting.

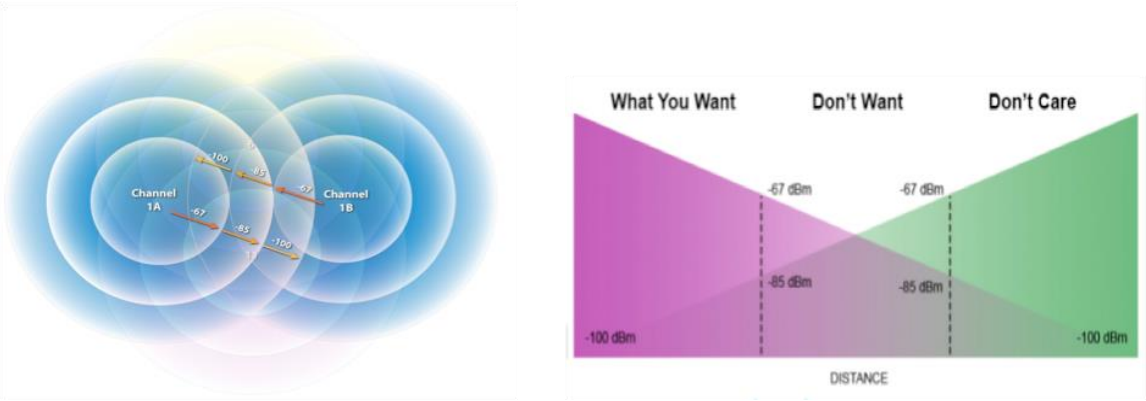

Fig. I-9 : On the Left Co-Channel Interference between 2 Different Channels in their spatial representations; On the Right, Thresholds of Desired Signals, Unwanted Signals and Fading Band.

The classic preventions to avoid this phenomenon are:

- Wider guard bands (if necessary);
- More proper frequency assignment.

I.3.1.10 *Adjacent Transponder Interference*

The Adjacent Transponder Interference happens when there is more than one transponder the satellite. In this case, cross-talk effect among different channels belonging to different lines might be experienced, so that the higher power level signal might interference and be processed together with the intended signal on the adjacent transponder. The source of this interference is on board transponders and the cause is

poor electromagnetic shielding of the involved transmission line. As prevention, it is possible to use accessories with standard compliant specifications or to make a study concerning the related electromagnetic compatibility.

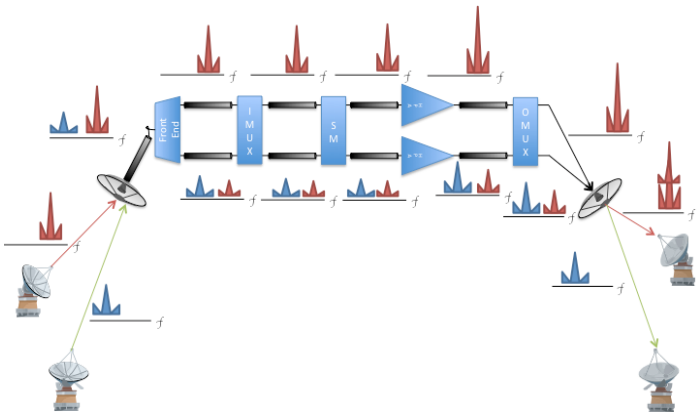

Fig. I-10 : Transponder Crosstalk over the Same Satellite.

I.3.1.11 *Adjacent Satellite Interference*

The Adjacent Satellite Interference occurs when satellites spacing is very short. This interference is due to poor inter-system coordination or operator error. Both affected satellite operators use full spectrum on a non-interference basis involuntary partially override or disturb other satellite channels.

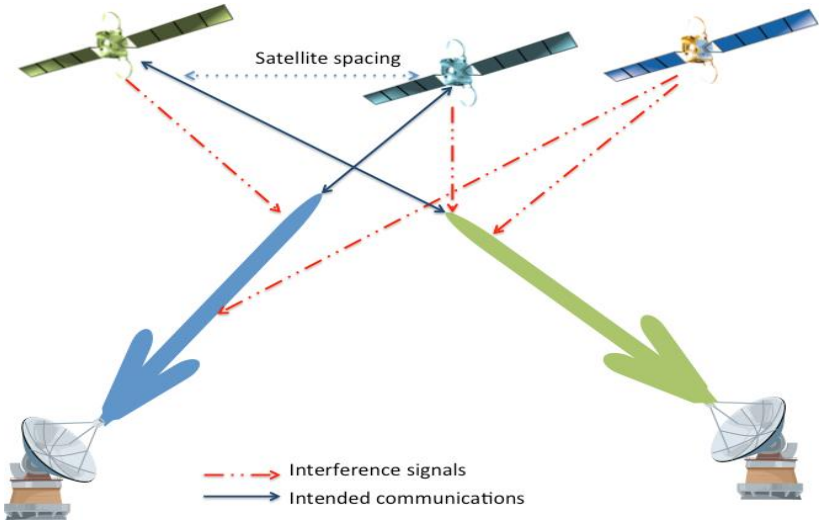

Fig. I-11 : Satellite Adjacent Interference Can Affect Communications Either at the Satellite Antenna and Ground Segment.

The source of this interference is the authorized satellite broadcast while the cause can be either a lack of cooperation between operators or operator errors.

Some preventions may be performed:

- Properly setting frequency channel assignment;
- Properly setting transmission power level;
- Better coordination between operators.

I.3.2 Intentional Interference

Two kinds of intentional interference must be considered. They differ from each other in their purpose:

- Jamming;
- Piracy.

Jamming consists of transmitting a signal on the legal traffic processed by the victim satellite. The interfering carrier is transmitted from an Earth Station within the Uplink footprint of the victim satellite or on the outer edge of the coverage. It is typically a high-power carrier, within the frequency band of the target carrier. When a carrier is jammed, a geolocation process is launched in order to establish, if possible, a target geographical area where the interference should be transmitted from. In this case, interference signals are tent to sever communications or broadcasts. According to communications experts, a RF link can be regarded as effective when a BER lower than 10^{-3} is achieved. The purpose of the jamming techniques is to make BER raise to 10^{-1} to degrade dramatically the communication channel and put it out of service. All different jamming strategies attempt to accomplish this, by transmitting electromagnetic energy towards the target by means of a signal carrier centred on its same frequency.

Piracy is a voluntary act aiming to use the space capacity without any legal or commercial agreement. Pirates normally access the space capacity to transmit contributions without being noticed. A pirate carrier is considered as interference since it occupies available capacity but it is quite different from the above-mentioned cases. Since the carrier is very often transmitted on the guard bands of the affected transponder or on any available frequency gap on the victim satellite, it "steals" a certain amount of the overall available power of the transponder and can degrade the performance of legitimate services. This degradation does not necessarily happen. The service disruption can be an unwanted side effect. In this case the aim is not to prevent communications but on the contrary to illegally use commercial leased bandwidth and transponders in order to spread some contents for either political purpose or hacker tests. Those carriers are usually detected upon transponder watch activities and look like any other modulated standard DVB carrier. An effective solution in order to mitigate piracy attack effectiveness might be provided by the implementation of a Carrier ID Strategy as suggested by Satellite Users Interference Reduction Group (SUIRG).

It has been assessed that intentional interference weights up to 10% of total experienced interference split between a 6% related to intentional jamming and 4% due to piracy attacks [6]. All different jamming strategies attempt to accomplish this by transmitting energy towards the target by means of a signal carrier centred on its same frequency.

Realistically effective radiated power (EIRP) of a tactical jammer is limited to about $100\,W$ for an airborne jammer and about $5\,KW$ for a large ground-based jammer [R. 7]. Each jamming technique is characterized by a particular assets management in terms of power distribution over time and frequency domain and power sharing among different targets.

An exhaustive literature and press overview suggested that unauthorized interference is a small but significant subset of all types of satellite communications problems experienced. Within this subset has been reviewed that, the cause of the most part of interference events was determined to be non-hostile. However, there are some interference events whose the causes could not be defined. In these cases, the events often join a similar "profiles" and make communication to be disrupted forcing operator to move transmissions to another satellite, another transponder or another band of the same transponder. When it happens, it is reasonable to deduce that at least some of these interferences have a hostile matrix. It can be called: "denial of service" attack, provided that jammers tent to compromise service provision.

Denial of service attack is conducted by hostile electromagnetic interference. This interference can affect:

- Ground segment, even called "downlink jamming", directed at local receiver;
- Space segment, even called "uplink jamming", presented at the satellite, affecting by mixing or overriding the intended carrier.

By mean of algorithm of direction finding, pointing and triangulation techniques downlink jamming can be easily detected and coped with. On the contrary, the vulnerability of commercial satellites to uplink jamming lies within its own structure and operational mode: a bent-pipe satellite transponder is designed to accept microwave energy over a certain band and to re-transmits it at the downlink frequency after proper amplification. So, that the presence of hostile signal (if it reaches satellite with an enough power level) could result in:

- A mixing with the intended signals, making reception of the legitimate signal unable (in other words making the E_b/N_0 less than the sensibility of the receiving satellite antenna);

- Raise the noise floor of the electronic equipment, like transponders, reducing carrier to noise ratio;
- Degradation or severing of all transponder's communications, by inducted saturation, if satellite receiver has limitation in term of received power.

It must be pointed out that due to the significant encoding gain employed in current commercial satellite communication modulation protocols, even a small decrease of Carrier-to-noise-ratio C/N_0, can force communication to go out of service [R. 1].

Intrinsic geosynchronous satellite vulnerability is the very easily targeting of it, since their orbital position is known. There is no need to use tracking equipment: just set intended satellite reference elevation and azimuth and transmit a continuous wave at the desired carrier frequency.

In terms of power needed to sever or disrupt commercial communications must be underlined that typical broadcast carrier to noise ratio are at least $20\,dB$ or more, so that to induce degradations of these carriers, it would be required large aperture antenna - $9\,m$ or more - and powerful amplifiers rated in thousands of watts [R. 8]. According to that has been noticed, all the documented cases of interference against commercial broadcast satellite have involved another commercial broadcast site.

In the case of the ground segment was operated using a Very Small Aperture Terminals (VSATs) (as it happens for example, when commercial satellites lease some of their transponders during wartime, to provide communications over a specific battlefield) equipment needed to implement uplink jamming becomes more affordable.

VSATs generally uses dish antenna with dimension between 1 up to $4\,m$ paired with receive-power limited rice-transmitter developing

carrier to noise ratio varying between $6 - 10\,dB$ above noise floor. Depending on the bandwidth of intended signal, interference signals one of $^1/_2$ powerful as target signal can sever communications. As mentioned before, due to extensive use of advanced coding techniques a relatively slight decrease of the carrier-to-noise ratio can put communication channel down. This aim can be accomplished with VSATs using a few watt power supplies.

Another major issue connected to uplink jamming is the coverage of geostationary satellite. When a jammer tries to attack a satellite, it might be in two different topological scenarios:

- *Around the Edge of Coverage*: if the jammer station is located in the outer nearby of the victim satellite feeder footprint. In this case, jammer would aim to gain his way toward satellite transponders through satellite antenna side lobes or lateral side of main lobe. This scenario requires a huge amount of power, for the attack to be effective.
- *Under Coverage*: if the jammer station lies within the victim satellite feeder footprint. As far as this scenario is concerned, jammer can reach transponders directly toward satellite antenna main lobe with required levels of power far lower than the previous case.

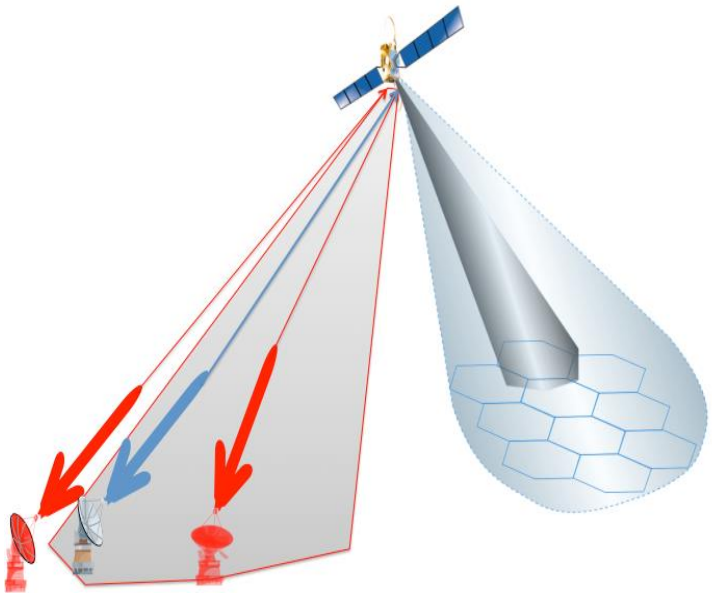

Fig. I-12 : Jamming Sources Outside and Inside the Feeder Coverage.

Either the jammer lies within the footprint contour or around its outer border, it has to be noticed that jammer may be anywhere throughout a geographical area of thousands of square kilometres, making localization very hard to pursue. Even if satellite was provided by a secondary antenna system for jammer localization in order to implement some algorithm of direction finding to locate interference transmitter angular position, jammer might be able to move or to operate only on a limited duty-cycle, or both. Moreover, a jammer geo-location on air is made even more difficult due to the high directivity antenna pattern used for uplink transmissions. Energy will be not broadcasted over a wide radiation pattern but concentred in a focused, quasi-pencil beam, making *de facto* threat signal very hard to triangulate.

In the following subparagraphs, main jamming strategies will be reviewed. In particular, will be emphasized the strategy used, the characterization of each kind of jamming and the effects produced.

I.3.2.1 *Noise Jamming*

In the noise jamming, limited band (generally Gaussian random noise waveform) is modulated over the carrier of interest. This type of jamming can be characterized depending on spectral occupation:

- Broadband Noise Jamming (BNJ), if it occupies a large bandwidth, typically all the attacked transponder bandwidth;
- Partial-band Noise Jamming (PNJ), if it occupies some channels bandwidth;
- Narrow-band Noise Jamming (NNJ), if it is spread over just one channel bandwidth.

This jammer can cause:

- A raised noise floor that affects consequently demodulation performances;
- Disruption of the channel. In fact, the more the coding gain of intended transmission is, the more the effective noise floor will be.

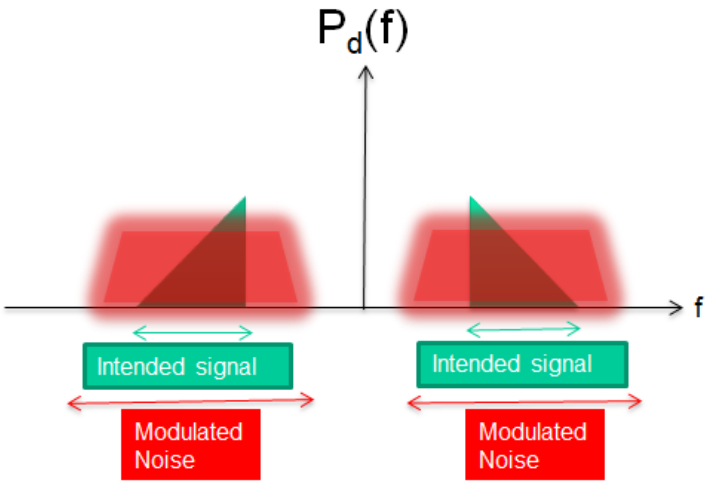

Fig. I-13 : White Gaussian Noise Modulated over Interested Carrier in order to Impair C/N_0 and Disturb Broadcast Signals.

I.3.2.2 *Tone Jamming or Continuous Wave*

In the Tone jamming one or more un-modulated carriers are radiated towards the victim antennas. The frequency of this continuous wave is generally set to be the same of the intended communication one

to be jammed. The characterization usually depends on carrier power and on number of carriers to be transmitted:

- Single Tone Jamming, if it is radiated just one carrier;
- Multi Tone Jamming, if more than one carrier is transmitted.

Since this kind of jamming is based on a transmitting of a continuous wave, it is a constant jammer that transmits continuously and this brings to the following drawbacks (for the jammer):

- It is easy to detect;
- It is great power consumption.

The Tone Jammer allows to keep the medium always busy, over the selected frequency, making a constant noise floor raise or making the affected channel unusable (for high transmitted power levels).

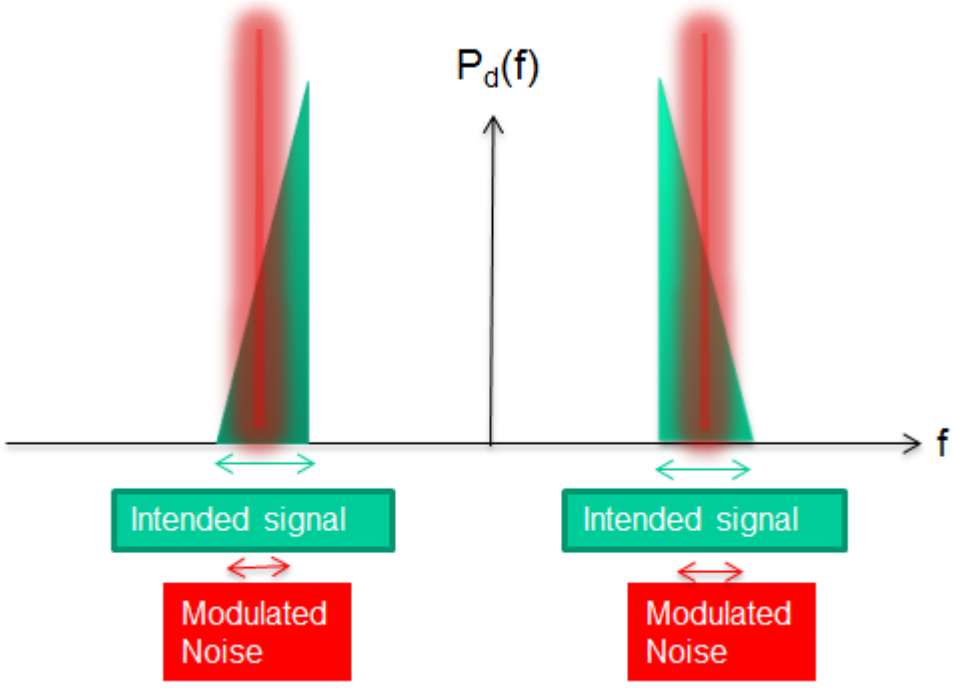

Fig. I-14 : Single Tone Intentional Interference Overriding Jammed Carrier

I.3.2.3 *Follower Jamming*

The follower jamming may disrupt communications if the satellite feeder link implement some sort of frequency hopping technology in order to avoid constant jammer (like tone jammers). A follower jammer

emits a single tone signal at a carrier that varies to follow frequency hops of the target receiver, making almost vain the countermeasure of frequency hopping. Greatest hopping rate is strictly related to the jammer's location. This kind of interference may be characterized by means of transmitted power level, number of hops and bandwidth of use and strikes in general satellite transponders (if frequency hopping is implemented).

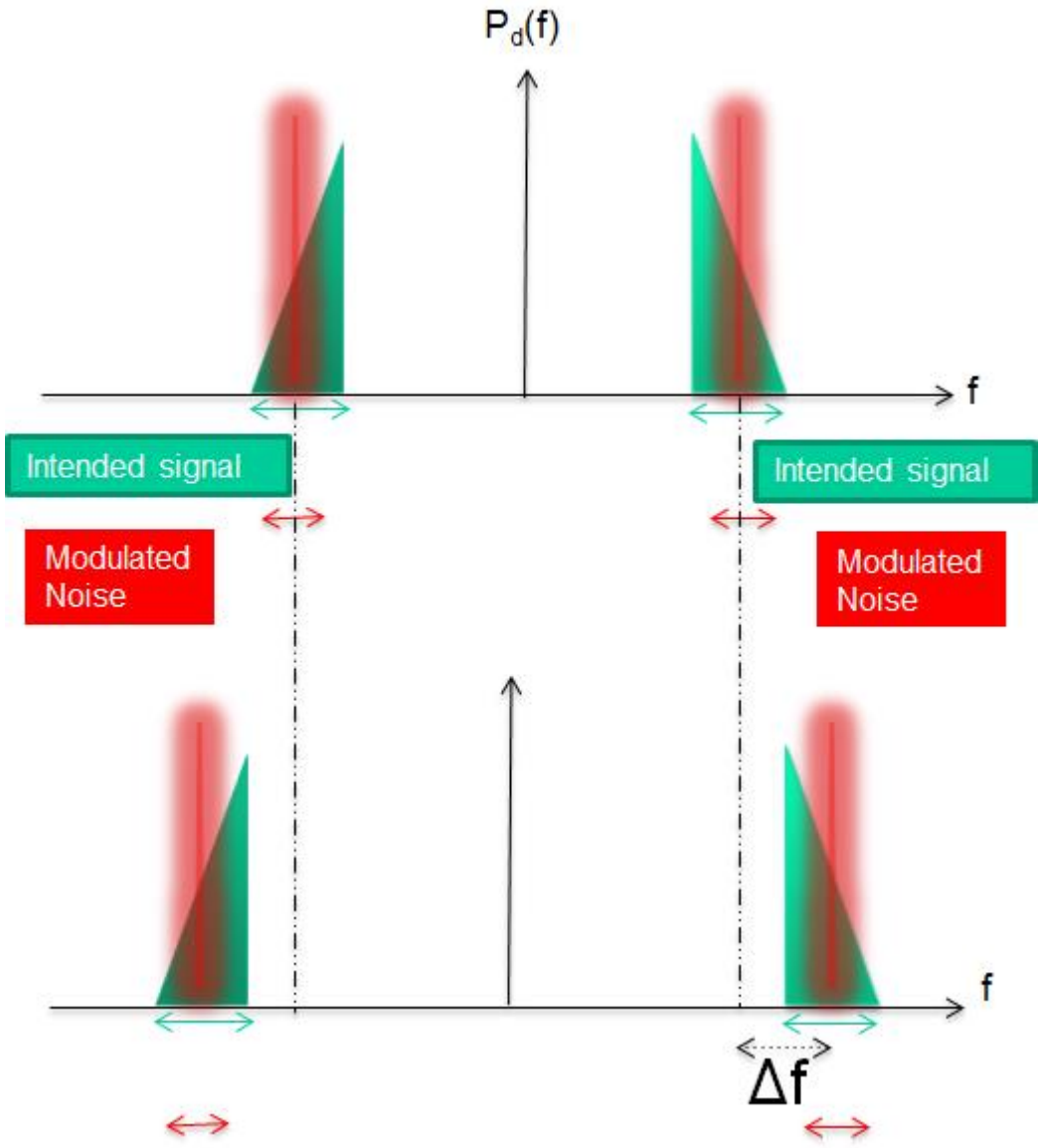

Fig. I-15 : Following Jamming where the Jammer Signal Hops through Bandwidth of Interest following Target Signal.

Sweep jamming aims to counter several different systems spread in frequency over a wide band by continuously sweeping the jamming

frequency across the band. This jamming is used when jammer does not know the target frequency, and then it sweeps across the probable spectrum either periodically or aperiodically jamming the affected networks temporarily. Sweep jamming is less efficient and effective than the spot jamming, but has the advantage of attacks several networks making imposing restrictions on freedom of frequency-hopping by the victim satellites. It is similar to Noise jamming. When a NBN, PBN, STJ signal is scanned in time across frequency band of interest in order to jam periodically the whole band. This jammer is characterized by transmitted power level, number of hops, bandwidth of swept signal and victim portions of the spectrum swept.

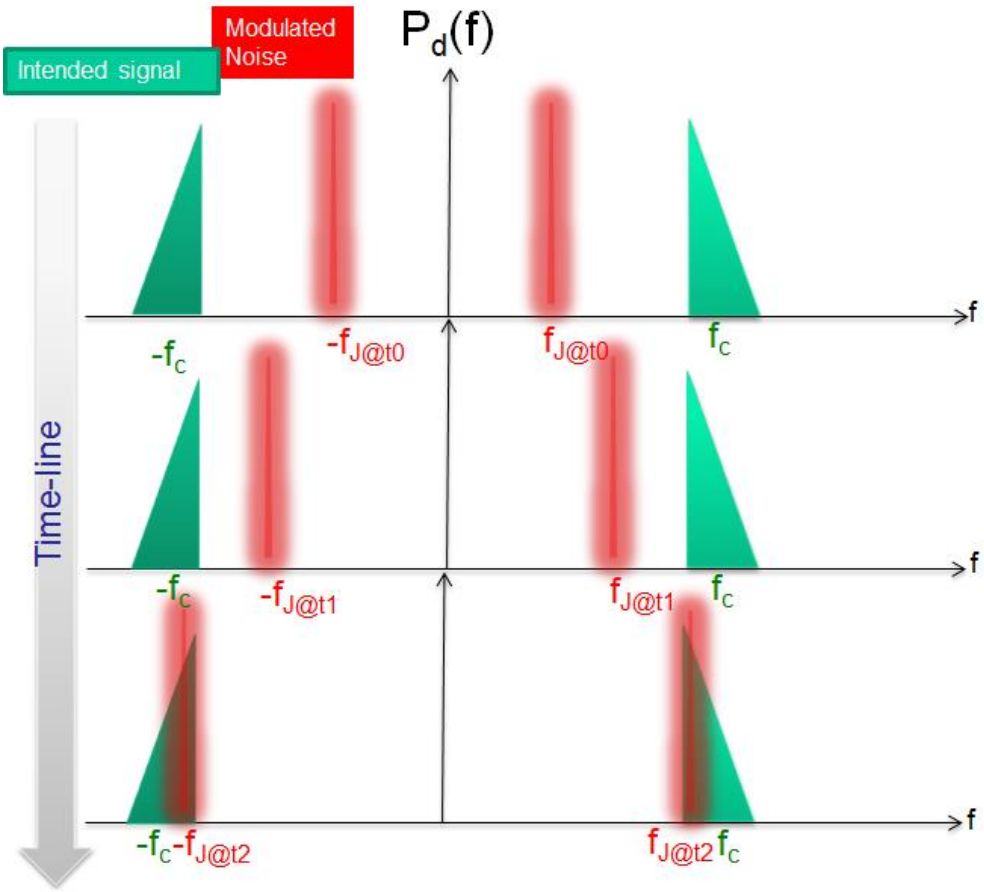

Fig. I-16 : Jamming Signal Sweeping over a certain Bandwidth of Interest.

I.3.2.4 *Barrage Jamming*

Barrage jamming is used when there is a need to jam several carrier frequencies simultaneously using a wide bandwidth. Thus, barrage jamming covers a large bandwidth of the radio spectrum leaving very little opportunities for the target network to avoid jamming. The problem of barrage jamming is in terms of power. In fact, the power has to be spread over a very wide band reducing the corresponding power spectral density. Barrage jammers require high RF power to maintain the required power spectral density of jamming. This is quite different from the previous kinds of jammers, whose entire transmitted power is concentrated in a relatively narrow bandwidth. Power is thus the critical success (or failure) factor associated with barrage jammers, while the advantage is that this kind of jamming can interfere with any signal belonging to its operative band. The characterization of this kind of jamming is in terms of bandwidth, emission mask and transmitted power level. The Barrage Jamming may strike satellites with large operative bands and transmissions whose the operative band is unknown.

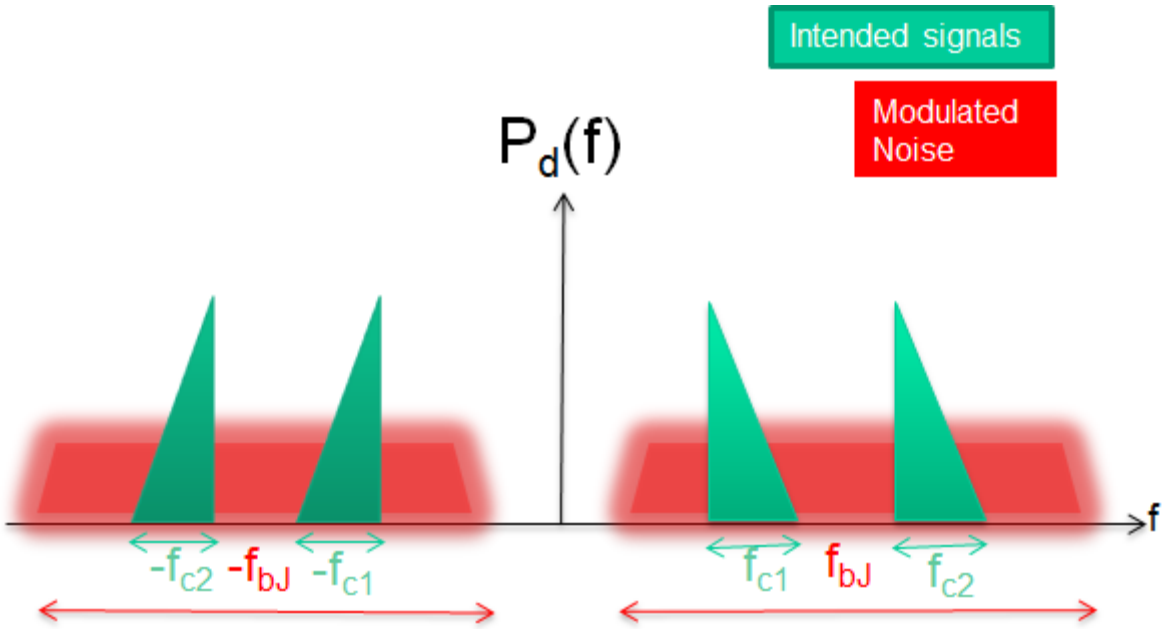

Fig. I-17 : A wide band signal overlapping all intended bandwidth to be jammed.

I.3.2.5 *Pulse Jamming*

In the Pulse Jamming regime an intermittent carrier is generally modulated by broadband noise. Jamming pulses are emitted for a specific time period then sleeps for another one. By varying their time duration, jammer changes emission mask and energy consumption. The characterization of this interference is based on the spectral power density mask, duty-cycle (if pulses are emitted randomly it is called *Random Jamming*), transmitted power level and bandwidth. The Pulse Jamming has effective against satellite provided with secondary wide lobe antenna for jamming threat geo-location: indeed intermittent transmission can make localization very hard.

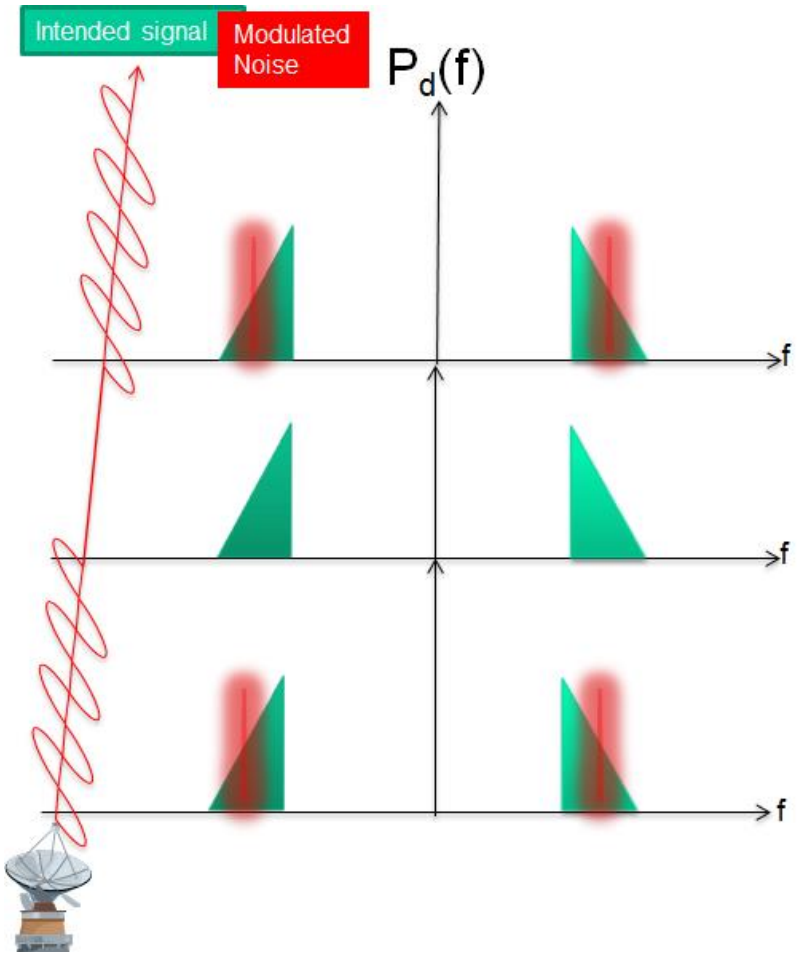

Fig. I-18 : Pulse Jamming: A tone jammer emitting only for a limited time period.

I.3.2.6 *Deception Jamming - Smart Jamming*

The Deception Jamming is a form of intelligent jamming which acts only on selected portions of the target signal, i.e. jamming only channels used for synchronization procedures. This jammer transmits a signal very like the one that has to be interfered. For this reason, data packets in transit on satellite seem to be identical to the true ones sent by the legitimate nodes. Since a deceptive jammer transmits jamming pulses in the form of regular packets, the probability of detection is lower if compared with constant jammer. Deceptive jammer consumes considerable energy and is not an energy efficient jammer. It works generally under the footprint coverage where jammer receives intended signals for later re-transmitting it towards the satellite feeder. When it works with memorized signals, it stores and then forwards back signal received. Enhanced version can forward coherent representation of the original signal, so the satellite will not be able to distinguish it from other legitimate signals it receives and processes as targets. The characterization is in terms of the spectral power density mask, transmitted power level, bandwidth and time delay for re-transmission. The Deception Jamming has effective against singular satellite channel.

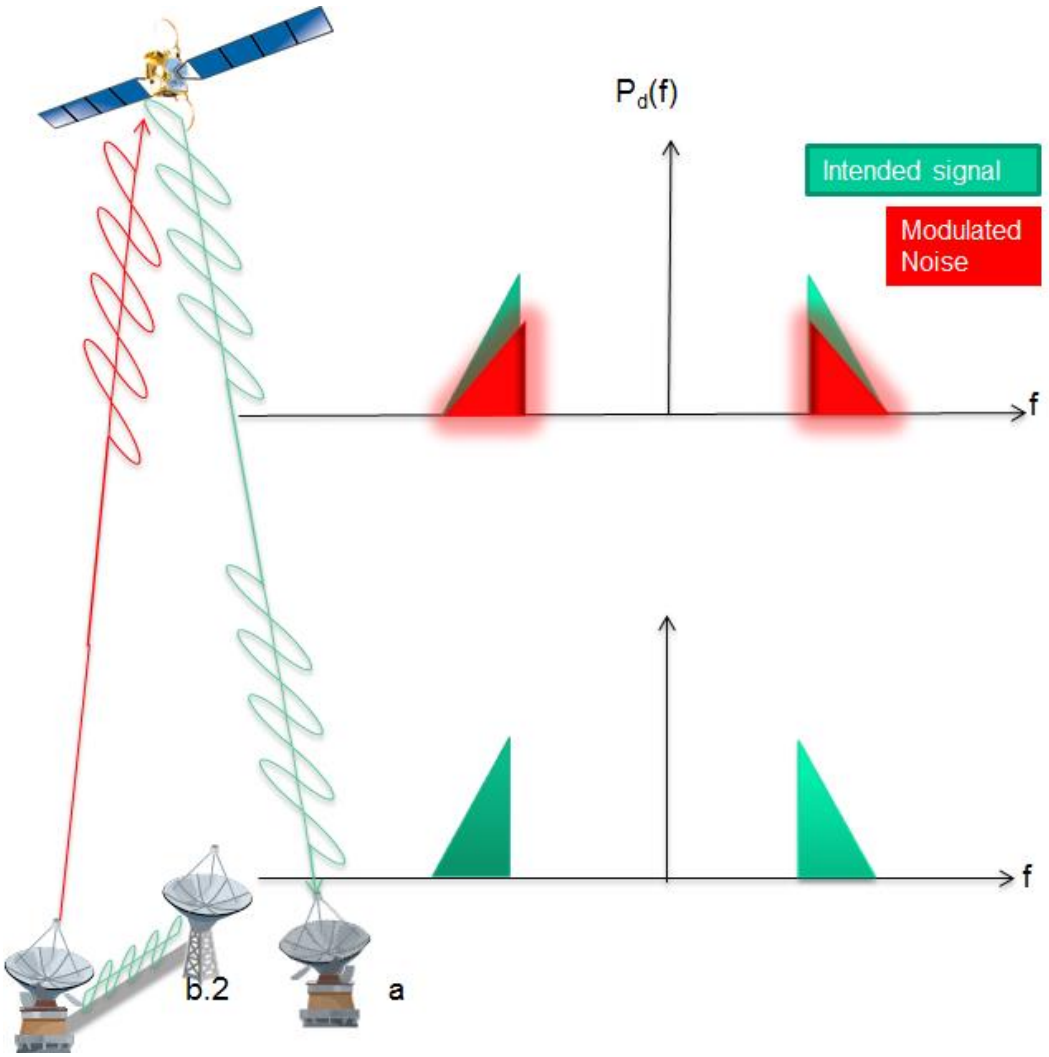

Fig. I-19 : Deception Jamming: Jammer Intercepting facility b.2 record signal to be jammed and then sends it to jammer transmitter b.1 that re-transmits it toward satellite feeder.

I.3.2.7 *Reactive Jamming: Smart Jamming*

Also, the Reactive Jamming is a form of intelligent jamming which acts only on selected portions of target signal, i.e. jamming only channels used for synchronization procedures. In particular, the Reactive Jammer emits pulses only when the satellite medium is busy. Data packets are thus able to degrade communication. Contrary to what happens with the previous jammers, reactive jammers sense if the medium is busy or not, optimizing the energy consumption [9]- [10]. The characterization is in terms of the emission mask, transmitted

power level and bandwidth. This interference strikes intermittent transmissions, like point-to-point communication.

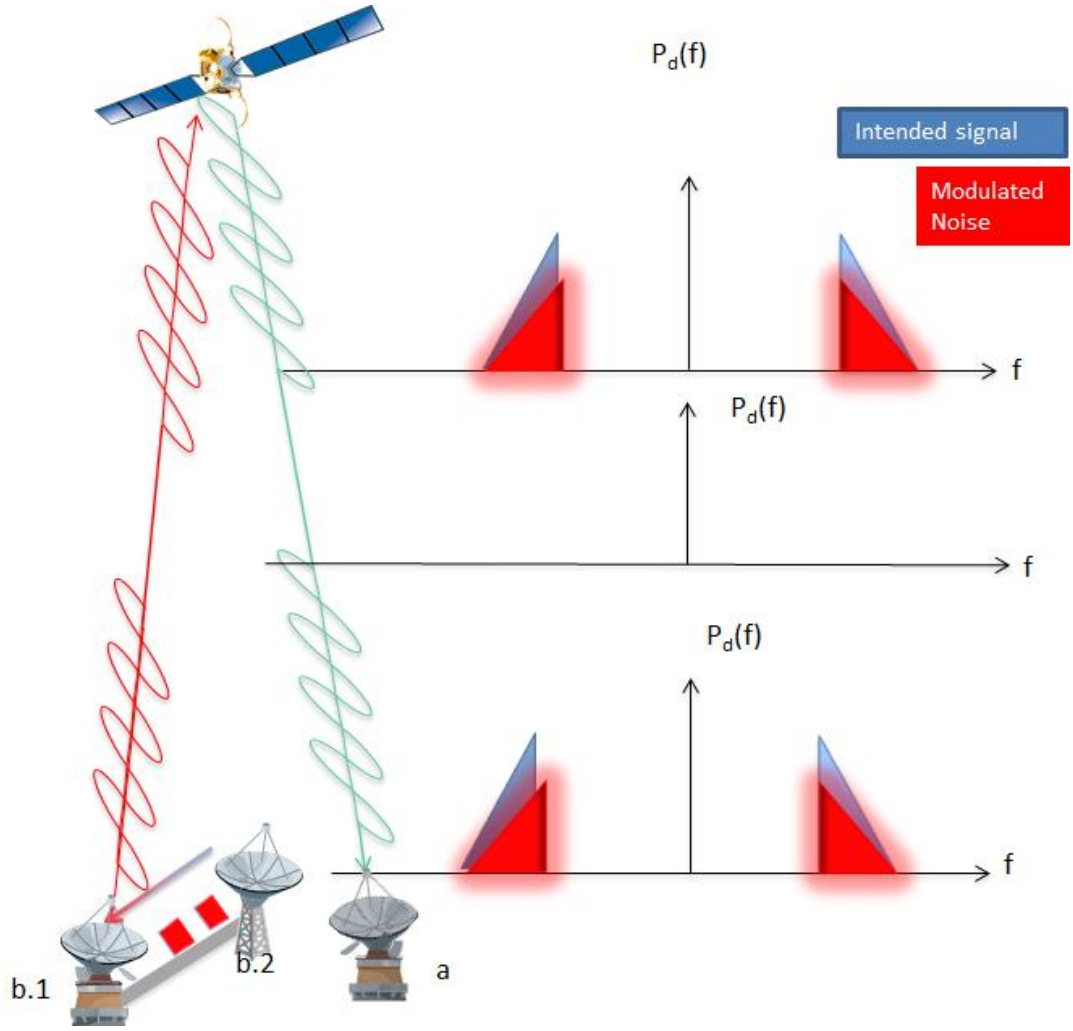

Fig. I-20 : Reactive Jamming: Jammer Sensing b.2 record signal to be jammed and then send it to jammer transmitter b.1 that re-transmits it toward satellite feeder.

I.4 Satellite Vulnerabilities

In this section the multitude of vulnerabilities will be carried out and analysed, considering those regarding the space segment. Typical bent-pipe satellites can be grouped into 3 gateways which might be susceptible to vulnerabilities:

- Antenna bulk
- TWTA
- Transponder

In addition, if satellites were provided with some kind of On-Board Processing Unit (like a router) even the on-board access router should be considered as a vulnerable access point.

The on-board satellite antennas may be susceptible to both environmental and human factors that can degrade operations intentionally or not. As mentioned in the previous chapter, the main causes of degradation related to unintentional interference at antenna levels are:

- Unintentional RF interference from side lobes on an adjacent satellite (ASI);
- Equipment error;
- Human Error;
- Ionospheric Interference during solar maximum activities;
- Unauthorized carries due to frequency spectrum congestion;
- Multipath;

In addition, being antennas one of the major object protruding from the satellite's surface, they are the most vulnerable even to physical damages, which could heavily compromise communications performance. These damages might be inflicted by:

- Space debris and possibly even meteoroids;
- Material out-gassing that can overheated devices;

- Sun released highly-energetic particles due to solar flares or coronal mass ejections.

These mechanical causes of malfunctioning will not be taken into account for the purpose of this study, but might be object of further investigations.

Provided that, antenna section is the main gateway through interference sources can enter into and affect the system. For this reason, particular attention ought to be paid in designing its radio-electrical features in order to make it stronger in rejection of interference, especially as far as concerned the following antenna figures:

- *Side Lobe Level*: the lower level of secondary side lobes can be reached, the lower gain will obtain not intended signals, intentional or unintentional;

- *Pointing accuracy*: the grater the pointing precision is, the lesser will be the risk of Adjacent Satellite Interference and Co-Channel Interference or jammer attack;

- *Polarization purity*: the greater polarization effectiveness will be implemented by the antenna, the lesser will be the impact of intentional or unintentional cross-polarization interference.

It has to be pointed out that although many different type of jamming strategies use antennas as gateway to access satellite payload, the most of these has impact mainly on TWTA or transponder level to accomplish their attack. In fact, once it enters through the antenna section, an interference signal at proper carrier in input to a bent-pipe transponder will be processed along with the intended signals and then re-transmitted down toward the receiver. The interference signal may act at this level in different way causing:

- Obscuration: when interference signals have a Signal-To-Noise-Ratio greater than the intended signal, making the receiver unable to discern the right payload signal;

- Noise Floor Raising: when interference signal make noise floor of the transponder to rise, causing strong reduction in the SNR of all intended signals. If payload signals get lost in the background noise, it cannot be recovered.

These impairments might be experienced due to a wide variety of causes involving intentional attack from a malicious jammer or unintentional occurrence of interference generation, like the ones mentioned in the previous section.

To enable each transponder to carry multiple signals, a multiple access scheme is generally used. Every different multiple access technology might be more prone to some kind of interference. According to that, it will be summarized in their pros and cons reported in the Tab. I-1.

ACCESS STRATEGY	Pros	Cons
CDMA	Protection against frequency jammer Reduced Co-channel interference	Weak against high power jamming attackers If LFSR are used to create the codes spoofing jamming becomes quite easy
FDMA		Prone to intermodulation interference Suffers from Co-Channel interference if channel spacing is too poor
TDMA	No Interference between different legitimate user signals	

Tab. I-1 Advantages and Disadvantages of Multiple Access Technologies.

The main TWTA vulnerability consists of its susceptibility to high voltage breakdown failures. When intentional or unintentional interference raise signal power level in input at the satellite power amplifier, it can force amplifier to work in saturation zone, with a consequent impairment of SNR, introduction of signal distortions and spurious emissions that could interfere with the intended signals. As the signal power level increases, might occur even the high voltage breakdown that result in TWT failure making the re-transmission chain unserviceable." [R. 56].

I.5 EFFECTS OF INTERFERENCE

In order to evaluate the effect of the intentional and unintentional interferences, a simulator model has been developed in association with the R&D section of the Telecommunication department of Thales Alenia Space Italia to analyse both the E2E satellite communication channel and the most representative intentional interference scenarios [R. 41]. The influence of jammer on satellite's devices and what happens to the communication satellite radio-link in presence of the voluntary interference has been assessed.

I.5.1 Interference effects on physical level of communication links

In order to evaluate the End-To-End chain, an implementation of the whole system has been developed using MATLAB's well-known block diagram environment Simulink. The simulation approach has been focused on the modelling of the ground and payload equipment with the RF impairments and propagation losses. Radio-frequency characteristic link parameters, such as EIRP or G/T, can be varied as well as interference waveform.

The baseline software simulation platform top level architecture will include the transmitter, channel models (both uplink and

downlink), satellite and the receiver sub-elements. The baseline model for simulator design will be the reference DVB-S2 standard. The services of interest taken into account are Fixed Satellite Service (FSS)/Broadcasting Satellite Service (BSS) provided by Ku-band broadband GEO satellite system. The simulator has been designed in order to model the abovementioned services implementing different modulations and wide range of Forward Error Correction (FEC) redundancy rate accordingly to the DVB-S2 standard.
The block diagram of the developed simulator end-to-end chain without the jamming is sketched in the next figure.

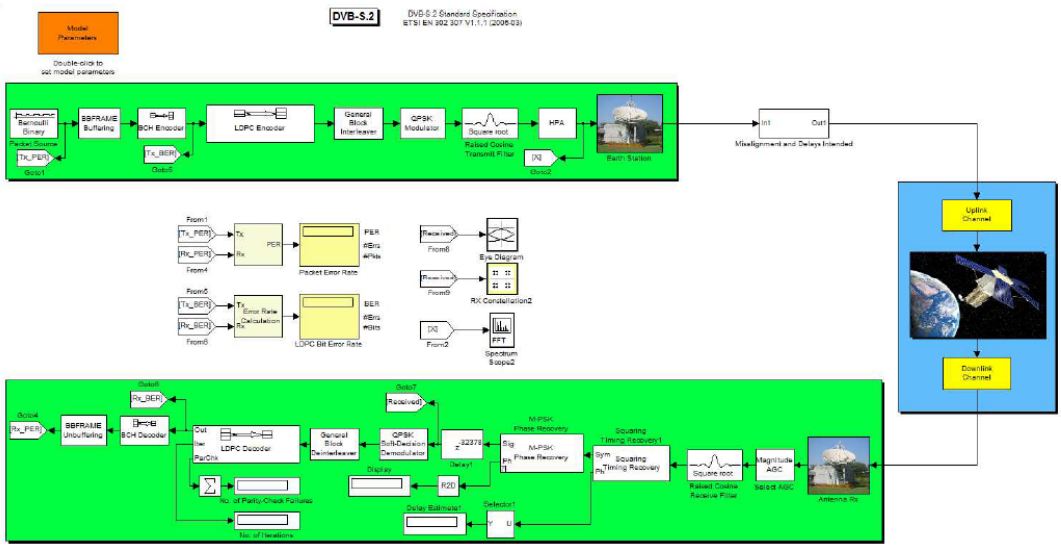

Fig. I-21 : End-To-End Chain Numerical Simulator [**R.** 41].

The blue region stands for the satellite and the uplink and downlink channels, while the green ones represent the feeder link and the user's segment. The orange block instead (placed in the upper corner on the left side), called Model Parameters, is the block where a user sets the values needed for the numerical simulation. Along the end-to-end chain a lot of intermediate scopes are introduced to verify what is happening to the information during the communication. The scopes inserted are:

■ Scatter plot that reveals the modulation characteristics showing it in terms of phase and quadrature;

■ Eye diagram that reveals how the waveforms used to send multiple bits of data can potentially lead to errors in the interpretation of those bits. In other words, it shows if there is Inter-Symbol Interference (ISI) and which is its impact in the communication chain;

■ FFT plot that displays the streams of data in the frequency domain making the Fast Fourier Transform of the packets.

In addition, the simulator is able to produce the SNR curves like E_b/N_0, E_s/N_0 and C/N_0 in function of BER and PER values.

Real scenarios are fixed to make the simulations more consistent with the reality. In particular, it has been chosen a satellite that is still in orbit for each Radiocommunication services, in such a way to have the values necessary for the simulation that are the most realistic as possible; all the satellites that have not a European coverage are filtered out, since it has been decided that the jammer is placed in one of the country found in literature; for the chosen satellite, it has been made a research of
which is the location of the teleport.

The entire simulator test activity has been validated through the comparison between the BER curves produced by the simulator with the theoretical BER ones [R. 12], as represented in the following figure where
simulator results are shown in red while the theoretical curves shown in
black.

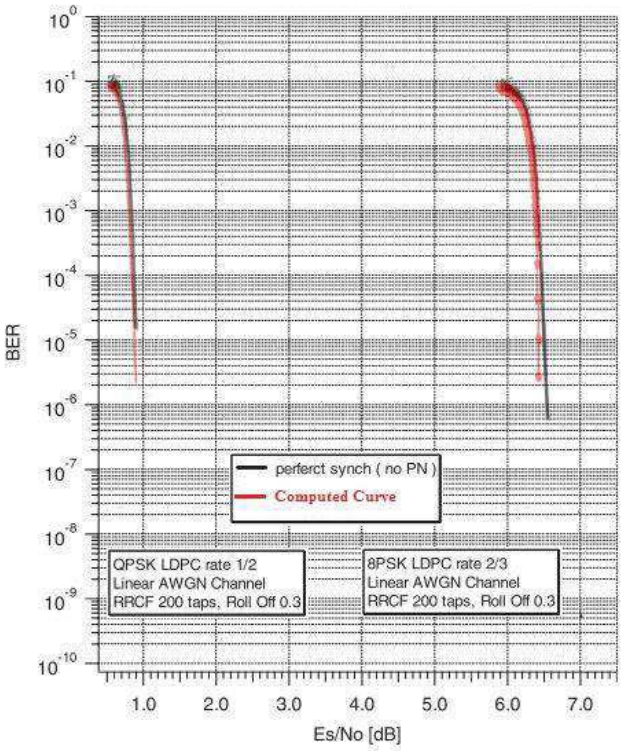

Fig. I-22 : Comparative test between theoretical curves [R. 41].

In particular, the curves on the left are computed with the mod cod (modulation and coding) QPSK 1/2, while the ones on the right are computed with the mod cod 8PSK 2/3. The implemented simulator can well analyse effects of interference phenomena on the communication link in presence of any kind of interference, either intentional or unintentional. It has been used to assess the impact of the intentional and unintentional interferers on the E2E chain and evaluate the performance obtained by using such anti jamming technique. Analyses have been carried out into three consequent phases. In the first place, the E2E DVB-S2 standard has been taken into account as reference for the simulator implementation. Once the simulator has been validated with the standard, the chain has been enhanced with the insertion of all the other blocks.

The whole simulator has been then compared with the results found in literature and the ones carried out by the link budget analysis, in order to verify the output accordance with the theoretical expected results.

In the TAS-I laboratory the simulator results have been validated by comparison with the ones obtained using of a satellite E2E radiofrequency emulator. The simulator has been then used to understand the impact of the jamming strategies on the communication link in terms of BER, PER and quality of received signal (eye diagrams and constellations). A jamming strategy can degrade communications by making the BER upper than 10^{-3}. The aim of the jamming techniques is to make BER raise to 10^{-1} in order to sever the communication channel and put it out of service. All different jamming strategies attempt to accomplish this, by transmitting electromagnetic energy towards the target by means of a signal carrier centred on its same frequency.

All the predicted interference sources presented in I.3 have been deeply analysed and its effects on E2E link communication evaluated by the means of this simulator. The presentation of all the simulated results is outside the purpose of this work but on representative case will be shown as example of the results can be carried out.

The most common interference observed by the satellite operators is the tone jamming, since it is the easiest to generate by a jammer. For this reason, the tone jamming is presented as example to understand the capability of the simulator, even if all the other jammers have been simulated. The tone jamming has the effect to generate pulses in the frequency domain that, if superposed on the pass-band of the intended carrier and if have a power level greater than the intended carrier itself, are able to sever the communication.

I.5.2 Analysis of the Tone Jamming Effect

The tone jamming has the effect to generate pulses in the frequency domain that, if superposed on the pass-band of the intended carrier and

if have a power level greater than the intended carrier itself, are able to sever the communication.

In the Fig. I-23 is shown the comparison between the situation in which no interference is active and the one in which the tone jamming is present (respectively Fig. I-23 a and Fig. I-23b). In the Fig. I-23b the red signal curve is the interference one that is superposed also on the pass-band of the intended carrier. From this figure, it is possible to note that the power of the interferer signal is quite greater than the intended carrier and this produce the severing of the communication. In fact, when the tone jamming is performed the BER is of 0.437 while the PER tends to the unitary value, i.e. the communication is compromised.

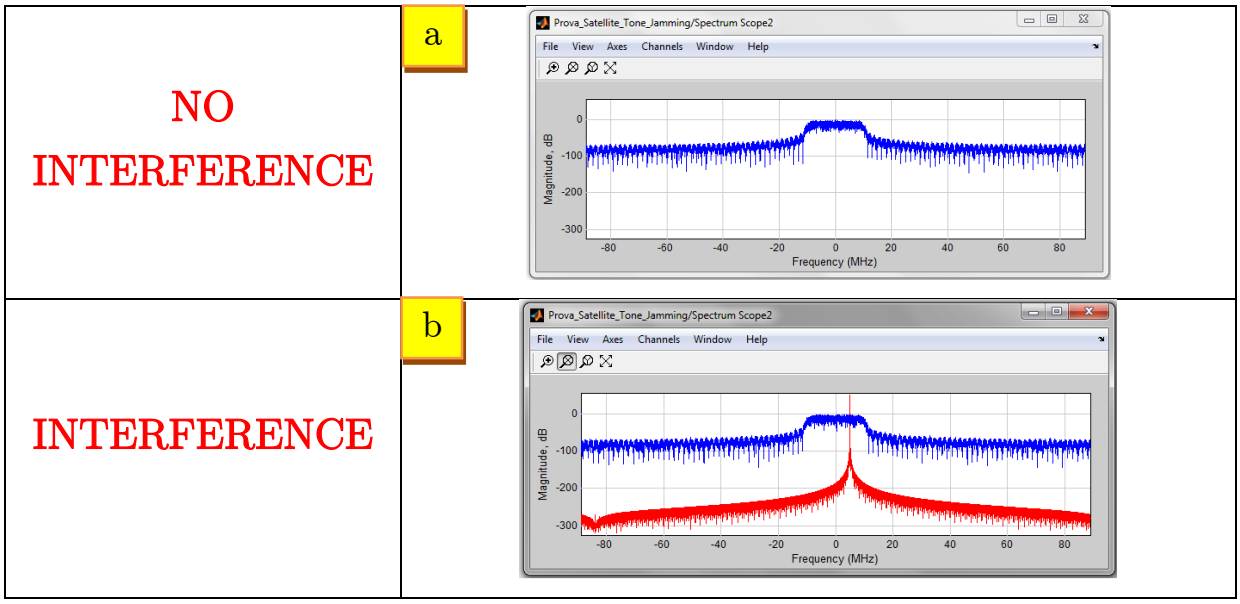

Fig. I-23 : FFT Scopes obtained by the Tone Jamming Simulations without the Interference (a) and with the Interference (b) [R. 41].

In the Fig. I-24 is represented the signal coming out from the satellite at the Tx antenna level, when the interference is absent (Fig. I-24a) and when it is present. The superposition of the interferer signal shown in the previous figure, is reflected in the Fig. I-24 b by the introduction of the unwanted peaks. The only peak visible in the figure

(the other is out of the dynamic range adopted to represents the output signals) appears in correspondence of the pulses due to the tone jamming and is highlighted by the yellow box.

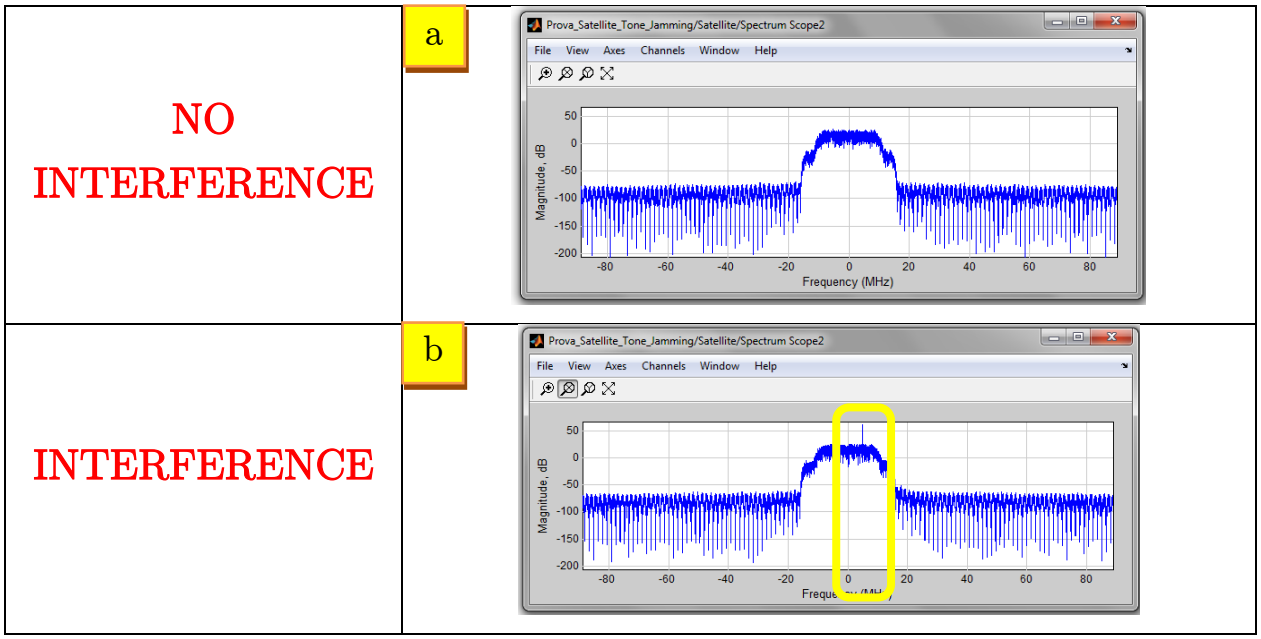

Fig. I-24 : FFT Scopes of the Output Satellite Signal obtained by the Tone Jamming Simulations without the Interference (a) and with the Interference (b) [R. 41]..

In the Fig. I-25b, in fact, it is clear the effect of the interference in the communication. The scatter plot in the Fig. I-25b is enlarged in amplitude and this causes the superposition of the symbols producing unrecoverable errors in the receiving phase by the user's segment. The enlargement is due to the fact that at each symbol is added a phase variation (that correspond to a frequency variation) and an amplitude variation of the quadrature and phase components caused by the interferer.

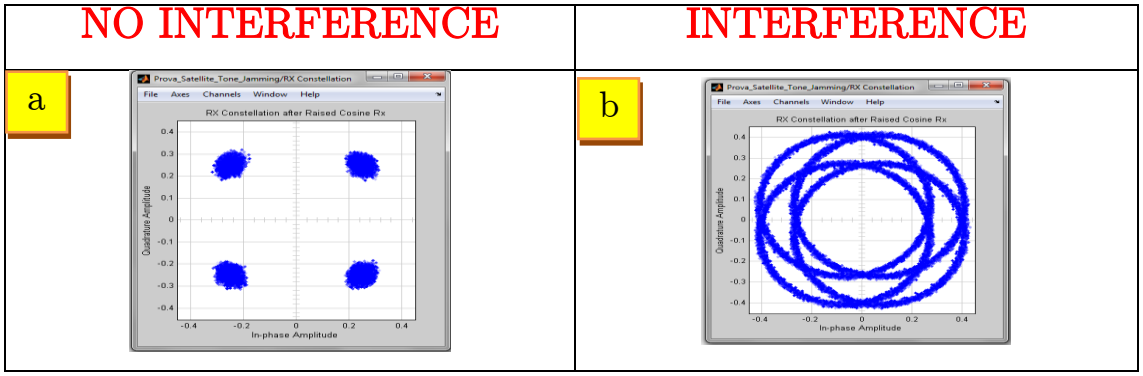

Fig. I-25 : Scatter Plots obtained by the Tone Jamming Simulations without the Interference (a) and with the Interference (b) [R. **41**].

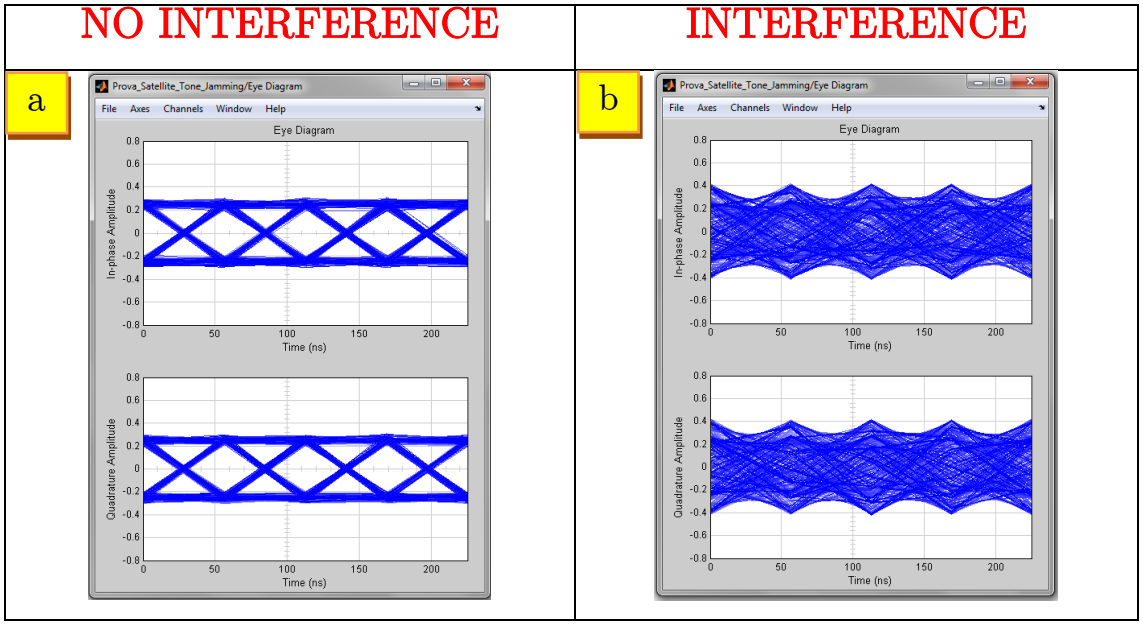

Fig. I-26 : Eye Diagrams obtained by the Tone Jamming Simulations without the Interference (a) and with the Interference (b) [R. 41].

In the Fig. I-26 is confirmed the goodness of the link in absence and in presence of the interferer. In fact, while in the Fig. I-26 the eye diagram shows an eye widely open both in the phase and in the quadrature quadrant, in the Fig. I-26 b these situations not happened and then the eye is completely closed both in the phase and in the quadrature quadrant.

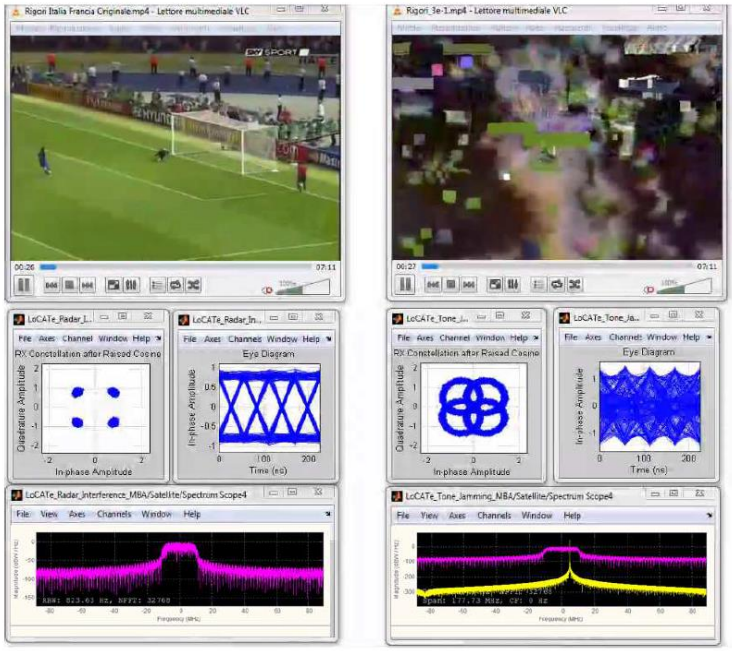

Fig. I-27 :QoS obtained in Absence (right) and in Presence of a Tone Jamming (left)as simulated by the developed emulator[R. 41].

I.5.3 Effects of Unmitigated Interference on Satellite link

Here as follows, two synoptic tables which synthetize the huge effort which has been spent in defining the impairments introduced by the interference sources in the satellite system.

Analytical Parameters		Cross-Pol Interference	Intermodulation interference	Raised Noise Floor	Adjacent Satellite Interference	Radar Interference
High Level	Detail Level	FSS/BSS (Ku-Band)	FSS/BSS (Ku-Band)	MSS (C/L Band)	FSS/BSS (Ku-Band)	FSS/BSS (Ku-Band)
Physical Layer	*C/N+I Reduction*	2.13 dB	13.01 dB	0 dB	10.85 dB	18.81 dB
Signalling Level	*Loss of access due to loss of signalling*	No Signalling due to FDMA	No Signalling due to FDMA	No Signalling due to FDMA	No Signalling due to FDMA	No Signalling due to FDMA
	Time to Resolve after end of interference	No Signalling due to FDMA	No Signalling due to FDMA	No Signalling due to FDMA	No Signalling due to FDMA	No Signalling due to FDMA
Network Level	*Time To Re-Sync*	Up to 20 sec	Up to 20 sec	Up to 20 sec	Up to 20 sec	Decoder cannot re-sync between 2 consecutive burst
	Time to Resolve after interference ends	Up to 20 sec	Up to 20 sec	Up to 20 sec	Up to 20 sec	Up to 20 sec
Capacity Level	*Generation of Capacity Loss*	Only if traffic planned on other pol and power margin	Strongly impacted	NDA	No	Always due to Radar signal high power level
	Amount of Capacity Loss	All	No differential capacity loss	NDA	None	total loss of Capacity on affected bandwidth
Availability Level	*Generation of Availability Loss*	Strongly impacted	If C/N+I > 5 dB might no be available depending on service	NDA	No	Always due to Radar signal high power level
	Amount of Availability Loss	Difficult to quantify	Difficult to quantify	NDA	None	Drop to 0
Other Effects	*Indirect Additional effects*	No	No	NDA	No	No

Tab. I-2: Assessment of Effects of Unmitigated Unintentional Interference [R. 40]

Analytical Parameters		Piracy	Tone Jamming (CW)		Multi-Tone Jamming	Sweep Jamming		Deceptive Jamming
High Level	Detail Level	FSS/BSS (Ku-Band)	FSS/BSS (Ku-Band)	FSS (Ka-Band)	FSS/BSS (Ku-Band)	FSS/BSS (Ku-Band)	MSS (C-L Band)	FSS/BSS (Ku-Band)
Physical Layer	*C/N+I Reduction*	No loss Power robbing	19.46 dB	20.73 dB	19.47 dB	20.28 dB	1.93 dB	18.46 dB
Signalling Level	*Loss of access due to loss of signalling*	No Signalling due to FDMA	No Signalling due to FDMA	No Signalling due to FDMA	No Signalling due to FDMA	No Signalling due to FDMA	No Signalling due to FDMA	No Signalling due to FDMA
	Time to Resolve after end of interference	No Signalling due to FDMA	No Signalling due to FDMA	No Signalling due to FDMA	No Signalling due to FDMA	No Signalling due to FDMA	No Signalling due to FDMA	No Signalling due to FDMA
Network Level	*Time To Re-Sync*	Not applicable	Up to 20 sec	Up to 20 sec	Up to 20 sec	Up to 20 sec	NDA	Up to 20 sec
	Time to Resolve after interference ends	Not applicable	Up to 20 sec	Up to 20 sec	Up to 20 sec	Up to 20 sec	NDA	Up to 20 sec
Capacity Level	*Generation of Capacity Loss*	No	Often due to CW signal high power level	Often due to CW signal high power level	Often due to CW signal high power level	Often due to Sweeping signal high power level	NDA	Yes
	Amount of Capacity Loss	No	Total loss of Capacity	Total loss of Capacity	Total loss of Capacity	Total loss of Capacity	NDA	Total loss of Capacity
Availability Level	*Generation of Availability Loss*	If TPX is 100% loaded and in saturation	Often due to CW signal high power level	Often due to CW signal high power level	Often due to CW signal high power level	Often due to CW signal high power level	NDA	Often due to CW signal high power level
	Amount of Availability Loss	Even drop to 0	Total outage	Total outage	Total outage	Total outage	NDA	Total outage
Other Effects	*Indirect Additional effects*	No	No	No	No	No	NDA	No

Tab. I-3: Assessment of Effects of Unmitigated Intentional Interference [R. 40]

I.6 ANTENNA SYSTEM ANTI-JAMMING TECHNIQUES

The purpose of this chapter is to identify and describe possible anti-interference techniques. These techniques must regard the commercial satellite field and then they should be as much as possible low cost. For this reason, the performance of the candidates' anti-interference techniques has to be linked with the impact in terms of mass, power budget and costs of the final TeLeCommunication (TLC) payload.

The techniques that will be taken into account are at antenna sub-system, to avoid injection of interference both in the receivers and in the payload sub-systems: these techniques are typically based on the beam-forming array technology.

I.6.1 Techniques at the Antenna Subsystem

Purpose of this frame of the activity has been to identify and describe antenna anti interference techniques identifying their impacts on the reference scenarios architectures as previously described

considering as trade-off elements their expected performances and anticipated cost impacts.

This activity has constituted the core of the entire work, providing the anti-interference techniques conceived for the utilisation on commercial satellites i.e. considering not only the performances but their impact in term of mass, power budget and costs of the final TLC payload (P/L).

To respect to the TLC P/L architecture the techniques which have been considered cover the antenna sub-system, to avoid injection of interference in the receivers and the sub-systems of the P/L: these techniques are typically based on the beam-forming technology.

The impact of the proposed techniques on the requirements at system level have been analysed in details. As continuation of this activity frame, a first iteration on the possible considered techniques will be traded-off describing their peculiarities, characteristics and possible space and ground segment design will be drawn.

For what concern the solution definition and implementation the antenna is the key element of an anti-interference sub-system, indeed it represents the transducer between the signal and the environment in which it must work, the antenna is the first line of defence against interference.

The directivity of the antenna in the transmission and reception modes allows space discrimination to be used as an Electronic Counter Countermeasures (ECCM) approach, i.e. it can discover the Direction of Arrival (DoA) of any malicious signal.

During the activity, several techniques for generating space discrimination or DoA have been considered and mainly two of those that do not require a huge design effort have been taken into account:

- Beamwidth control: smaller antenna beamwidth, or correspondingly higher antenna gain, can be employed to spotlight a target and to achieve burn-through jamming.

- Antenna coverage: an antenna with multiple beams can be used to delete the beam containing a jammer while still maintaining detection capabilities for the remaining beams.

The first technique is effective if the jammer is at great distance from the signal source (higher is the distance higher is the antenna isolation vs the interference). The second one is acceptable if it is acceptable to lose beam connectivity towards the direction of the interferer.

Adaptive array systems, representing the technique at the forefront of research and development efforts (as Antenna Nulling) with promises of superior performance against side-lobe and main beam jammers.

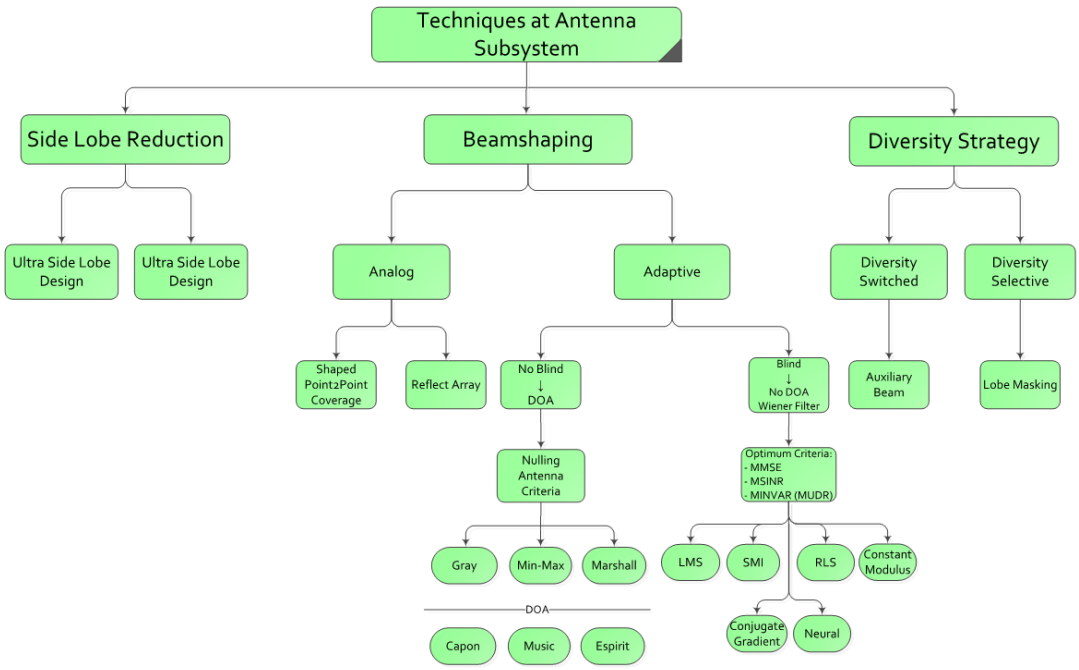

Fig. I-28 : Antenna Interference Mitigation Synoptic Table

Antenna directivity realises inherently space discrimination of transmitted or received (due to reciprocity) electromagnetic signals, which are spatially filtered with respect to their propagation direction angle.

Therefore, a smart shaping of antenna radiation pattern allows to use antenna as an effective Electronic Countermeasure (ECM) in order to reduce and eventually cut off interference impact on satellite system. Types of interference countermeasure, based on antenna capability to discern signal from different geometrical angle of arrival, goes by the name of "Spatial Processing". Spatial processing allows interference detection and mitigation when interference is spatially separated from the wanted signals and especially where signal source channels are de-correlated or the sources are spatially separated.

They have been successfully used in a quite extensive way in military applications, where interfering signals power level can be very high and civilian satellite systems are nowadays experiencing such severe jamming events as well. Many of the strategies and the algorithms, implementing special processing, rely on having multiple antenna elements for their operation, or can be extended to use multiple antenna elements to provide improved performance. Multiple Antenna techniques such as beam-shaping, diversity or source separation can be particularly effective against spatially separated interferer but on the other hand, the price one pays for such performance is not just in the additional processing, but also the additional antennas and RF processing equipment required. For all those reasons, in spite of their performances, spatial processing has not been implemented on large scale in satellite systems in the previous years, until reconfigurable payloads and multiple beam antennas becomes a major requirement of operator in order to keep up with the market pace. Since the demands for broadband services by satellite communications are growing so rapidly, future satellite systems shall provide many new services such as high-speed internet access and broadband multimedia services. In order to fulfil these souring requests, it will be crucial to improve

spectrum efficiency to enhance the system capacity. One of the most promising approaches toward a capacity improvement is the employment of a Smart Antenna technology, which allows to modulate different multiple beams to realise a Space Division Multiple Access (SDMA), by dividing the service area into a large number of cells, where each cell is served by one beam. Both analog or digital beams generation approach, called beam-forming, need a multiple antenna technology and a beam-forming control network to be implemented, thus even spatial processing techniques for interference mitigation might be embedded in satellite system without a major impact on payload architecture. Typical interference signals, affecting by RF systems, are received as a plane incident electromagnetic wave at antenna effective area. Effective aperture of an antenna is defined as the area of an ideal antenna that would absorbs the same power from an incident plane wave as the antenna in question under the matched polarization. According to that, effective aperture represents the ratio of the radiation density in an angular direction in space to the total input power to the antenna. The aim of this strategy is to maximize this ratio in the direction of arrival of intended signals and to minimize it in the angle of arrival of interference signals. The term beam-shaping relates to the function performed by a device or apparatus in which energy radiated by an aperture antenna is focused along a specific direction in space: the objective is either to preferentially receive a signal from that direction or to preferentially transmit a signal in that direction. This technique allows to provide a versatile form of spatial filtering to separate signals that have overlapping frequency content but originate from different spatial locations. Systems designed to receive spatially propagating signals often encounter the presence of interference signals. If desired signal and interferers occupy the same temporal frequency band, temporal filtering cannot be used to separate signal from interference. However, the desired and interfering signals usually originate from different spatial locations so it's possible to separate signals implementing a spatial filtering by means of antenna. An antenna may

be considered to be a device that maps spatial-temporal signals into the time domain, thus making them available for further analysis in a digital signal processor. In this philosophical framework, an ideal antenna is one that converts the spatial-temporal signals arriving at an antenna into a temporal signal without distortion. On transmit the far field of an antenna is the time derivative of the input transient waveform fed to its input terminal. While on receive, the same antenna acts as a spatial integrator of the fields that are incident on it. Hence, the temporal and spatial properties of an antenna are intimately related and the beam- forming strategy takes advantage of both these domains. Thanks to electromagnetic reciprocity property, as in transmission, beam- former network can be seen as the apparatus which allows to maximize antenna gain towards a preferred direction, so in reception the beam-forming network can be interpreted as the equipment that decide the complex weighting factor by the means of which can be coherently – or un-coherently- summed all the received field component coming from different spatial locations. All the beam-forming strategies are focused on the weighting determination pursuing some purpose in term of radiation pattern achievement. Whereas for the former an antenna acts as a spatial filter, and therefore processing occurs in the angular domain, a signal-processing algorithm can be applied in the temporal domain to determine the proper weighting values. Thus beam-forming can be seen as a joint technique between antenna technology and signal processing technology for what concerning the appropriate weighting system.

The beam-shaping technology and architecture are strictly correlated. The basic alternatives from the technological (and then architectural) point of view, are:

- Antenna Optics: Direct Radiating Array, Multi Beam Antenna or Multi Feed Antenna;
- Beam Forming network: Analog or Digital;
- Blind or not Blind: If needed DoA determination;
- Beam-Forming weights calculation algorithm: On board or on Ground.

Considering as above detailed (see bullets) the two basic solutions for the antenna optics are: Direct Radiating Array (DRA) or Multi-beam antenna (MBA).From the qualitative point of view, once fixed the aperture, the main difference is that the DRA requires a high number of feeds to fully sample the aperture. The MBA has a reduced number of feeds, magnified by an optical device (reflector). These two technologies have been examined by the point of view of their capacities of nulling depending on the equivalent antenna aperture and on the number of the necessary elements and spacing. For a given antenna dimension, a first discriminator has been the antenna flexibility and resolution Vs. nulling and a second discriminator has been the antenna spectral resolution to the interference source and users' locations. Once the antenna family have been selected many parameters affecting the antenna nulling capability like the antenna nulling resolution Vs user-interference source relative positions and number can be investigated. Regarding the DOA, the main difference between the two solutions is that with the DRA solution any signal arriving from a direction (θ, ϕ), has relative phase on each feed which is function of the direction of arrival (θ, ϕ). The use of an MBA implies, on the contrary, that the relative phase of the signal onto each feed is not function of the direction of arrival (θ, ϕ). As described in the evaluation of the optimum radiating aperture of the Antenna Nulling Algorithm Technique (ANAT) on the basis of the following items:

- ANAT ground resolution
- Max embarkable and realisable radiating aperture.
- Number of requested active RF chains
- External coverage protection against far-out interference sources in terms of granted I/S

I.7 Analytic problem formulation

To carry out the reference benchmark analyses in the beam-space, it is necessary to choose a suitable element beam model. The analytic model should consider the main antenna aperture parameters as the correct antenna aperture model and the supposed illuminating field distribution.

In the first place, it will be described the simple rectangular aperture model with a uniform field feeding over the aperture itself which will represents the single element of the DRA.

I.7.1 Rectangular Aperture Radiation Pattern

The aperture geometrical variables are ***a*** and ***b***, which controls the aperture width and height respectively as reported in Fig. I-29.

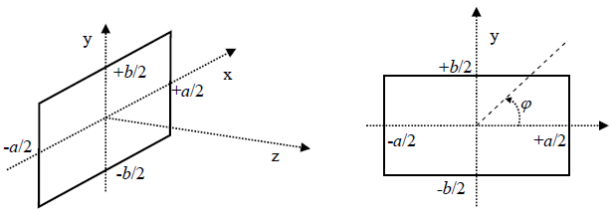

Fig. I-29 : Rectangular Aperture Reference system

It is possible to focus our attention on 3 cases of interest according to the relative modal distribution on the aperture: TE_{m0} , TE_{10} , TE_{mn} .

The field distribution over the aperture can be described as:

$$T(x\,,y) = C\ \cos\left(\frac{m\pi}{a}x\right)\cos\left(\frac{n\pi}{b}y\right) \tag{I.1}$$

where a , b are the rectangular waveguide side and C is a multiplying constant.

By taking into account the first case (m, 0) the modal distribution of the field on aperture is :

$$TE_{m0} \Rightarrow T(x\,,y) = C\ \cos\left(\frac{m\pi}{a}x\right) \overset{\text{def}}{=} f_y^{(x)}(x) * f_y^{(y)}(y)$$

$$= C\ \cos\left(\frac{m\pi}{a}x\right)\left[\Pi\left(\frac{x}{a}\right)\Pi\left(\frac{y}{b}\right)\right] =$$

$$= C\ \cos\left(\frac{m\pi}{a}x\right) e^{-jk_z\frac{x^2}{2R_a}}\ e^{-jk_z\frac{y^2}{2R_b}} \tag{I.2}$$

Thus the related radiation function can be written as:

$$F_y(\,\theta\,,\varphi\,) = \int_{-\infty}^{+\infty} f_y^{(x)}(x)\, e^{-jk_0\sin(\theta)\cos(\varphi)x}\ dx$$

$$* \int_{-\infty}^{+\infty} f_y^{(y)}(y)\, e^{-jk_0\sin(\theta)\sin(\varphi)y}\ dy =$$

$$= \int_{-a/2}^{+a/2} C\cos\left(\frac{m\pi}{a}x\right) e^{-jk_z\frac{x^2}{2R_a}}\ e^{-jk_0\sin(\theta)\cos(\varphi)x}\ dx$$

$$* \int_{-b/2}^{+b/2} e^{-jk_z\frac{y^2}{2R_b}}\, e^{-jk_0\sin(\theta)\sin(\varphi)y}\ dy = \qquad \text{(I.3)}$$

By considering $k_z = 2\pi/\lambda$, $S_a = \Delta_a/\lambda = A^2/8\lambda R_a$ and $S_b = \Delta_b/\lambda = B^2/8\lambda R_b$ it is worth noting that $k_z\,\Delta_a$ e $k_z\,\Delta_b$ represent the maximum radiation phase deviation expressed in radians, so by introducing these variables:

$$= C\int_{-a/2}^{+a/2} \cos\left(\frac{m\pi}{a}x\right)\ e^{-j\left(\frac{\pi A^2}{4\lambda R_a}\right)}\ e^{-jk_0\sin(\theta)\cos(\varphi)x}\ dx$$

$$* \int_{-b/2}^{+b/2} e^{-j\left(\frac{\pi B^2}{4\lambda R_b}\right)}\, e^{-jk_0\sin(\theta)\sin(\varphi)y}\ dy = \qquad \text{(I.4)}$$

Now by introducing $\sigma_a^2 = 4\,S_a = A^2/2\lambda R_a$ *and dually* the $\sigma_b^2 = 4\,S_b = B^2/2\lambda R_b$,

$$= C\int_{-a/2}^{+a/2} \cos\left(\frac{m\pi}{a}x\right)\ e^{-j\left(\frac{\pi}{2}\right)\sigma_a^2\left(\frac{2x}{A}\right)^2}\ e^{-jk_0\sin(\theta)\cos(\varphi)x}\ dx$$

$$* \int_{-b/2}^{+b/2} e^{-j\left(\frac{\pi}{2}\right)\sigma_b^2\left(\frac{2y}{B}\right)^2}\, e^{-jk_0\sin(\theta)\sin(\varphi)y}\ dy = \qquad \text{(I.5)}$$

Now by changing the variable, in accordance with:

$$\begin{cases} \xi_a = \dfrac{2x}{A} \rightarrow x = \dfrac{\xi A}{2} \Rightarrow dx = \dfrac{A}{2} d\xi \\ \hat{\xi}_a = m\xi_a \rightarrow d\hat{\xi}_a = m d\xi_a \end{cases} \tag{I.6}$$

It can be obtained:

$$= \frac{AC}{2} \int_{-1}^{+1} \cos\left(\frac{m\pi A\xi_a}{2A}\right) e^{-j\left(\frac{\pi}{2}\right)\sigma_a^2\xi_a^2} e^{-jk_0(\sin(\theta)\cos(\varphi))\xi_a\frac{A}{2}} d\xi_a$$

$$* \frac{B}{2} \int_{-1}^{+1} e^{-j\left(\frac{\pi}{2}\right)\sigma_b^2\xi_b^2} e^{-jk_0(\sin(\theta)\sin(\varphi))\xi_b\frac{B}{2}} d\xi_b =$$

$$= \frac{ABC}{4} \int_{-1}^{+1} \cos\left(\frac{m\pi\xi_a}{2}\right) e^{-j\left(\frac{\pi}{2}\right)\sigma_a^2\xi_a^2} e^{-j\frac{2\pi}{\lambda}(\sin(\theta)\cos(\varphi))\xi_a\frac{A}{2}} d\xi_a$$

$$* \int_{-1}^{+1} e^{-j\left(\frac{\pi}{2}\right)\sigma_b^2\xi_b^2} e^{-j\frac{2\pi}{\lambda}(\sin(\theta)\sin(\varphi))\xi_b\frac{B}{2}} d\xi_b =$$

$$= \frac{ABC}{4} \int_{-1}^{+1} \cos\left(\frac{m\pi\xi_a}{2}\right) e^{-j\left(\frac{\pi}{2}\right)\sigma_a^2\xi_a^2} e^{-j\pi v_x\xi_a} d\xi_a * \int_{-1}^{+1} e^{-j\left(\frac{\pi}{2}\right)\sigma_b^2\xi_b^2} e^{-j\pi v_y\xi_b} d\xi_b =$$

$$= \frac{ABC}{4m} \int_{-1}^{+1} \cos\left(\frac{m\hat{\xi}_a}{2}\right) e^{-j\left(\frac{\pi}{2}\right)\sigma_a^2\frac{\hat{\xi}_a^2}{m^2}} e^{-j\pi v_x\frac{\widehat{\xi_a}}{m}} d\hat{\xi}_a$$

$$* \int_{-1}^{+1} e^{-j\left(\frac{\pi}{2}\right)\sigma_b^2\xi_b^2} e^{-j\pi v_y\xi_b} d\xi_b = \tag{I.7}$$

These integral formula can be solved by using the Fresnel Integral Form. By adopting the following variables position:

$$\begin{cases} \hat{\sigma}_a^2 = \dfrac{\sigma_a^2}{m^2} \\ \hat{v}_x = \dfrac{v_x}{m} \end{cases} \tag{I.8}$$

They can be written as:

$$= \frac{ABC}{4m}\ F_1(\hat{\sigma}_a\ ,\ \hat{\upsilon}_x)\ F_0\left(\sigma_b\ ,\ \upsilon_y\right) \tag{I.9}$$

Now extending the previous case to the most general $\mathrm{TE}_{\mathrm{mn}}$ modes, the field distribution on aperture can be written as:

$$TE_{mn}\ \Rightarrow\ T(x\ ,y) =\ C\ \cos\left(\frac{m\pi}{a}x\right)\cos\left(\frac{n\pi}{b}y\right)\ \stackrel{\text{def}}{=}\ f_y^{(x)}(x) * f_y^{(y)}(y)$$

$$=$$

$$=\ \ C\ \cos\left(\frac{m\pi}{a}x\right)\cos\left(\frac{n\pi}{b}y\right)\left[\Pi\left(\frac{x}{a}\right)\Pi\left(\frac{y}{b}\right)\right] =$$

$$=\ \ C\ \cos\left(\frac{m\pi}{a}x\right)\cos\left(\frac{n\pi}{b}y\right)e^{-jk_z\frac{x^2}{2R_a}}\ e^{-jk_z\frac{y^2}{2R_b}} \tag{I.10}$$

Whose the radiation function can be derived as:

$$F_y(\ \theta\ ,\varphi\ )\ =\ \int_{-\infty}^{+\infty} f_y^{(x)}(x)\ e^{-jk_0\sin(\theta)\cos(\varphi)x}\ dx$$

$$* \int_{-\infty}^{+\infty} f_y^{(y)}(y)\ e^{-jk_0\sin(\theta)\sin(\varphi)y}\ \ dy \tag{I.11}$$

According to the previous paragraph, it can be obtained:

$$\begin{aligned} &F_y(\ \theta\ ,\varphi\ ) \\ &= \frac{ABC}{4m}\int_{-1}^{+1}\cos\left(\frac{m\hat{\xi}_a}{2}\right)\ e^{-j\left(\frac{\pi}{2}\right)\sigma_a^2\frac{\hat{\xi}_a^2}{m^2}}\ e^{-j\pi\upsilon_x\frac{\widehat{\xi_a}}{m}}\ d\hat{\xi}_a \\ &* \int_{-1}^{+1}\cos\left(\frac{n\pi\xi_b}{b}\right)e^{-j\left(\frac{\pi}{2}\right)\sigma_b^2\xi_b^2}\ e^{-j\pi\upsilon_y\xi_b}\ d\xi_b\ = \end{aligned} \tag{I.12}$$

By a variables position as follows: :

$$\begin{cases}\hat{\xi}_b =\ n\xi_b \\ d\hat{\xi}_b = nd\xi_b\end{cases} \tag{I.13}$$

Thus the radiation pattern is :

$$\begin{aligned} & F_y(\theta,\varphi) \\ & = \frac{ABC}{4mn}\int_{-1}^{+1}\cos\left(\frac{m\hat{\xi}_a}{2}\right) e^{-j\left(\frac{\pi}{2}\right)\sigma_a^2\frac{\hat{\xi}_a^2}{m^2}} e^{-j\pi\upsilon_x\frac{\hat{\xi}_a}{m}}\, d\hat{\xi}_a \\ & * \int_{-1}^{+1}\cos\left(\frac{m\hat{\xi}_b}{2}\right) e^{-j\left(\frac{\pi}{2}\right)\sigma_b^2\frac{\hat{\xi}_b^2}{n^2}} e^{-j\pi\upsilon_y\frac{\hat{\xi}_b}{n}}\, d\hat{\xi}_b = \end{aligned} \tag{I.14}$$

With the following position:

$$\begin{cases} \hat{\sigma}_b^2 = \dfrac{\sigma_b^2}{n^2} \\ \hat{\upsilon}_y = \dfrac{\upsilon_y}{n} \end{cases} \tag{I.15}$$

The known radiation pattern can be written as:

$$\begin{aligned} & F_y(\theta,\varphi) \\ & = \frac{ABC}{4mn}\int_{-1}^{+1}\cos\left(\frac{m\hat{\xi}_a}{2}\right) e^{-j\left(\frac{\pi}{2}\right)\sigma_a^2\frac{\hat{\xi}_a^2}{m^2}} e^{-j\pi\upsilon_x\frac{\hat{\xi}_a}{m}}\, d\hat{\xi}_a \\ & * \int_{-1}^{+1}\cos\left(\frac{m\hat{\xi}_b}{2}\right) e^{-j\left(\frac{\pi}{2}\right)\hat{\sigma}_b^2\hat{\xi}_b^2} e^{-j\pi\hat{\upsilon}_y\hat{\xi}_b}\, d\hat{\xi}_b = \end{aligned} \tag{I.16}$$

So accordingly to what has been evaluated for the Tm_0 modes we find :

$$F_y(\theta,\varphi) = \frac{ABC}{4mn}\; F_1(\hat{\sigma}_a\,,\,\hat{\upsilon}_x)\, F_1\left(\hat{\sigma}_b\,,\,\hat{\upsilon}_y\right) \tag{I.17}$$

The chosen radiation pattern for a Direct Radiating Array formed by a squared tapered horn can be assumed as a rectangular aperture radiation pattern with an uniform field excitation over the input port.

The one-dimensional field distribution of the a unitary length aperture can be easily express as in (2.1).

$$\prod(x) = \begin{cases} 1\ , & -1/2 < x < 1/2 \\ 0\ , & x < -1/2\ ;\ x > 1/2 \end{cases} \qquad \text{(I.18)}$$

from which we can derive the functional form of the uniform field distribution over a 2 dimensional aperture sustained by the TE_{10} (along y direction):

$$f_y(x,y) = f_y^{(x)}(x)\, f_y^{(y)}(y) \equiv \prod\left(\frac{x}{a}\right) \prod \qquad \text{(I.19)}$$

By Fourier transformation of the field distribution, the beam pattern related to the chosen field distribution can be derived as follows:

$$F_y(\theta,\varphi) = F_y^{(x)}(\theta,\varphi) * F_y^{(y)}(\theta,\varphi) =$$

$$= \int_{-\infty}^{+\infty} \Pi\left(\frac{x}{a}\right) e^{+jk_0(\sin(\theta)\cos(\varphi))x}\, dx$$

$$* \int_{-\infty}^{+\infty} \Pi\left(\frac{y}{b}\right) e^{+jk_0(\sin(\theta)\sin(\varphi))y}\, dy =$$

$$= \int_{-a/2}^{+a/2} e^{+jk_0(\sin(\theta)\cos(\varphi))x}\, dx * \int_{-b/2}^{+b/2} e^{+jk_0(\sin(\theta)\cos(\varphi))y}\, dy =$$

$$= \frac{e^{+jk_0(\sin(\theta)\cos(\varphi))x}}{jk_0(\sin(\theta)\cos(\varphi))x}\Bigg|_{-a/2}^{+a/2} \qquad \text{(I.20)}$$

$$* \frac{e^{+jk_0(\sin(\theta)\sin(\varphi))y}}{jk_0(\sin(\theta)\sin(\varphi))}\Bigg|_{-b/2}^{+b/2}$$

Which can be easily modified, as follows in order to reduce it to and easier mathematical expression:

$$F_y(\theta,\varphi) = \left(\frac{2}{2}\right)\frac{1}{jk_0(\sin(\theta)\cos(\varphi))}\frac{\left(a/2\right)}{\left(a/2\right)} * \left(e^{+jk_0(\sin(\theta)\cos(\varphi))\frac{a}{2}} - e^{-jk_0(\sin(\theta)\cos(\varphi))\frac{a}{2}}\right) *$$

$$\left(\frac{2}{2}\right)\frac{1}{jk_0(\sin(\theta)\sin(\varphi))}\frac{\left(b/2\right)}{\left(b/2\right)} * \left(e^{+jk_0(\sin(\theta)\sin(\varphi))\frac{b}{2}} - e^{-jk_0(\sin(\theta)\sin(\varphi))\frac{b}{2}}\right) =$$

$$= 4 * ab * \frac{\sin(k_0(\sin(\theta)\cos(\varphi))\frac{a}{2}}{k_0(\sin(\theta)\cos(\varphi))\frac{a}{2}} * \frac{\sin(k_0(\sin(\theta)\sin(\varphi))\frac{b}{2}}{k_0(\sin(\theta)\sin(\varphi))\frac{b}{2}} = \qquad \text{(I.21)}$$

Starting from (2.4) we can easily express the beam pattern by the means of the radiation variables $\boldsymbol{u}$ and $\boldsymbol{v}$ according to the (2.5).

$$F_y(\theta,\varphi) = 4 * ab * \frac{\sin(u)}{(u)} * \frac{\sin(v)}{(v)} \qquad \text{(I.22)}$$

$$= ab * sinc(u) * sinc(v)$$

For a DRA antenna configuration, the square shape and the aperture illumination is taken as uniform in order to maximize the beam directivity and thus the beam analytical form of the I.26 by adding the reference efficiency of the antenna.

I.7.2 Circular Aperture Radiation Pattern

Following the same approach, can be easily derived the beam pattern as generated by a circular aperture antenna with an uniform field distribution along the y- direction (TE_{11} mode). The reference geometry is shown in Fig. I-30

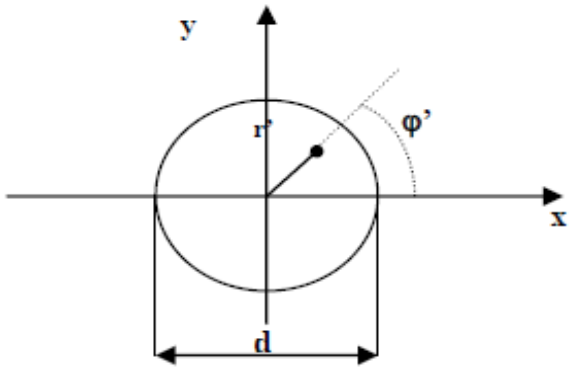

Fig. I-30 : Circular Aperture reference geometry.

The beam pattern, as generate by the y -direction TE_{11} mode can be expressed as:

$$F(\theta,\varphi) = \int_A f(x', y')\, e^{jk_0 \sin(\theta)(x'\cos(\varphi)+ y'\sin(\varphi))}\, dx'\, dy' =$$

$$= \int_{-d/2}^{+d/2} \int_0^{2\pi} f(r', \varphi')\, e^{jk_0 r' \sin(\theta)(\cos(\varphi')\cos(\varphi)+ \sin(\varphi')\sin(\varphi))}\, r' dx'\, d \qquad \text{(I.23)}$$

With the variable changing described as follows:

$$\begin{cases} x' = r' \cos(\varphi') \\ y' = r' \sin(\varphi') \end{cases} \tag{I.24}$$

According to the transformation described in (2.7), the (2.6) results :

$$F(\theta, \varphi) = \left(\frac{d}{2}\right)^2 \int_0^1 \int_0^{2\pi} f(\rho', \varphi') \, e^{j\frac{\pi d}{\lambda}\varphi' \sin\theta \cos(\varphi - \varphi')} \, \rho' \, d\rho' \, d\varphi' \tag{I.25}$$

Where introducing the radial symmetry of the field distribution and the radiation variable u, defined as follows:

$$\begin{cases} u = \left(\frac{\pi d}{\lambda}\right) \sin\theta \\ \rho' = \left(\frac{2r'}{d}\right) \Rightarrow r' = \left(\frac{d\rho'}{2}\right) \end{cases} \tag{I.26}$$

It turns out that the problem will be dependent only on the φ variable:

$$F(\theta, \varphi) = \left(\frac{d}{2}\right)^2 \int_0^1 \int_0^{2\pi} f(\rho') \, e^{ju\varphi' \cos(\varphi - \varphi')} \, \rho' \, d\rho' \, d\varphi' \tag{I.27}$$

Where the integral form in the ρ' differential is defined as :

$$\int_0^{2\pi} e^{ju\varphi' \cos(\varphi - \varphi')}\, d\rho' \ \stackrel{\text{def}}{=}\ 2\pi J_0(u\rho') \tag{I.28}$$

Which is the Bessel function of first kind and first order. Now by extending the integration domain to $+\infty$, the beam formula turns out to be:

$$F(\theta) = F(u) = 2\pi * \left(\frac{d}{2}\right)^2 \int_0^{\infty} f(\rho') J_0(u\rho')\rho' d\rho' \tag{I.29}$$

Which is named *Hankel Transform*.

It is worth noting that the rectangular aperture radiation pattern is the Fourier transform in the spatial domain of the aperture field distribution. As far as Circular Aperture concerns, it stands a similar relation between the radiation pattern and the field distribution which are related by the Hankel Transform. Thus it can be expressed the radiation pattern of circular aperture by the (2.13) where $H\{*\}$ represents the symbolic operator of the Hankel transform.

$$\frac{F(u)}{2\pi\left(\frac{d}{2}\right)^2} = H\{f(\rho')\} \tag{I.30}$$

Since in the uniform case, the field distribution can be written as $f(\rho') = 1$ per $0 \le \rho' \le 1$. It is worth noting that the Hankel transform of a constant is the $besinc(u)$ function, as defined below:

$$H\{f(\rho')\} = besinc(u) = \frac{J_1(u)}{u} \tag{I.31}$$

Where J_1 is the Bessel function of first kind and first order.

For completeness, the third studied analytical model is always related to a circular aperture with a tapered field distribution. The amplitude tapering for side lobe reduction reduces the spatial efficiency (or

aperture efficiency) of the antenna. Along with the reduction of peak directivity, amplitude tapering also results in a broadening of the main beam. While reduced side, lobes are usually desirable, reduced peak directivity is usually not, therefore a correct understanding of the aperture efficiency is a valuable design too

For a general aperture antenna, we can define the tapering parameter t which is the ration between the amplitude of the feeding field at the border of the aperture w.r.t. the feeding field at the aperture centre. Thus, for a circular aperture with diameter a, we can define the taper parameter as:

$$t = \frac{\left|E\left(\frac{a}{2}\right)\right|}{E(0)} \tag{I.32}$$

A taper parameter is as high as it approaches to one. It means that the higher taper parameter we define the similar filed distribution we have between the aperture border s and its center. When $t \to 1$, it can be experienced higher side lobe level but we experience even higher gain.

Different tapering function may be chosen. Among them we can cite the following ones:

- *Raised Cosine tapering*: A cosine function increased by a constant rate:

$$f = t + (1 - t)\cos\left(\frac{\pi}{a}x\right) \tag{I.33}$$

In this function the order of the cosine may be changed to increase the tapering. ;

- *Hamming Tapering*: it represents a particular case of the raised cosine tapering:

- $$f = t + (1-t)\cos^2\left(\frac{\pi}{a}x\right) \qquad \text{(I.34)}$$

- *Raised parabolic tapering*: this kind of tapering is particularly suitable for circular aperture :

$$i(r) = t + (1-t)\,(1-r^2)^p \qquad \text{(I.35)}$$

This kind of function offers even a very good advantage for the evaluation of the tapering itself due to the fact that an integral transform of such function can be achieved by developing the first kin d Bessel function of order one as a power series.

Thus, the radiation pattern related to the Raised parabolic tapering can be expressed as follows:

$$F(\theta,\varphi) = \int_{-\infty}^{+\infty}\int_{-\infty}^{+\infty} T + (1-T)(1-r^2)^p\, e^{jk_0(\sin(\theta)\cos(\varphi)+\sin(\theta)\sin(\varphi))}\,dx\,dy \qquad \text{(I.36)}$$

Which can be specialized, in the case of a circular aperture fo diameter $\boldsymbol{d}$ as follows:

$$2\pi\left(\frac{d}{2}\right)^2\int_0^{+\infty} f(\rho')J_0(u\rho')\rho'\,d\rho'$$

$$= 2\pi\left(\frac{d}{2}\right)^2\int_0^R [T + (1-T)(1-r^2)^p]J_0(u\rho')\rho'\,d\rho' =$$

$$= 2\pi r^2 * \left[\int_0^R TJ_0(u\rho')\rho'\,d\rho' + \int_0^R (1-T)(1-r^2)^p J_0(u\rho')\rho'\,d\rho'\right] =$$

$$= 2\pi r^2 * \left[T\int_0^R J_0(u\rho')\rho'\,d\rho' + (1-T)\int_0^R (1-r^2)^p J_0(u\rho')\rho'\,d\rho'\right] =$$

$$= 2\pi r^2 * \frac{TJ_1(u)}{u} + r^2\int_0^1\int_0^{2\pi}(1-T)\left[1-r^2\rho'^2\right]^p e^{+ju\rho'\cos(\varphi-\varphi')}\,\rho'\,d\rho'\,d\varphi' =$$

$$= 2\pi r^2 * \frac{TJ_1(u)}{u} + r^2(1-T)\int_0^1\int_0^{2\pi}\left[1 - r^2\rho'^2\right]^p e^{+ju\rho'\cos(\varphi-\varphi')}\,\rho'\,d\rho'\,d\varphi' =$$

$$= 2\pi r^2 * \frac{TJ_1(u)}{u} + 2\pi r^2(1-T)\int_0^1\left[1 - r^2\rho'^2\right]^p J_0(u\rho')\,d\rho' =$$

$$= 2\pi r^2 * \frac{TJ_1(u)}{u} + 2\pi r^2(1-T)\pi 2^p p!\,\frac{J_{p+1}(u)}{u^{p+1}} \qquad \text{(I.37)}$$

This results derives directly from the properties of the Fourier-Bessel Transform for the function $i(r)$:

$$F(u) = 2\pi a^2 \int_0^1 i(r)\,J_0(ur)\,r\,dr = \pi a^2\,\frac{2^{p+1}\,p!\;J_{p+1}(u)}{u^{p+1}} \qquad \text{(I.38)}$$

It is worth noting that increasing the value of p, taper increases and the distance on u-axis between the zeros crossing of the function increases as well.

The same result can be obtained by Hankel Transform of the field over the aperture. Starting from a generic function f(r), the Hankel transform will have analytical form as follows:

$$F(u) = \int_0^1 f(r)\,J_0(ur)\,r\,dr \qquad \text{(I.39)}$$

By changing the variable according to the one used in the parabolic taper function, we obtain:

$$r \rightarrow x = 1 - r^2 \qquad \text{(I.40)}$$

By developing in Taylor Series the above-mentioned function:

$$f(x) \rightarrow f(r) \sim \sum_{n=0}^{N} a_n (1 - r^2)^n \tag{I.41}$$

And by Hankel transform the (I.28):

$$F(u) = \int_0^1 \sum_{n=0}^{N} a_n (1 - r^2)^n J_0(ur)\, r \, (\tag{I.42}$$

Now by inverting the integral form with the summation:

$$\sum_{n=0}^{N} a_n \int_0^1 (1 - r^2)^n J_0(ur)\, r\, dr \tag{I.43}$$

The I.30 is analytically similar to the field form of the pattern function of the circular aperture radiation that has been derived in the previous paragraph in the case of uniform feeding.

By analysing the I.24, considering the taper $T = 1 - A$ the formula form the radiated pattern can be easily derived as:

$$= \pi r^2 (1 - A) \left[\frac{2J_1(u)}{u}\right] + \pi r^2 A \left[2^{p+1} p! \frac{J_{p+1}(u)}{u^{p+1}}\right] =$$

$$= \pi r^2 \left[(1 - A) 2 \frac{J_1(u)}{u} + A 2^{p+1} p! \frac{J_{p+1}(u)}{u^{p+1}}\right] =$$

$$= \pi r^2 (1 - A) \left[\frac{2J_1(u)}{u} + \frac{A}{(1 - A)} 2^{p+1} p! \frac{J_{p+1}(u)}{u^{p+1}}\right] \tag{I.44}$$

The I.31 represents the mathematical function of the radiation pattern of the single beam radiated pattern from a multibeam antenna, focused by a reflector fed by circular horn.

So the analytic beam model corresponding to this illumination is:

$$F(u,v) = \pi r^2(1-A)\left[\frac{2J_1(u)}{u} + \frac{A}{(1-A)}2^{p+1}p!\frac{J_{p+1}(u)}{u^{p+1}}\right]$$

I.7.3 Reference Planar Phased Array

In order to acquire a clear understanding of the effectiveness of the nulling performance of the antenna, different planar array configuration are taken into account. The DRA technology is compared with the MBA configuration to define the optimum radiating aperture based on realistic antenna able to satisfy the requirement and minimizing the H/W complexity.

Taking into account an array of element distributed along the z-axis as reported in the following figure.

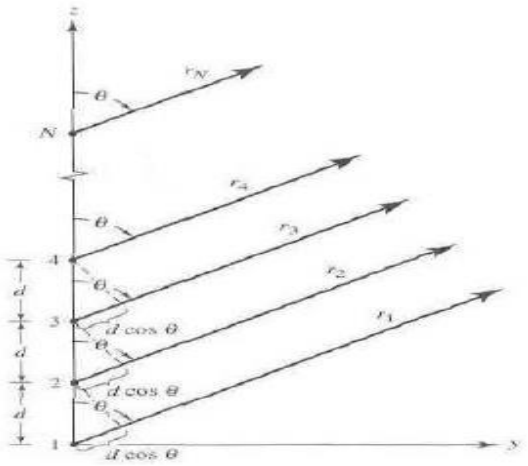

Fig. I-31 : Linear Array Example

Then the transverse electric field radiated by a single element can be written as:

$$E = \frac{j\eta kI\Delta l}{4\pi r}\, e^{-jkr}\, \sin(\theta)\, \hat{\theta} \tag{I.45}$$

So the total radiated field by N homogenous elements, by supposing no significant couplings between elements can be written as the vector sum of the radiated field of the elements:

$$E_{TOT} = E_1 + E_2 + \cdots E_N \tag{I.46}$$

If the feeding amplitude and phase is the same among all the elements and the feeding phase is equal to β then the total field is:

$$\begin{aligned} E_{TOT} = \frac{j\eta kI\Delta l}{4\pi r}\, e^{-jkr} \big(1 &+ e^{j(kd_i \cos(\theta) + \beta_i)} \\ &+ e^{j2(kd_i \cos(\theta) + \beta_i)} + \cdots \\ &+ e^{j(N-2)(kd_i \cos(\theta) + \beta_i)} \\ &+ e^{j(N-1)(kd_i \cos(\theta) + \beta_i)}\big)\, \sin(\theta)\hat{\theta} \end{aligned} \tag{I.47}$$

Where $kd_i\, cos(\vartheta)$ is the phase variation between adjacent elements due to geometrical variation and β_i stands for the constant phase variation due to excitation.

It is worth noting that the electric field as reported in equation I.51 can be seen as the signal element pattern multiplied by an Array Factor which depends only by the geometrical distribution of the element.

$$E_{TOT} = E_{Single\ Element} * AF \tag{I.48}$$

Array Factor (AF) can be easily evaluated as:

$$AF = 1 + e^{j(kd_i\cos(\theta)+\beta_i)} + e^{j2(kd_i\cos(\theta)+\beta_i)} + \cdots + e^{j(N-1)(kd_i\cos(\theta)+\beta_i)} =$$

$$= \sum_{1}^{N} e^{j(n-1)(kd_i\cos(\theta)+\beta_i)} = \sum_{1}^{N} e^{j(N-1)(\psi_i+\beta_i)} \tag{I.49}$$

By defining $\psi = kd_i\cos(\theta)$, it can be obtained:

$$AF = \sum_{0}^{N-1} e^{ji\psi_i} = \frac{1 - e^{jN\psi_i}}{1 - e^{j\psi_i}} \Rightarrow \frac{1 - e^{jN\psi_i}}{1 - e^{j\psi_i}} = \frac{e^{j\frac{N}{2}\psi_i} - e^{-j\frac{N}{2}\psi_i}}{e^{j\psi_i} - e^{-j\psi_i}} * e^{j\left(\frac{N-1}{2}\right)\psi_i} =$$

$$= \frac{\sin\left(\frac{N}{2}\psi_i\right)}{\sin\left(\frac{\psi_i}{2}\right)} * e^{j\left(\frac{N-1}{2}\right)\psi_i} \tag{I.50}$$

Which can be written as:

$$AF = \frac{\sin\left(\frac{N}{2}\psi_i\right)}{\sin\left(\frac{\psi_i}{2}\right)} \tag{I.51}$$

It is worth noting that the maximum of (I.51) can be obtained with $\psi=0$ and it is equal to N. So, it can be obtained the normalized array facto as:

$$(AF)_n = \frac{1}{N} \frac{\sin\left(\frac{N}{2}\psi_i\right)}{\sin\left(\frac{\psi_i}{2}\right)} \tag{I.52}$$

Nulls of the (I.52) are carried out when:

$$\sin\left(\frac{N}{2}\psi_i\right) = 0 \quad \mapsto \quad \frac{N}{2}\psi_i = \pm\, n\pi \qquad \begin{cases} n = 1\,,2\,,3\,,\ldots\ldots \\ n \neq N\,,2N\,,\ldots\ldots \end{cases} \tag{I.53}$$

These values are defined as follows:

$$\theta_n = \cos^{-1}\left[\frac{\lambda_i}{2\pi d_i}\left(-\beta_i \pm \frac{2n}{N}\,\pi\right)\right] \qquad \begin{cases} n = 1\,,2\,,3\,,\ldots\ldots \\ n \neq N\,,2N\,,\ldots\ldots \end{cases} \tag{I.54}$$

The model that will be employed for the scope of the analyses reported in this document are related to the extension of this concept to a planar element distribution.

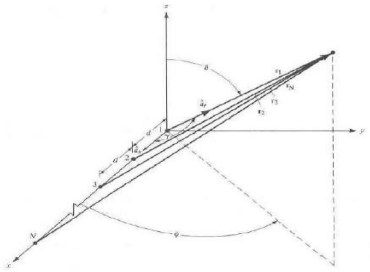

Fig. I-32 : Distribution along x -axis

Array factor for an element distribution along x axis is :

$$AF = \sum_{1}^{N} I_n \; e^{j(n-1)(kd_{xi}\cos(\gamma) + \beta_{xi}) + \xi_{xi}} \tag{I.55}$$

where I_n is the n-element excitation coefficient and d_x and β_x represents geometrical shift and e phase shift between adjacent element respectively.

Since $cos(\gamma)$ can be expressed as the dot product between $\hat{x}$ e $\hat{r}$:

$$\cos(\gamma) = \hat{x} * \hat{r}$$
$$= \hat{x} * (\sin(\theta)\cos(\phi)\hat{x} + \sin(\theta)\sin(\phi)\hat{y} + \cos(\theta)\hat{z}) =$$
$$= \sin(\theta)\cos(\phi) \tag{I.56}$$

Than (I.55) turn out to:

$$\sum_{1}^{N} I_n \; e^{j(n-1)(kd_{xi}\sin(\theta)\cos(\phi)+\beta_{xi})+\xi_{xi}} \tag{I.57}$$

Thus for an M elements array, which are elements of a N array spaced d_y along y-axis with a phase shift of βy a rectangular planar array can be built as in Fig. I-33:

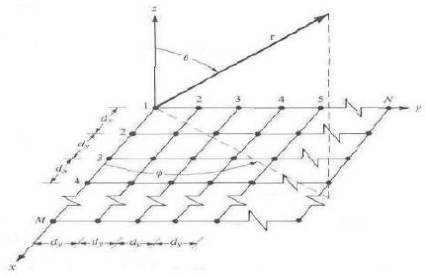

Fig. I-33 : Array composto da MxN elementi

The whole array factor can be expressed as:

$$AF = \sum_{1}^{N} I_{1n} \left[\sum_{1}^{M} I_{1m} \, e^{j(m-1)(kd_{xi}\sin(\theta)\cos(\phi)+\beta_{xi})+\xi_{xi}} \right] e^{j(n-1)\left(kd_{yi}\sin(\theta)\cos(\phi)+\beta_{yi}\right)+\xi_{yi}}$$
$$=$$
$$= S_{xm} * S_{yn} \tag{I.58}$$

Where:

$$\begin{cases} S_{xm} = \sum_{1}^{M} I_{1m}\ e^{j(m-1)(kd_{xi}\sin(\theta)\cos(\phi)+\beta_{xi})+} \\ S_{ym} = \sum_{1}^{N} I_{1n}\ e^{j(n-1)(kd_{yi}\sin(\theta)\cos(\phi)+\beta_{yi})+} \end{cases} \quad \text{(I.59)}$$

If the array elements are uniformly excited :

$$I_{mn} = I_0 \quad , \quad m = 0\,,1\,,2\,,\dots M \quad , \quad n = 0\,,1\,,2\,,\dots N \quad \text{(I.60)}$$

Thus the array factor expression is:

$$AF = I_0 \sum_{m=1}^{M} e^{j(m-1)(kd_{xi}\sin(\theta)\cos(\phi)+\beta_{xi})+\xi_{xi}} \sum_{n=1}^{N} e^{j(n-1)(kd_{yi}\sin(\theta)\sin(\phi)+\beta_{yi})+\xi_{yi}} \quad \text{(I.61)}$$

For which the normalized expression is:

$$AF_n(\theta\,,\phi\,) = \left\{\frac{1}{M}\,\frac{\sin\left(\frac{M}{2}\psi_{xi}\right)}{\sin\left(\frac{\psi_{xi}}{2}\right)}\right\}\left\{\frac{1}{N}\,\frac{\sin\left(\frac{N}{2}\psi_{yi}\right)}{\sin\left(\frac{\psi_{yi}}{2}\right)}\right\} \quad \text{(I.62)}$$

where:

$$\begin{cases} \psi_{xi} = (kd_{xi}\sin(\theta)\cos(\phi) + \beta_{xi}) + \xi_{xi} \\ \psi_{yi} = \left(kd_{yi}\sin(\theta)\sin(\phi) + \beta_{yi}\right) + \xi_{yi} \end{cases} \quad \text{(I.63)}$$

In the case of rectangular array distribution, the maximum of the array factor:

$$\begin{cases} \psi_{xi} = (kd_{xi}\sin(\theta)\cos(\phi)) = \pm 2m\pi & , \quad m = 0, 1, 2 \\ \psi_{yi} = (kd_{yi}\sin(\theta)\sin(\phi)) = \pm 2n\pi & , \quad n = 0, 1, 2 \end{cases} \quad \text{(I.64)}$$

I.7.4 Reference Satellite Antenna System Description and Definition

As reported in I.6.1 the most effective way to fight the interference at antenna level is represented by a beam-shaping approach [R. 67]. A very effective way to remotely and adaptively control the shape of the satellite coverage on earth is represented by active antenna systems. Such systems can be tuned to implement different kind of shaped footprints on ground accordingly with some specific law, chosen by satellite operator. More precisely, a Phased Array Antenna is an antenna system which can create the desired coverage by creating several simultaneous spot beams. Those beams can be combined pursuing mainly two kind of objectives: generating wider and more complex composite beams or producing different nulls in the gain pattern toward direction of arrivals of interfering signals.

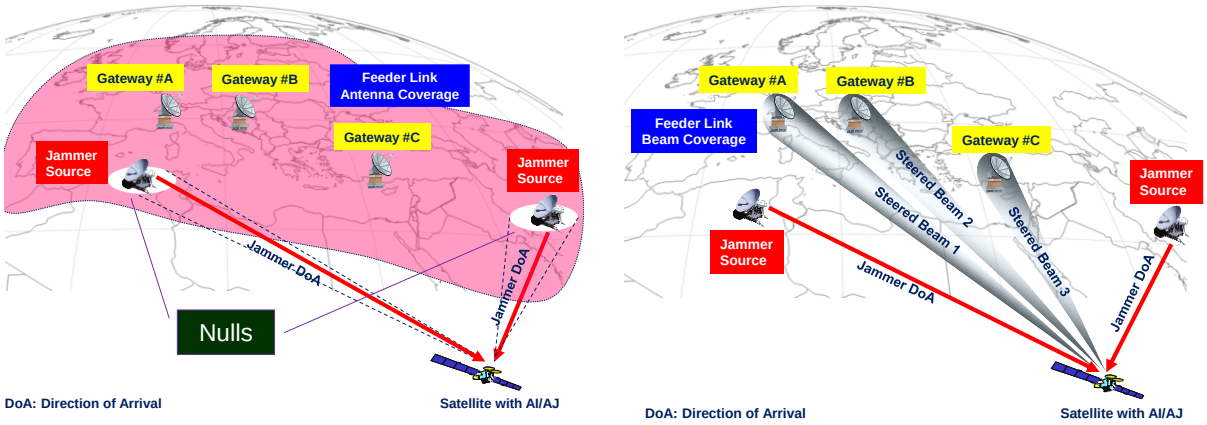

Fig. I-34 : Nulling and Ground Station beam Techniques [R. 44]

As far as satellite system antenna concerns, the reference Antenna radiation aperture choice for implementation of a phased array lead typically to two different concurring technologies. The two basic solutions for the antenna optics are: Direct Radiating Array (DRA) or Multi-beam antenna (MBA).

From the qualitative point of view, once fixed the aperture, the main difference is that the DRA requires a high number of feeds to fully sample the aperture. The MBA has a reduced number of feeds, magnified by an optical device (reflector). These two technologies have been examined by the point of view of their capacities of nulling depending on the equivalent antenna aperture and on the number of the necessary elements and spacing. For a, given antenna dimension, a first discriminator has been the antenna flexibility and resolution Vs. nulling and a second discriminator has been the antenna spectral resolution to the interference source and users locations. Once the antenna family have been selected many parameters affecting the antenna nulling capability like the antenna nulling resolution Vs user-interference source relative positions and number can be investigated. Regarding the DOA, the main difference between the two solutions is that with the DRA solution any signal arriving from a direction (θ, ϕ), has relative phase on each feed which is function of the direction of arrival (θ, ϕ). The use of an MBA implies, on the contrary, that the relative phase of the signal onto each feed is not function of the direction of arrival (θ, ϕ). As described in the evaluation of the best radiating aperture of the Antenna Nulling the model of the two antennas is properly constructed as described in the following paragraph.

As far as *MBA* concerns, a suitable model turns out to be an array of circular aperture horn element in which the field distribution on the aperture can be describe in accordance with:

$$F(r) = b + (1-b)\left[1 - \left(\frac{2r}{D}\right)^2\right]^P \tag{I.65}$$

Where D is antenna reflector diameter and the tapering parameter p and b are chosen in order to maximize antenna efficiency and evaluated as:

$$\begin{cases} P = 1 \\ b = 0.335 \end{cases} \tag{I.66}$$

These assumption lead to an analytic beam formula of :

$$B(u,v) = \sqrt{\eta}\frac{\pi D}{\lambda}\left[b\frac{2J_1(\rho)}{\rho} + (1-b)\frac{2J_2(\rho)}{\rho^2}\right] \tag{I.67}$$

Where the radiation variables are:

$$\begin{cases} u = \dfrac{\pi D}{\lambda}\sin(\theta)\cos(\phi) \\ v = \dfrac{\pi D}{\lambda}\sin(\theta)\sin(\phi) \\ \rho = \sqrt{u^2 + v^2} \end{cases} \tag{I.68}$$

As far as the DRA benchmark reference architecture, a planar array of squared tapered horn has been selected. The analytical formulation is similar to the one described in §I.7.1 by imposing both dimension the same. Thus, for the squared horn element, the field distribution on the aperture can be describe in accordance with:

$$F(r) = \left(\prod\nolimits_D(x)\prod\nolimits_D(y)\right) \tag{I.69}$$

Where D is the horn side and the feeding is uniform for both the side of the horn aperture.

These assumption lead to an analytic beam formula of:

$$B(u,v) = \sqrt{\eta 4\pi \left(\frac{D}{\lambda}\right)^2}\,\frac{\sin u}{u}\,\frac{\sin v}{v} \tag{I.70}$$

Where the radiation variables are:

$$\begin{cases} u = \dfrac{\pi D}{\lambda}\,\sin(\theta)\cos(\phi) \\ v = \dfrac{\pi D}{\lambda}\,\sin(\theta)\sin(\phi) \end{cases} \tag{I.71}$$

In order to assess the benchmark for satellite coverage that shall be achieved with the selected antenna, taking as reference the service area described in I.2, the target earth coverage to be implemented is the one called EU+MENA (European Union + Middle East + Northern Africa). The antenna is supposed to be mounted on a GEO Satellite system at 13 ° East.To cover the abovementioned area from the geostationary arch, an antenna field of view of [-3.5 °, 3.5 °] is requested.

Taking as reference a standard satellite DVB-S2 standard link budget, which is the communication standard currently implemented in most communication satellite systems, it can be derived the following parameters for the Satellite Receiving antenna.

A typical G/T value of 4 dB/ ° K can be achieved with a reference satellite antenna working at 13.75 GHz with equivalent noise temperature of 250 ° K, by a 27 dBi Antenna Receiving Gain. This Gain value, according to the performed link budget analyses can grant a Carrier-To-Noise Ratio (C/N) in rain condition with a positive margin of almost 5 dB. This value can grant the correct use of a typical 36 MHz satellite transponder Channel for a DVB-S2 QPSK (3/4) waveform with a Quasi-Error Free Condition (BER=10^{-7}).

A preliminary antenna loss budget can be made to estimate the target directivity to be requested by the antenna system in accordance to the following table:

	Losses Budget MBA [dB]	Losses Budget DRA [dB]
Reflector Losses (CFRP)	0.05	0.0
Feed+Polarized Loss	0.1	0.1
Waveguide losses	0.2	0.2
Front-end filter Loss	0.4	0.4
Implementation losses	0.5	0.5
Total Loss:	1.15 dB	1.10 dB

Tab. I-4 Typical Loss budget for both reference cases

For DRA, no Carbon fibre reinforced polymer made reflector losses has been considered due to the fact that any reflector in employed to magnifies the beam,

For both the technology, the antenna system block scheme can be reported as follows.

The reference mission scenario of interest is represented by a commercial standard satellite systems at geo-synchronous altitude operating over the earth field, designed to provide Broadcast Satellite Services with 24 transponders. We supposed to have M + N transmitting stations within the uplink coverage. The ground stations are parted in two different sub-sets: N interfering stations J_n located in (θ_{nJ} ; ϕ_{nJ}) and M authorized users Am located in (θ_{mA} ; ϕ_{mA}), where every station has been geo-located accordingly to elevation and azimuth angles, by which it is viewed by the satellite antenna. Two specific operative laws are considered: a regional coverage mode, in which one

aims to null the N interfering sources while realizing the best possible earth coverage communications link over the remaining earth field of view and a gateway beam mode, where one desires only to maximize the signal to M authorized users while nulling the N interfering sources.

We assume that the nulling algorithm, in both operational modes, will be implemented in the "beam space" domain instead of the "element"(or excitation) space domain. The purpose of this assumption is to present, without loss of generality, the different performance achievable by an ideal radiating aperture able to generate an proper number of element beams, consistent with the assigned aperture, independently by the number of radiating elements necessary to build the ideal analytic beams and independently by the type of optics.

The analytic beams have been considered generated by a radiating aperture optimally illuminated for maximum antenna efficiency and considered aberration free.

The general statement of the problem is explained with the aid of the following figure

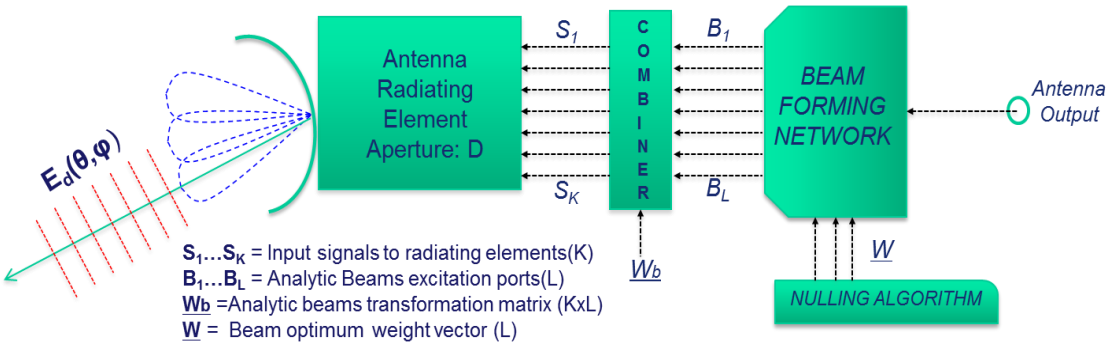

Fig. I-35 :: Multiple Beam Antenna system block diagram

The antenna input (output) vectors $[S_1 \ldots S_K]$ lies in the K-dimensional "element-space", the vectors of analytic beams outputs $[B_1 \ldots B_L]$ lies in the L-dimensional "beam-space". The K x L beam matrix $[W_b]$, maps the "element-space" into the "beam-space". In this configuration, the nulling algorithm works in the "beam-space"

generating the beam optimum weight vector W (L-elements). From the beam excitation coefficients, the element excitations can be computed using the transformation matrix.

The L analytic beams are generated combining the K electrical antenna ports as follows:

$$B_i(\theta,\varphi) = \sum_{j=1}^{K} W_{b(i,j)} S_j(\theta,\varphi) \quad i = 1 \dots M \tag{I.72}$$

Where $S_j(\theta, \varphi)$ is the radiation pattern of the single radiating element.

The antenna output in terms of angular coordinates (θ,ϕ) will be:

$$E(\theta,\varphi) = \mu * \sum_{i=1}^{L} W_i B_i(\theta,\varphi) \tag{I.73}$$

Where μ is a suitable pattern normalization factor.

In order to mitigate the effects of interfering sources in communication link operating at the same frequency, the system is to have the capability of nulling any desired direction over the field of view. The optimum nulling technique for forming N nulls in a desired radiation pattern is to point N maximum directivity beams in the N directions to be spatially filtered and appropriately weight these beams with the physical realization of the desired pattern. The procedure to determine the functional form of the maximum directivity beams $B_{max}(\theta,\varphi)$ that can be shaped by a given aperture directly descend by the Floquet expansion over the region of coverage of the aperture distribution corresponding to the principal polarization of interest.

Under such hypothesis, the radiation pattern $\mathrm{E}_d(\theta,\varphi)$ can be expressed in terms of normalized transform variables:

$$u = \frac{k_0 D}{2} sin\theta \cos\varphi \text{ and } v = \frac{k_0 D}{2} sin\theta \sin\varphi.$$

The target radiation pattern of the nulling configuration of shaped regional coverage can be expressed as:

$$\begin{aligned} &\mathrm{E}_{nd}(\theta,\varphi) \\ &= \sum_{\mathrm{k}=-\infty}^{+\infty} \sum_{l=-\infty}^{+\infty} \left\{ \iint_{u^2+v^2 \le (4\pi A/\lambda^2) sin^2(8.7^\circ)} \psi_{k,l}(u,v)\,du\,dv \right\} \psi_{k,l}(u,v) \\ &- \frac{\lambda_n}{2} \sum_{\mathrm{n}=1}^{N} B_{max}\left(\theta - \theta_{\mathrm{n}J}, \varphi - \varphi_{\mathrm{n}J}\right) \end{aligned} \tag{I.74}$$

Where the $\psi_{k,l}(u,v)$ functions are the Schmidt ortho-normalized set of basis functions deduced by the beam space basis function.

In the formula, the set of values λ_n, with n=1,…,N, are the coefficient needed to operate the linear combination between the desired coverage and the desired nulling beams. Those coefficients can be derived by constrained maximization of the $\mathrm{E}_{nd}(\theta,\varphi)$ and, more precisely, they represent the Lagrange multipliers of the above-mentioned maximization process. The above described optimum procedure to generate nulls is basically based on the generation of a maximum directivity beam in the direction of each null to be formed, appropriately weighted and subtracted from the desired radiation pattern.

I.8 Analyses and Results

In this chapter are reported the fundamental analyses and results achieved during this work.

To compare and evaluate the different proposed solution in terms of Antenna sub-system (DRA vs MBA) a complex tool of simulation has been developed. This tool takes into account the two different antenna

technologies and emulate the reference scenario as described in 0 for a Ku-Band satellite payload. The intended signal is supposed to be a DVB-S2 waveform for a full transponder bandwidth of 36 MHz.

The User location is supposed to be a priori known. For the purpose of the study, since no interference sources can affects the Transmit antenna, only the receiving Antenna of the satellite is simulated. All the jammer and interference sources as described in I.5.1 are evaluated by the simulation but since the supposed antenna implements a spatial filtering only based on the direction of arrival (DoA) of the interferer, a barrage jamming can be employed for analyses without loss of generality.

As reference Ground segment feeder station, has been adopted the general location of one of the major Satellite operator, reported in the following table.

	Longitude	Latitude
London	-0.13	51.51
Rambouillet	1.78	48.55
Frankfurt	8.68	50.10
Athens	23.73	38.00
Warsaw	21.00	52.25
Fucino	13.60	41.98
Makarios	33.37	35.14

Tab. I-5: Reference Ground Station [R. 58, R. 59]

According to the reference scenario the system evaluation has been taken into account for a standard 36 MHz Transponder, centred around fc=13.9 GHz linked with a space segment satellite infrastructure located at GEO arch 13 ° E with a beam Pointing Error of 0.05 °, a reference G/T equal to 4 dB/K and a reference Ground Station transmission EIRP= 70 dBW.

Within the reference EU27+MENA coverage as reported in Fig. I-36.

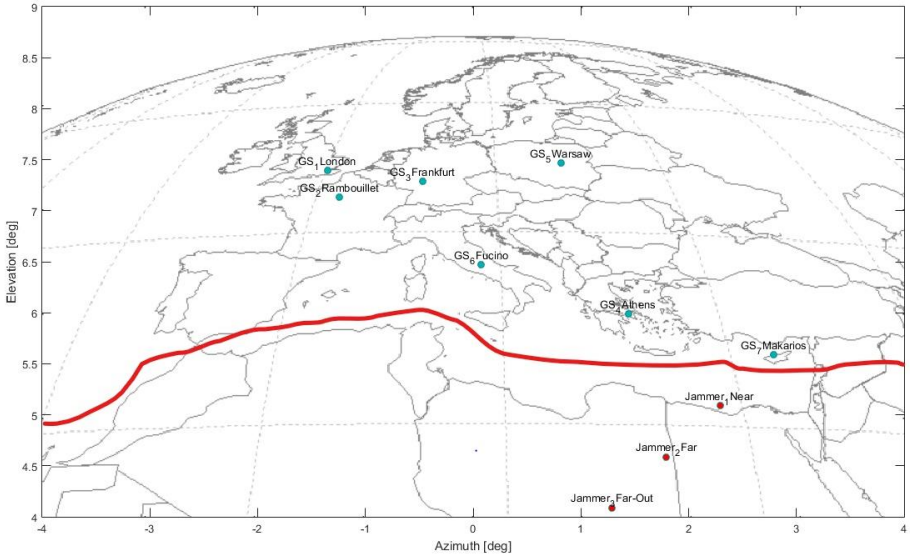

Fig. I-36 : Reference Scenario coverage

In Fig. I-36 the reference scenario is reported. The green spots represent the authorised ground station, which can forward signals towards satellite space segment. The red spots represent the typical jammer location, parted on the basis of their distance w.r.t. the intended ground station (in this case, Makarios Station). Red line represents the line below which is most likely interference sources were located in.

In the first two paragraph, will be presented the reference antenna performance in the so-called:" cold condition", i.e. when the nulling function is not activated because no interferer is active. In the following paragraphs, different operative scenario is presented with the antenna nulling activated.

I.8.1 Reference Benchmark – MBA Configuration

As far as the MBA configuration concerns, in the first place the number of element must be evaluated. Different analyses have been performed to estimate an effective aperture diameter and peak directivity for each beam, taking into account the beam spacing θ_s and the triple cross-over point over the adjacent beam [R. 28]. The reference architecture will provide a 16 beams configuration displaced on a rectangular lattice with a 32 λ parabolic reflector. This leads to a single beam, with a 3 dB beam width of $\theta_{3dB} = 1.7^\circ$ and a typical Triple Cross over Point of -4.4 dB w.r.t. peak beam directivity of 39.76 dBi [R. 36].

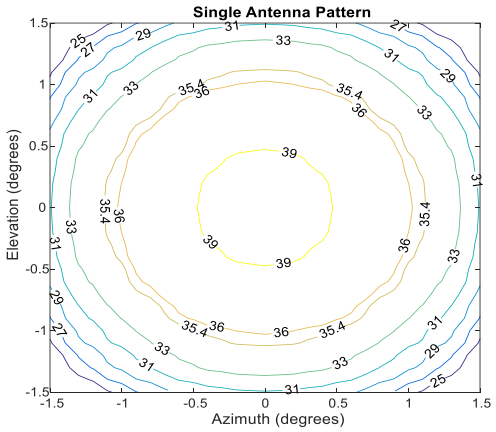

Fig. I-37 : Single beam Footprint with contour directivity level [dBi].

The single beam radiation pattern is reported in the following figure.

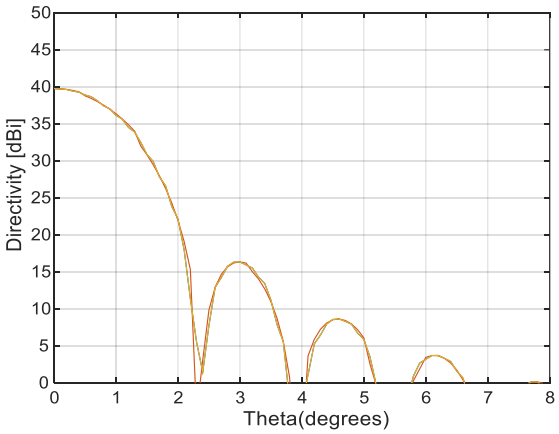

Fig. I-38 : Analytic Beam Directivity Pattern ϕ=0,45.

Selected triangular array lattice is presented as follows:

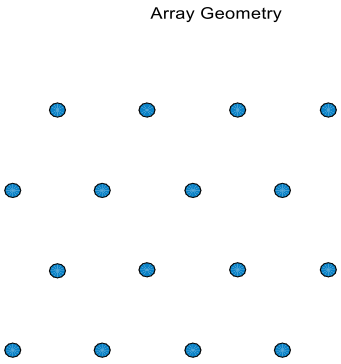

Fig. I-39 : Triangular lattice configuration

In Fig. I-40 is reported the related 16 analytic beams set over the service area Field of view in a triangular lattice configuration which represent the operative cold configurations.

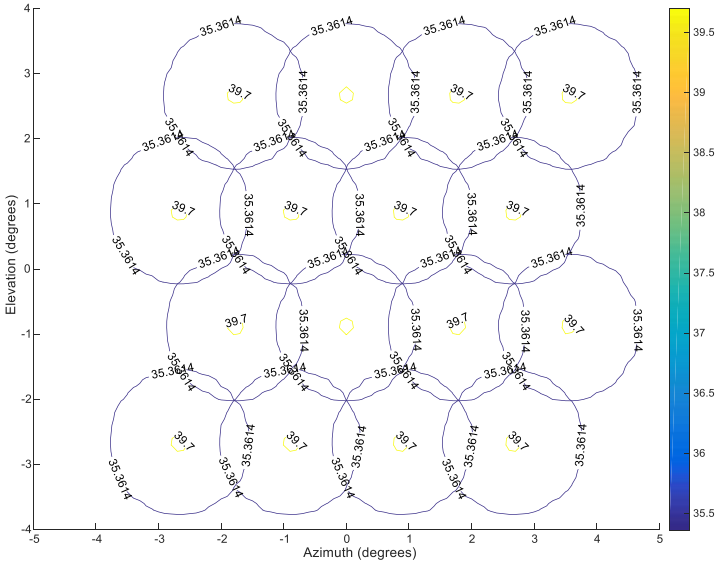

Fig. I-40 : Beam Distribution over [-3 ° ;+3 °] Field of view with directivity values [dBi]

The composite footprint form MBA Solution is reported in Fig. I-41. As can be easily seen the coverage requirement for directivity (min directivity 26.1 dBi) is fulfilled even in the composite beam solution.

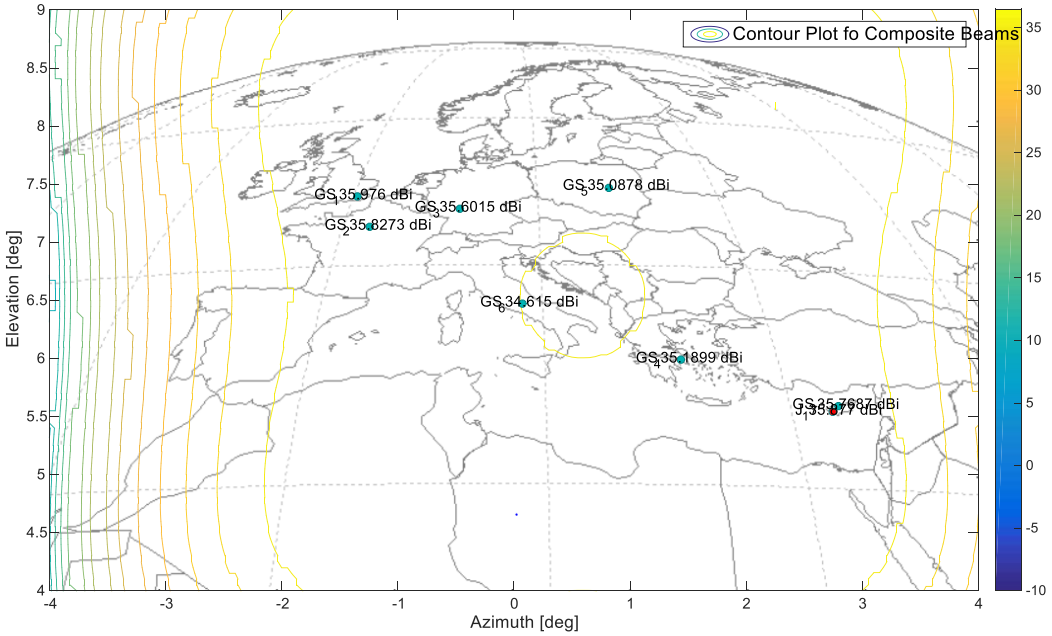

Fig. I-41 : Composite Directivity Beam Pattern ϕ=0,45 $^{\circ}$.

I.8.2 Reference Benchmark – DRA Configuration

As far as the DRA configuration concerns, in the first place the number of element must be evaluated. Different analyses have been performed to estimate an effective aperture width. This value is inner related to the single element interspacing. The interspacing can be chosen to avoid that the antenna pattern grating lobes fall inside the earth visibility circle. Thus, an element spacing in both the x and y axis of 3 λ can avoid grating lobes within the field of view visibility circle. The reference architecture will provide a 64 beams configuration displaced on a rectangular lattice with a 3 λ inter-elements spacing. This leads to a single beam, with a 3 dB beam width of θ_{3dB} =2.3 $^{\circ}$ and

a peak beam directivity of 20.63 dBi. A U-V space representation of the single element footprint is reported:

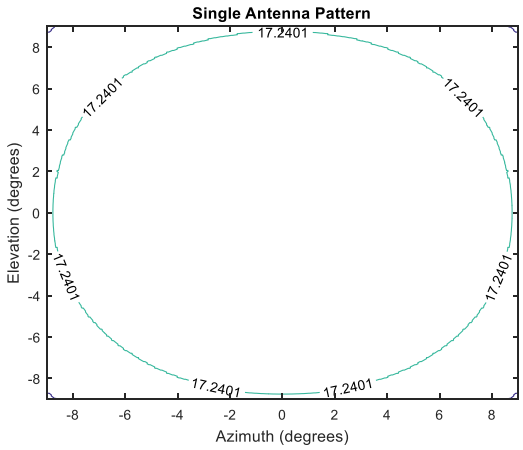

Fig. I-42 : Single DRA tapered squared horn footprint with uniform excitation with contour directivity level [dBi].

The analytic beam radiation pattern is reported for both the principal planes:

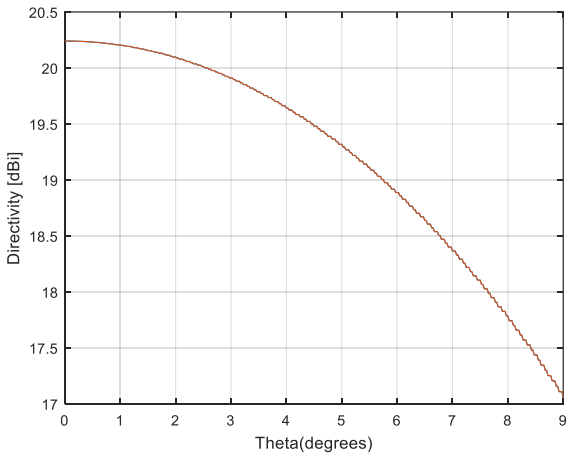

Fig. I-43 : Analytic Beam Pattern, in red ϕ=0, in yellow ϕ=45°.

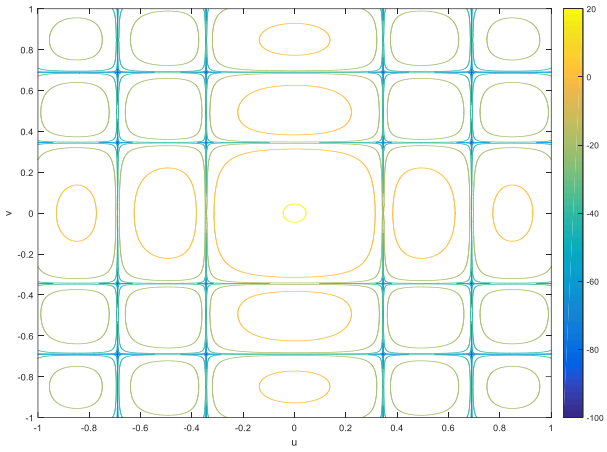

Fig. I-44 : Analytic Beam Directivity Pattern, in u-v space

The selected triangular lattice of the DRA 8*8 elements configuration is reported as follows:

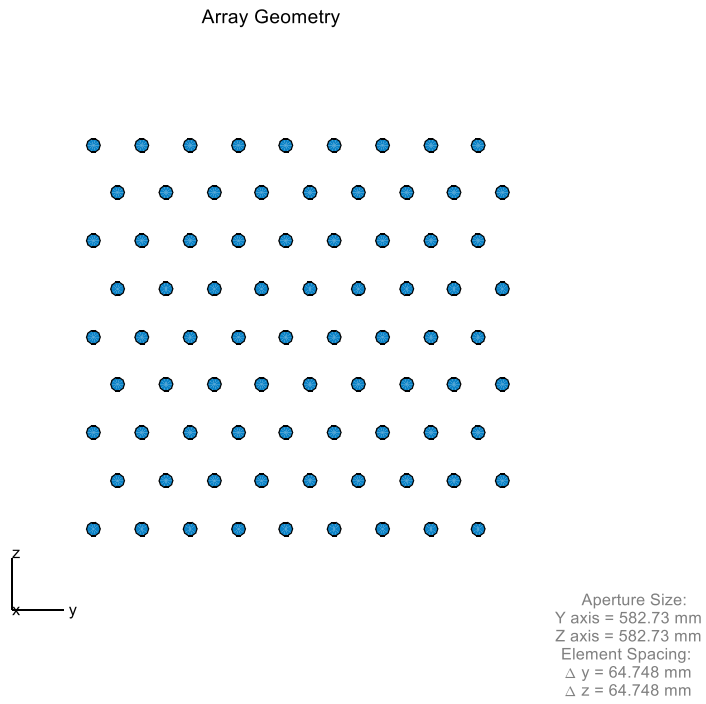

Fig. I-45 : Triangular DRA lattice

The composite array beam resulting from the uniform weighting of the antenna elements is reported as follows.

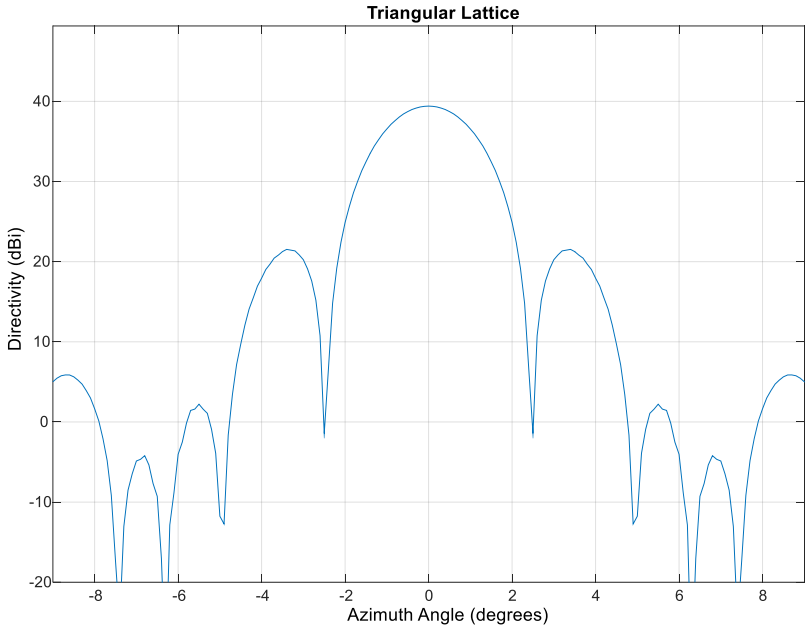

Fig. I-46 : Composite analytic beam from the 8*8 Array configuration.

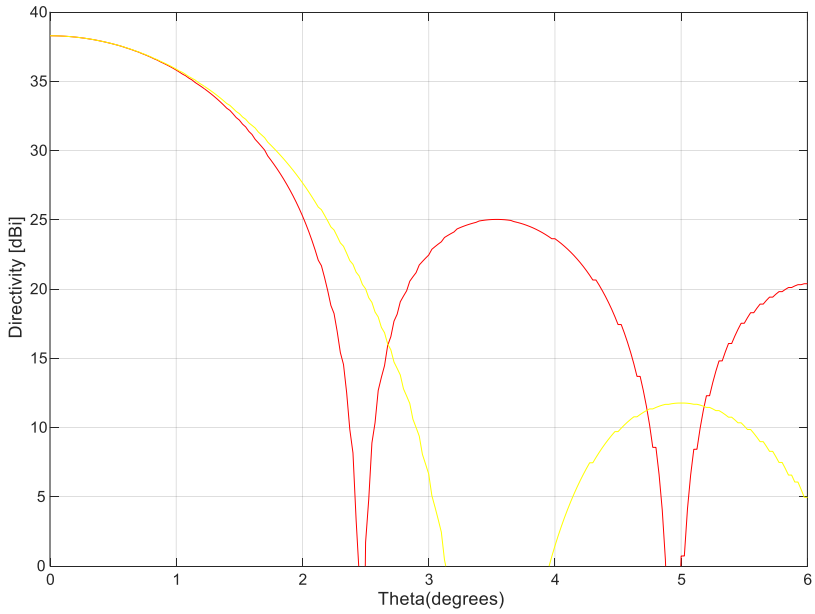

Fig. I-47 : Composite analytic beam from the 8*8 Array configuration, zoom in Field of view, in red ϕ=0, in yellow ϕ=45°.

As can be seen, an analytical beam of 39.83 dBi of Directivity can be synthetized with an angular beamwidth of 2.2°.

I.8.3 Jammer Mitigation in Reference Scenario and target required isolation definition

A DRA and MBA layout antenna are compared in this paragraph to estimate their nulling capability of interference mitigation.

For both the antenna configuration, an antenna system simulator has been developed. An intended signal has been defined and a barrage wide-band jamming is simulated in accordance to its power and spectral features as described in I.3.2.4.

In the reference scenario, intended signal is supposed to be transmitted by one of the ground station reported in 0 . The interferer signal is assumed to be transmitted by an unauthorised station located in the area called MENA (Middle East -North Africa). The choice of the interferer location in based upon a statistical analysis of the proved inference events as reported by Media.

To better prove the antenna nulling capability, the analysis is performed for three different kind of jammers classified by the mean of their angular separation from the intended source.

Interferer	Azimuth Position [deg]	Linear Distance [Km]
Jammer J_{Near}	$0.5^{\circ}+I_{Azimuth}^{\circ}$	312,29
Jammer J_{Far}	$1^{\circ}+I_{Azimuth}^{\circ}$	624,55
Jammer $J_{Far-Out}$	$1.5^{\circ}+I_{Azimuth}^{\circ}$	936,77

Tab. I-6:: Jammer location and its relative Azimuth position with respect to the intended station azimuthal position $I_{Azimuth}$.

Three jammers scenario are presented, a near jammer with an angular separation of 0.5° from the intended, A far jammer which is 1° far and a far-out jammer which is within a 1.5° of angular distance from

the authorised ground station. The reference scenario is reported in Fig. I-48 where the blue line is the contour of the interferers jammer origin region while the European Area is the service area for intended communication [R. 21,R. 22,R. 23,R. 24,R. 26].

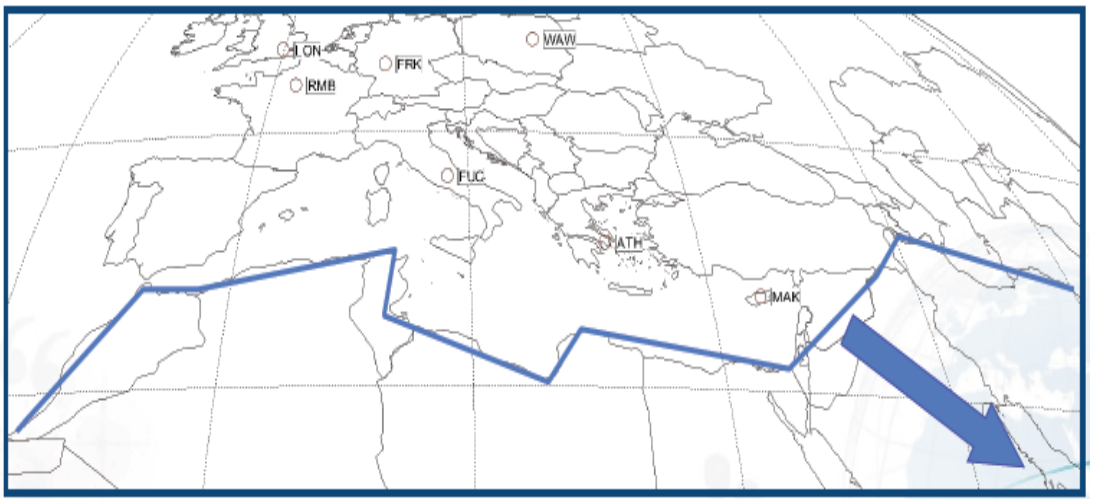

Fig. I-48 : Reference Operative scenario Region.

The reference scenario has been considered for a standard 36 MHz Transponder, centred around fc=13.9 GHz linked with a space segment satellite infrastructure located at GEO arch 13 ° E with a beam Pointing Error of 0.05 °. A reference G/T equal to 4 dB/K and a reference Ground Station transmission EIRP= 70 dBW for the downlink and uplink section of the link has been considered respectively. The transmitting signal is supposed to be a DVB-S2 QPSK (2/3) waveform, with 36 MHz bandwidth, which represents a standard for satellite commercial communications. According to the link budget analyses performed for this reference scenario and to the losses of the antenna system as reported in , the requested minimum antenna directivity to correctly use the satellite channel is 26.15 dB for MBA antenna and 26.1 dB for DRA.

As far as the jammer concerns a reference EIRP of 90 dBW has been taken into account into the footprint scenario.

Impacts on communication link has been taken into account evaluating threat for the payload of commercial satellites at physical layer by extensive link budget analyses. In these analyses, physical link features have been evaluated in accordance to ITU recommendations which are the industrial standard reference for radio link design and dimensioning.

Effects of interferers has been considered by their peculiar RF and spectral characterization as carried out by theoretical analysis and by the impairments, they introduce in radio link as assessed by the simulation activities described in I.5.1.

The abovementioned analyses allow to define a target Isolation required to the antenna nulling system. The relevant methodology developed, that lead to the definition of required antenna isolation is described as follows.

By indicating with I the time-averaged interference power and S the time-averaged useful signal power, the ratio I/S defines how much the jamming power is greater than the useful one. Regardless of the signal and jamming waveforms, it is possible to define the equivalent bit energy-to-jammer noise ratio as in (1):

$$\frac{E_b}{N_J} = \frac{B \cdot S}{R_b \cdot J} \tag{I.75}$$

where E_b is the useful energy per bit, N_I is the equivalent jamming noise single-sided power spectral density, B is the total available noise bandwidth, Rb (bit/s) is the bit rate of the useful payload signal . When considering signal reception in practical scenarios, AWGN with an equivalent power spectral density of N_0 is also present besides interference, and thus the relevant figure of merit becomes the Signal-to-Noise-plus-Interference Ratio (SNIR):

$$SNIR = \frac{E_b}{N_0 + N_I} \tag{I.76}$$

For transparent satellite link, the value of C/N_0 used in order to assess Signal-to-Noise Ratio or the $C/(N_0+I)$ to evaluate Signal-to-Noise-plus-Interference Ratio with respect of carrier power level can be calculated by SNIR:

$$\frac{C}{N_0 + I_I} = \frac{E_b \cdot R_b}{N_0 + N_I} \tag{I.77}$$

The impact of in-band interference on the on useful signals can be developed a methodology based on link budget, as described in the following steps:

In the first place, an estimation of the minimum allowable carrier-to-noise power density ratio $(C/N_0)_{req}$ requested at the input of the baseband part of the useful receiver in order to grant desired performance in terms of BER. This $(C/N_0)_{req}$ is the target reference value to be obtained in function of the RF receiving chain figure of noise and in its phase loop features.

A computation of the carrier-to-noise power density ratio under no interference (C/N0)uni at the input of the base-band part of the receiver, according to:

$$\left(\frac{C}{N_0}\right)_{uni} = \frac{P_r \cdot G_r}{kT_0 N_f L} \qquad \text{(I.78)}$$

Where:

Pr :received signal power level in Watt;

Gr :receiver antenna gain;

k : Boltzmann's Constant = 1.38*10-23 (W*sec/K);

T0 :is the thermal noise reference temperature in K ;

Nf :receiver noise figure including antenna and cable loss;

L :implementation loss plus A/D conversion loss.

Pr level can be evaluated through a link budget analysis based on :

i. Architectural Network structure, reference Satellite system and multiple access strategies;
ii. Geographical location, Modulation, coding and reference radio parameters for transmission and receiving;

$(C/N)_{unj}$ has been carried out both for clear sky condition or rain condition.

Computation of the critical interference-to-signal power ratio I/C value that can result in a loss of desired performance level, if overcome:

$$\left(\frac{I}{C}\right)_{\max} = \left\{ \cdot \frac{B \cdot Q_p}{\left[\left(\frac{C}{N_0}\right)_{uni} - \left(\frac{C}{N_0}\right)_{req}\right]} \right\} \tag{I.79}$$

Where:

B : is signal bandwidth

Q_p : is an dimensionless adjustment factor that depends on the interference bandwidth occupation calculated as $\rho_I = \frac{B_I}{B}$, i.e. the fraction of the total band affected by interference.

Computation of the received interference power corresponding to the critical interference level :

$$I_{r\max} = \left(\frac{I}{C}\right)_{\max} \cdot C_r \tag{I.80}$$

Once it has been calculated maximum critical received interference signal power, it can be derived the total interference signal level, for provided amplitude spectrum density, as far as unintentional interference concerns, or for a given jammer's Equivalent Isotropic Radiated Power, regarding intentional interference. Generally, the received interference signal level can be written as:

$$C_r = \frac{EIRP_I \cdot G_r\left(\vartheta_{doa}, \varphi_{doa}\right)}{L_p L_i} \tag{I.81}$$

Where:

$EIRP_I$: is the interference equivalent isotropic radiated power derived

from the source of the interference

$G_r(\vartheta_{doa}, \varphi_{doa})$: in the receiver antenna gain in the direction of arrival of interference signal

L_p : is a cumulative figure that takes into account all the propagation losses.

L_i : is a cumulative figure that takes into account other impairments may occur in the transceiver chain.

In the end, received SINR could be calculated in a two steps procedure. First of all, it shall be evaluated interference spectral density, as follow:

$$N_I = \frac{I_r}{B_I} = \frac{I_r}{B}\frac{B}{B_I} = \frac{N_{I_{bb}}}{\rho_I} \tag{I.82}$$

Where:

N_I : is the interference power spectral density in its transmission band

B_I : is the portion of total available signal bandwidth superimposed with a partial band interference signal.

B : is the total available signal bandwidth

$N_{I_{bb}} = \frac{I_r}{B}$: is the equivalent interference noise single-sided power spectral density

$\rho_I = \frac{B_I}{B}$: is the fraction of the total band affected by interference

And so the SINR has been taken into account as C/N ratio defined as:

$$\left(\frac{C}{N+I}\right)_{tot} = \frac{E_b \cdot R_b}{N_0 + N_{I_{bb}}} \tag{I.83}$$

Once $\left(\frac{C}{N+I}\right)_{tot}$ has been calculated, it has been possible to carry out the magnitude of affection of each type of interference under test, in term of total loss of C/N ratio with respect to the un-interfered C/N ratio.

Thus for the reference satellite system scenario a total available margin for the communication link of 4 dB has foreseen for clear sky condition (0,2 dB for Rain condition) with a probability of 99,9% of out of service in accordance to ITU Standards. Additional link parameters are described in the following table[R. 59,R. 60,R. 61,R. 62,R. 63,R. 64,R. 65].

Link Parameter	Value [dB]
Total Available (C/N) Margin without interference (Clear)	4,04
Total Available (C/N) Margin without interference (Rain)	0,2
Total (C/N+I) (Clear)	-7,98
Total (C/N+I) (Rain)	-11,04
Total loss of (C/N+I) (Clear)	-19,47
Total loss of (C/N+I) (Rain)	-18,68

Tab. I-7: Link Budget analyses reference scenario results

Now evaluating the total un-interfered $\frac{I}{C_{max}}$ of the link and the unmitigated C_r , as can be seen even by comparison the the Total Available (C/N) Margin and the Total (C/N+I) (Clear), it can be defined the isolation requirement at 25 dB.

In the following antenna analyses that level of isolation is considered as required by the Antenna system performance.

To prevent possible local minima, a general global optimizer has been used to search the complex weight configuration for implementing the nulling algorithm. Specifically, a global search minimax algorithm with constrains which depends on the coverage that must be achieved. The target radiation pattern of the nulling configuration of shaped regional coverage can be expressed as:

$$\mathrm{E}_{nd}(\theta,\varphi) \tag{I.84}$$
$$= \sum_{\mathrm{k}=-\infty}^{+\infty}\sum_{l=-\infty}^{+\infty}\left\{\iint_{u^2+v^2\leq(4\pi A/\lambda^2)sin^2(3^\circ)} \psi_{k,l}(u,v)du\,dv\right\}\psi_{k,l}(u,v)$$
$$-\frac{\lambda_n}{2}\sum_{\mathrm{n}=1}^{N} B_{max}\left(\theta-\theta_{\mathrm{n}J},\varphi-\varphi_{\mathrm{n}J}\right)$$

Where the $\psi_{k,l}(u,v)$ functions are the Schmidt ortho-normalized set of basis functions deduced by the beam space basis function.

In the formula, the set of values λ_n, with n=1..,N, are the coefficient needed to operate the linear combination between the desired coverage and the desired nulling beams. Those coefficients can be derived by constrained maximization of the $\mathrm{E}_{nd}(\theta,\varphi)$ and, more precisely, they represent the Lagrange multipliers of the above-mentioned maximization process.

In the following paragraphs coverage plots are reported in order to analyse the impact on the whole footprint of the nulling and the

capability of nulling technique in mitigate interference sources in such satellite scenario.

A lead parameter which affects antenna nulling maximum achievable performance is the beam pointing error (BPE). The BPE together with the Beam Error Uncertainty (BPU) define somewhat the maximum achievable precision of the Antenna Nulling system. The BPE is related to the accuracy, nulling direction can be known at antenna level with. The Beam Pointing Uncertainty is related to the precision, the position of the interferer is known with. In order to keep low the complexity of the embarked antenna system, no geolocation of the interference is considered to be performed on board, on the contrary the position is assumed to be known by the operator which manages the satellite. Some Private company offers such service [i.e., http://www.kratostts.com/solutions/satellite-and-space/rf-interference-mitigation] and for the purpose of the study is supposed to know the position of the interferer with a 0.05° of uncertainty (≈63 Km). All the analyses presented in the following take as reference a BPU value of 0.05°.

An antenna nulling algorithm has been implemented based on a MINIMAX global search algorithm, to be employed in the investigation. The algorithm takes into account all the parameters of physical link, as defined in reference benchmark link budget analyses, so thus the implemented algorithm can minimize the total received power of the jammer. This simulator, ex novo developed by the theoretical background is one of the lead achievement of this work, since it provides a powerful way to investigates nulling capabilities of different antenna solutions both at directivity level and then directly at antenna system levels. A scope of example, the behaviour at signal level has been reported, as it comes out from the simulation tool in the following figure.

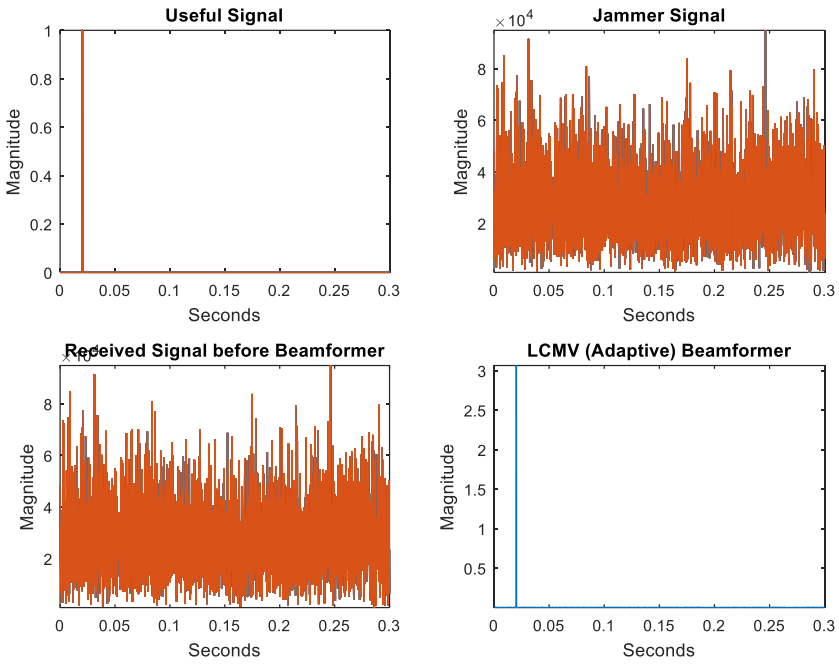

Fig. I-49: Output of Simulator at Signal level.

In Fig. I-49: Output of Simulator at Signal level. the signal level output of the simulator has been presented. In the first plot the reference useful signal is reported in time domain, the second upper plot, clockwise, shows the reference jammer signal, in the lower left plot, useful signal, white Gaussian antenna noise and Interferer signal as they arrive at antenna aperture, in the last plot the signal as filtered by the beam forming network. The simulator can implement even constrained maximum likehood algorithm and the reported plot referrers to that, but for the purpose of this work, only a MINIMAX algorithm has been employed.

I.8.4 MBA Antenna Nulling Analyses

A MBA antenna layout with triangular lattice over the presented scenario is chosen. Phase and Amplitude coefficients of the array has been optimized by a minimax algorithm. According to Tab. I-7 the requested minimum antenna directivity to correctly use the satellite channel is 26.15 dB for MBA antenna. The required S/I isolation is 25 dB. The Multi Beam Antenna Coverage is represented for the cold case in Fig. I-50, when it is working in single beam per feed mode and no nulling is working.

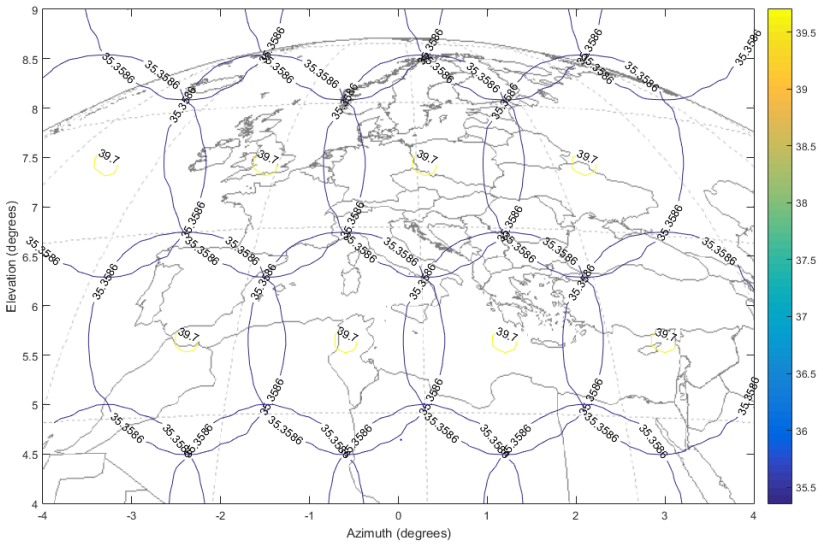

Fig. I-50 : MultiBeam Antenna Configuration in Cold Case.

In the following plots are reported the coverage produced by the selected MBA antenna in different nulling scenario. In order to set which is the minimum distance can be effectively nulled by the antenna system, a progressive sweep analysis is performed. Taking as reference a Ground Station on the Cyprus Island (GS_7) which is the nearest to the most probable interferer origin geographical location. Thus, it will be verified the performance of the nulling system by evaluating the

capability to mitigate interferer located from 0.05 ° to 0.4 ° from the authorised station to establish the minimum nullable distance.

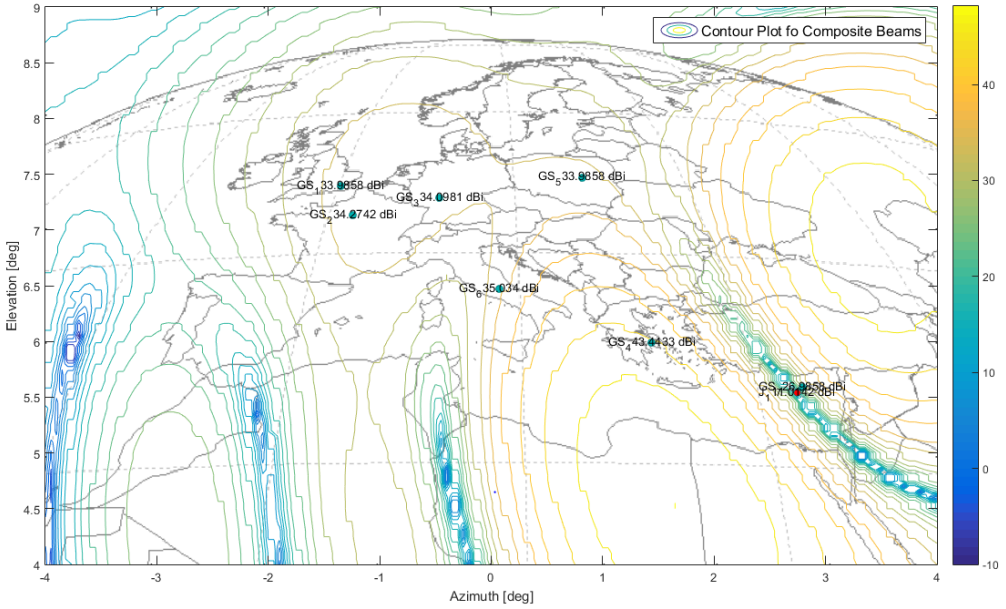

Fig. I-51 : Hot Case: Nulled Pattern with authorised station GS_7 and a 0.05 ° far interferer J_1

An angular separation of 0.05 ° (62,7 Km) does not allow to reach the required isolation level w.r.t. the interferer, a maximum of 18.8 dB of isolation is provided.

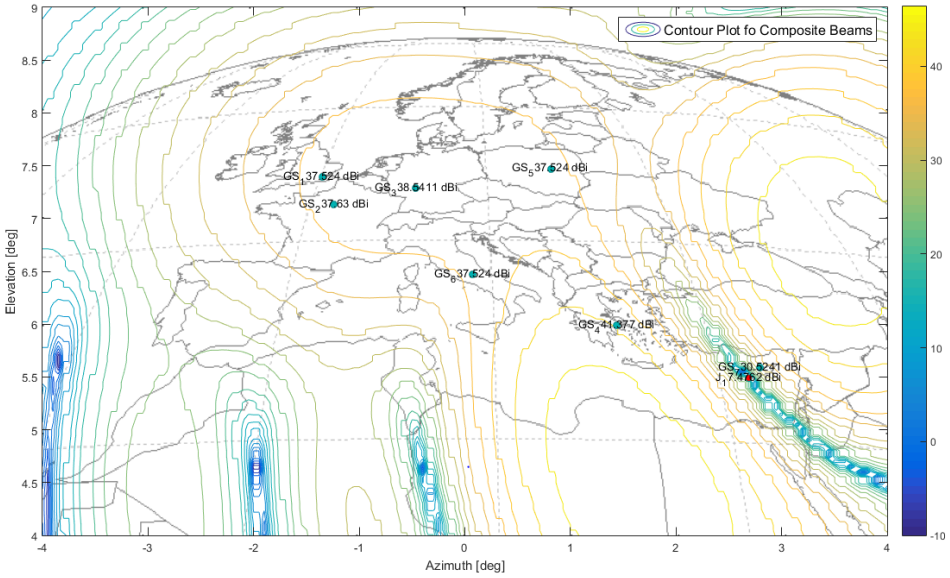

Fig. I-52 : Hot Case: Nulled Pattern with authorised station GS_7 and a 0.1 ° far interferer J_1

An angular separation of 0.1 ° (125,3 Km) does not allow to reach the required isolation level w.r.t. the interferer, a maximum of 18.8 dB of isolation is provided.

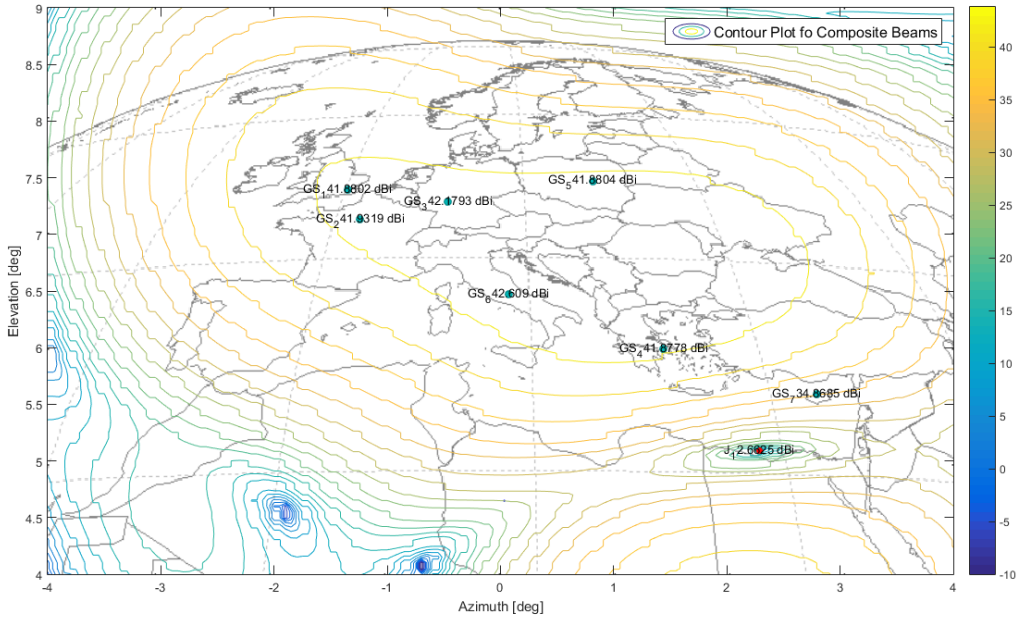

Fig. I-53 : Hot Case: Nulled Pattern with authorised station GS_7 and a 0.5 ° far interferer J_1

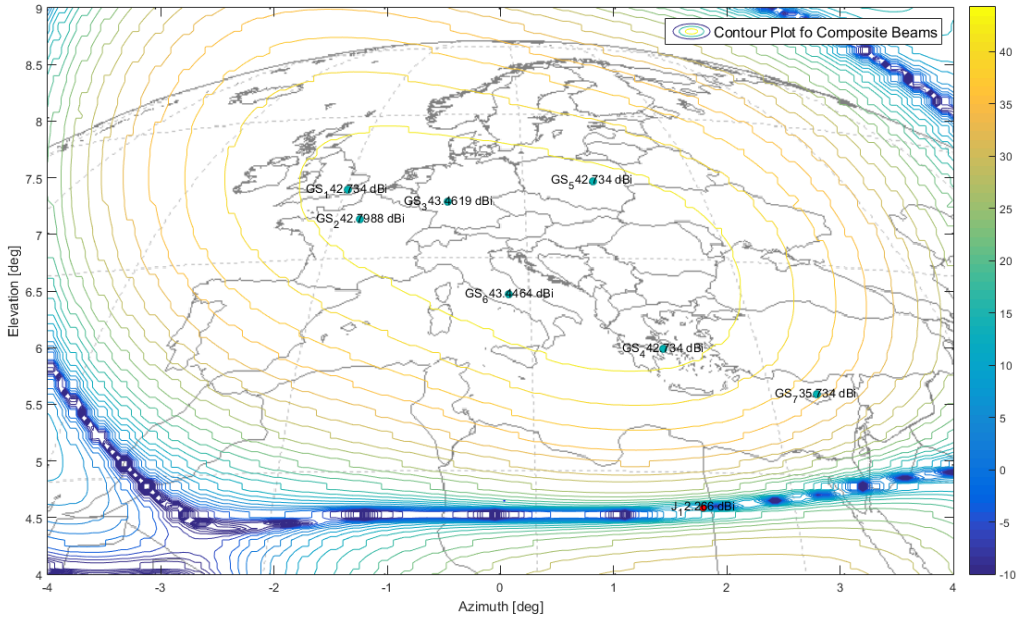

Fig. I-54 : Hot Case: Nulled Pattern with authorised station GS_7 and a 1 ° far interferer J_1

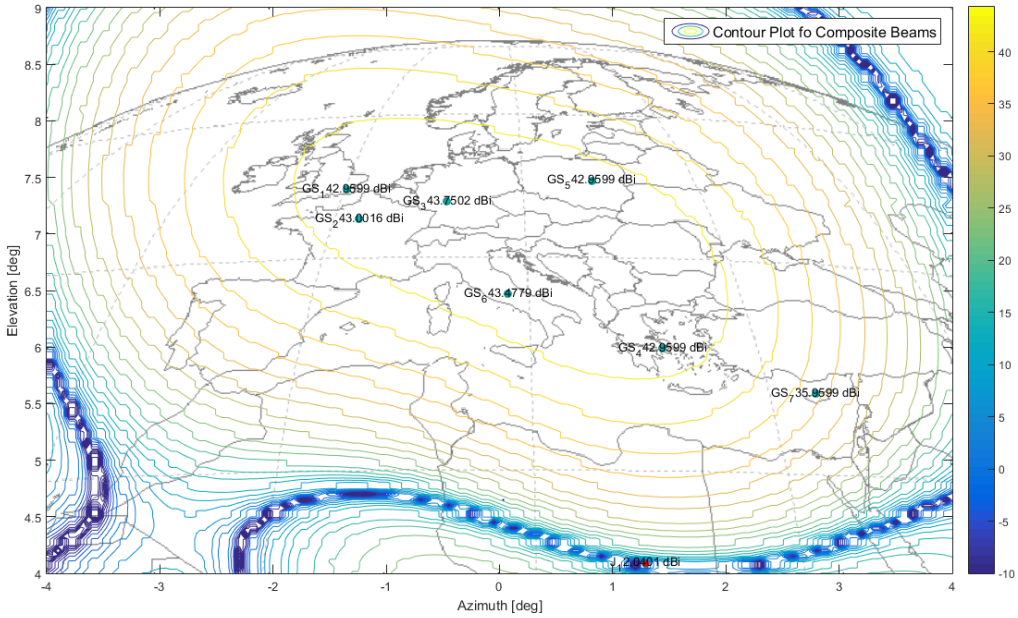

Fig. I-55 : Hot Case: Nulled Pattern with authorised station GS_7 and a 1.5 ° far interferer J_1

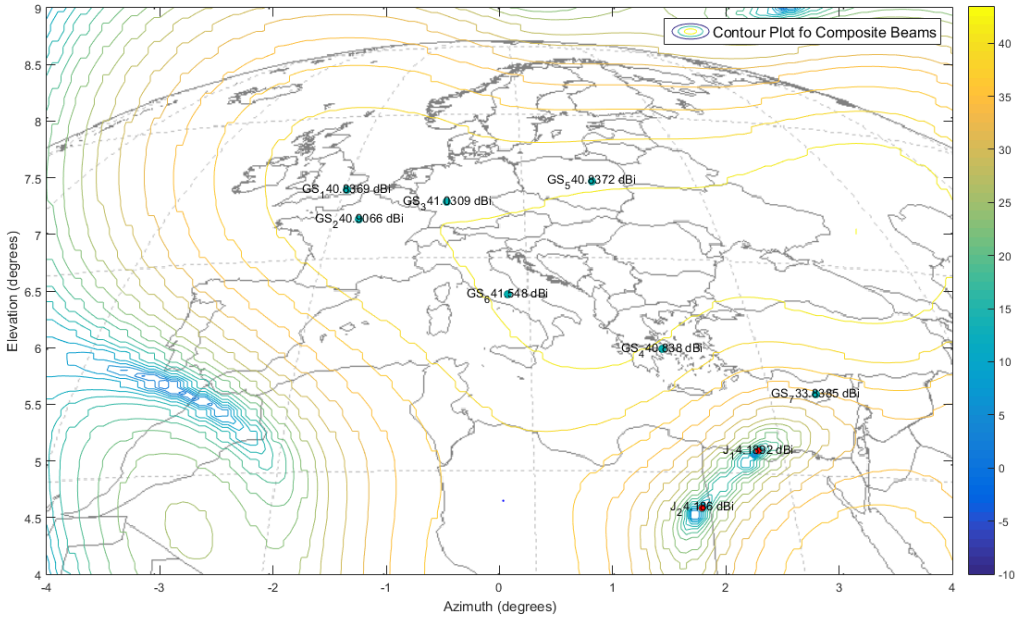

Fig. I-56 : Hot Case: Nulled Pattern with authorised station GS_7 and 3 interferers: a near J_1 (0.5 $^\circ$) and a far J_2 (1 $^\circ$) interferer

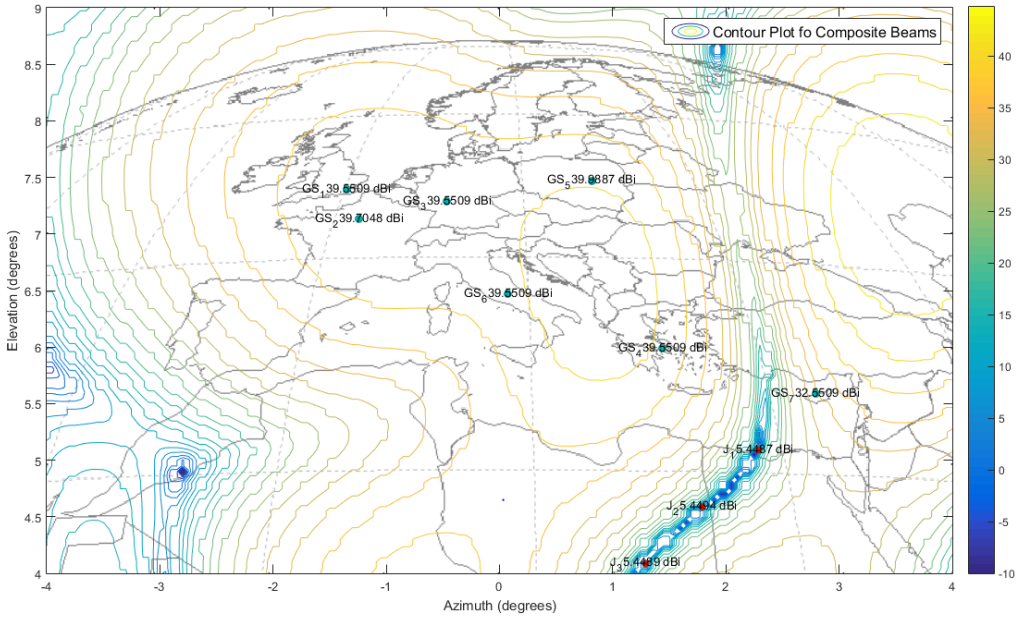

Fig. I-57 : Hot Case: Nulled Pattern with authorised station GS_7 and 3 interferers: a near J_1 (0.5 $^\circ$) and a far J_2 (1 $^\circ$) and far out interferer J_3 (1.5 $^\circ$)

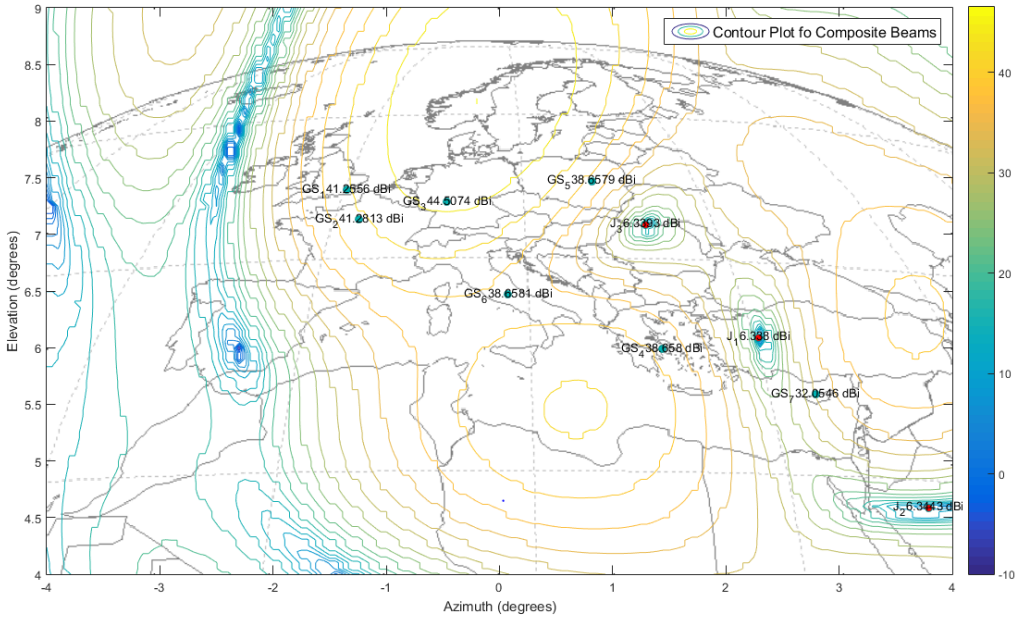

Fig. I-58 : Hot Case: Nulled Pattern with authorised station GS_7 and 3 interferers: a near J_1 (0.5 °) and a far J_2 (1 °) and far out interferer J_3 (1.5 °)

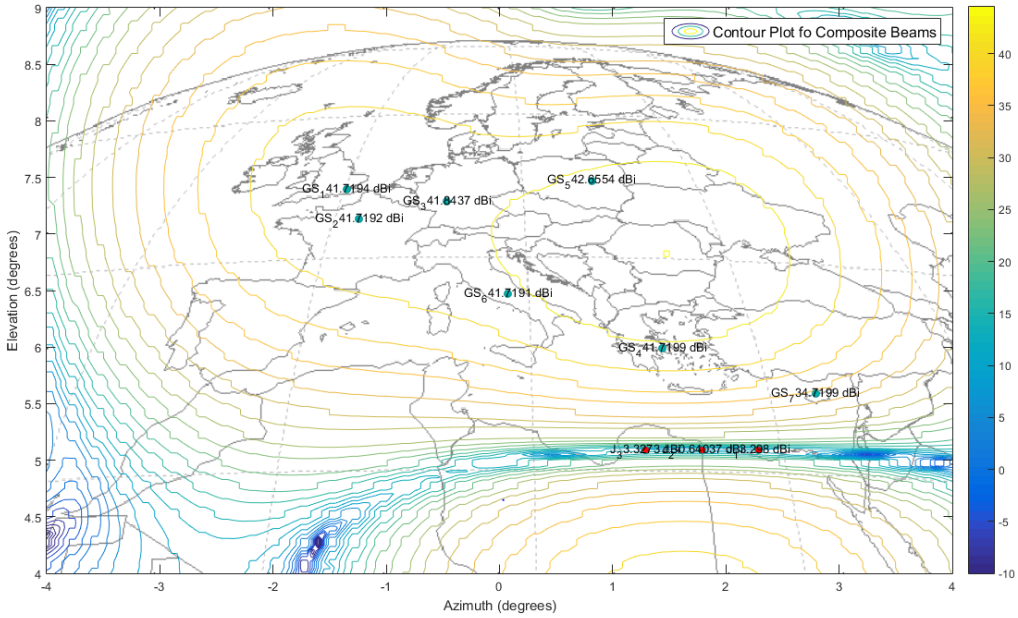

Fig. I-59 : Hot Case: Nulled Pattern with authorised station GS_7 and 3 interferers: a near J_1 (0.5 °) and a far J_2 (1 °) and far out interferer J_3 (1.5 °)

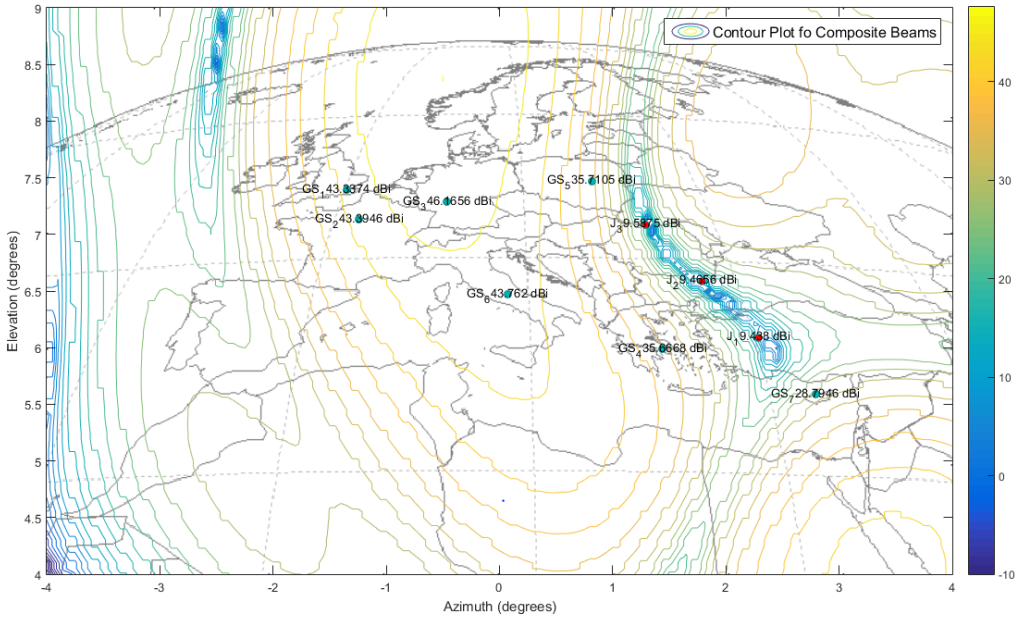

Fig. I-60 : Hot Case: Nulled Pattern with authorised station GS7 and 3 interferers: a near J_1 (0.5 °) and a far J_2 (1 °) and far out interferer J_3 (1.5 °)

A synoptic table will summarize the achieved isolation performances for each of the presented scenario.

J_3	J_2	J_1	Minimum Directivity User [dBi]	Maximum Directivity Jammer [dBi]	Achieved isolation [dBi]	Isolation Req. [dBi]	Delta Isolation [dBi]
		0.05	26,98	17,04	9,94	25	-15,06
		0.1	30,52	7,47	23,05	25	-1,95
		0.5	34,86	2,66	32,20	25	7,2
	1		35,734	2,66	33,07	25	8,07
1,5			35,95	2,04	33,91	25	8,91
	1	0,5	33,83	4,20	29,64	25	4,64
1,5	1	0,5	32,55	5,44	27,11	25	2,11
1,5	1	0,5	32,05	6,338	25,71	25	0,71
1,5	1	0,5	34,72	3,30	31,42	25	6,42
1,5	1	0,5	28,80	9,43	19,37	25	-5,63

Tab. I-8: MBA 32λ performance table

It is worth noting that whenever the requested isolation is not achieved only toward the ground Station nearest to the interferer the receiving Satellite antenna shows a C/I ratio below the requested value and loose the link towards the satellite. The rest of the ground station keep the connection.

An additional sweep of results are presented for a 16 feed MBA with 45 λ parabolic reflector. This leads to a single beam, with a 3 dB beam width of θ_{3dB} =1.2 ° and a Triple Cross over Point of -4.2 dB w.r.t. peak beam directivity of 42.08 dBi.

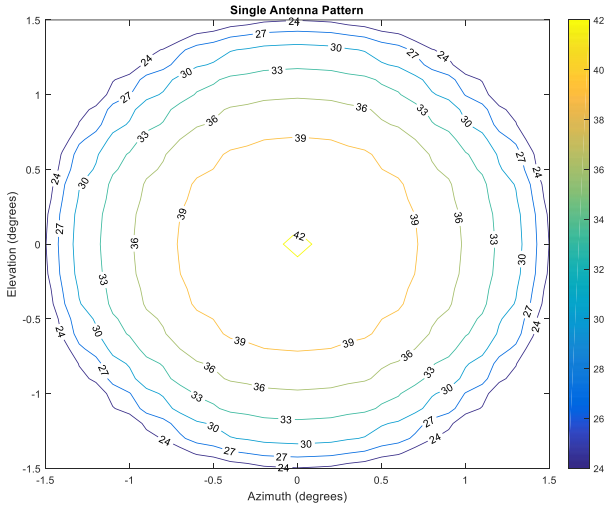

Fig. I.61 : Single beam Footprint with countour directivity level [dBi].

The single beam radiation pattern is reported for both the principal planes.

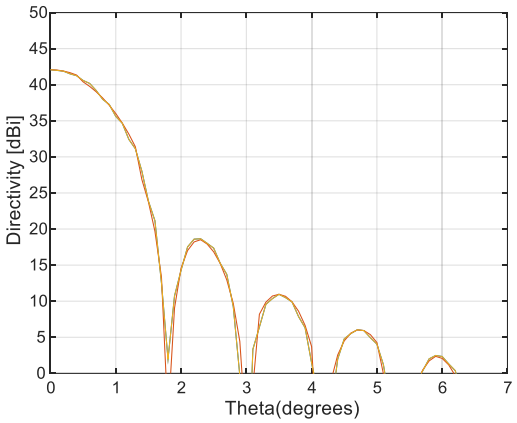

Fig. I.62 : Analytic Beam Directivity Pattern ϕ=0,45.

In Fig. I-40 is reported the related 16 analytic beams set over the service area Field of view in a triangular lattice configuration which represent the operative cold configurations.

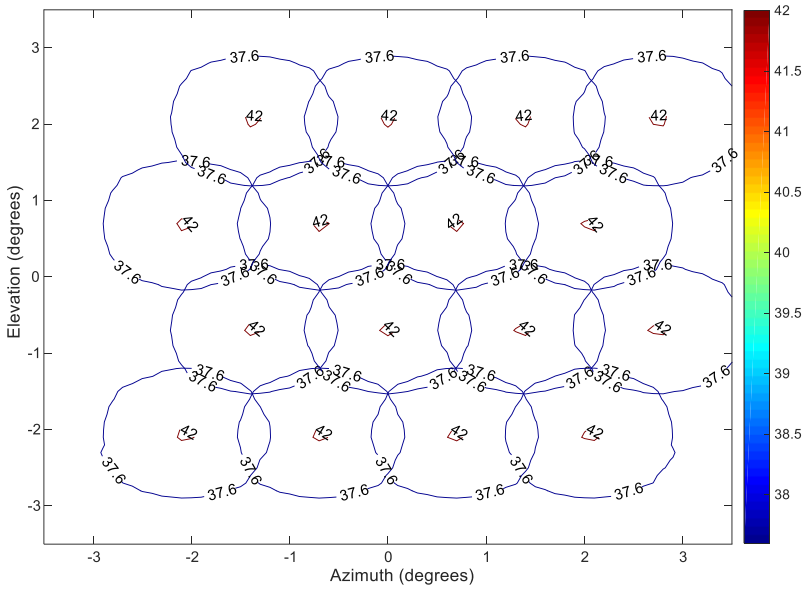

Fig. I.63 : Beam Distribution over [-3 ° ;+3 °] Field of view with directivity values [dBi]

he composite pattern form MBA Solution is reported in Fig. I-41. As can be easily seen the coverange requirement for directivity (min directivity 26.1 dBi) is fulfilled even in the composite beam solution.

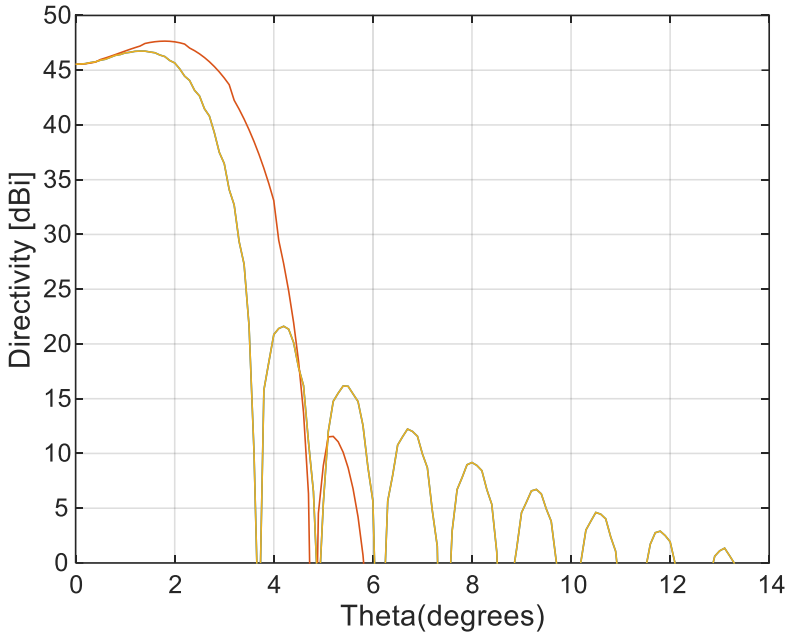

Fig. I.64 : Composite Directivity Beam Pattern ϕ=0,45.

In the following plots are reported the coverage produced by a 45λreflector wide MBA antenna in different nulling scenario. In order to set which is the minimum distance can be effectively nulled by the antenna system, a progressive sweep analysis is performed. Taking as reference a Ground Station on the Cyprus Island (GS_7) which is the nearest to the most probable interferer origin geographical location. Thus, it will be verified the performance of the nulling system by evaluating the capability to mitigate interferer located from 0.05° to 0.4° from the authorised station to establish the minimum nullable distance. An angular separation of 0.05° (62,7 Km) does not allow to reach the required isolation level w.r.t. the interferer, a maximum of 17.92 dB of isolation is provided.

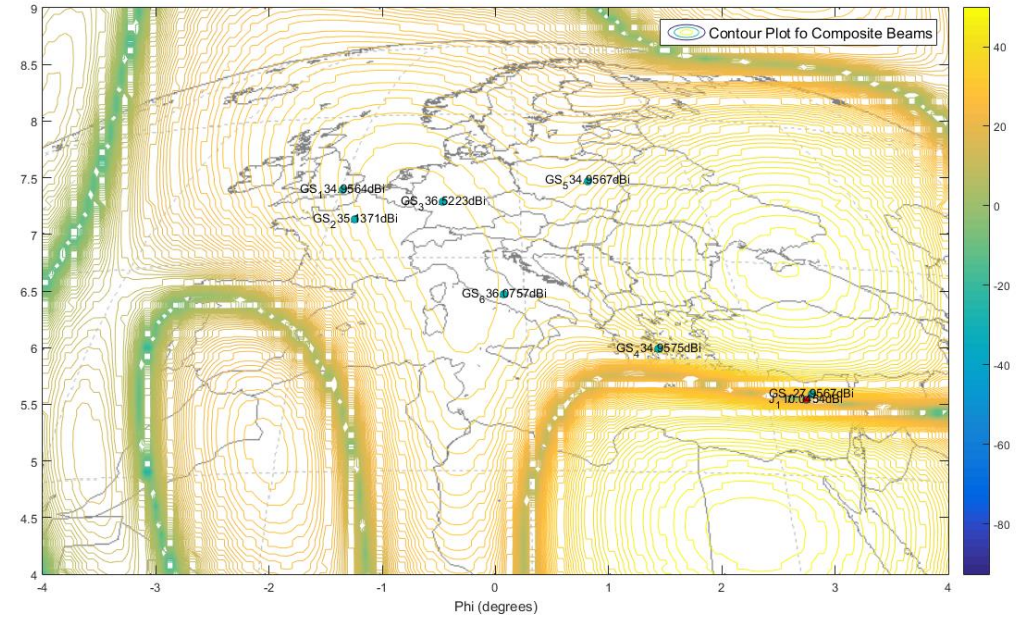

Fig. I-65 : Hot Case: Nulled Pattern with authorised station GS_7 and a 0.05 ° far interferer J_1

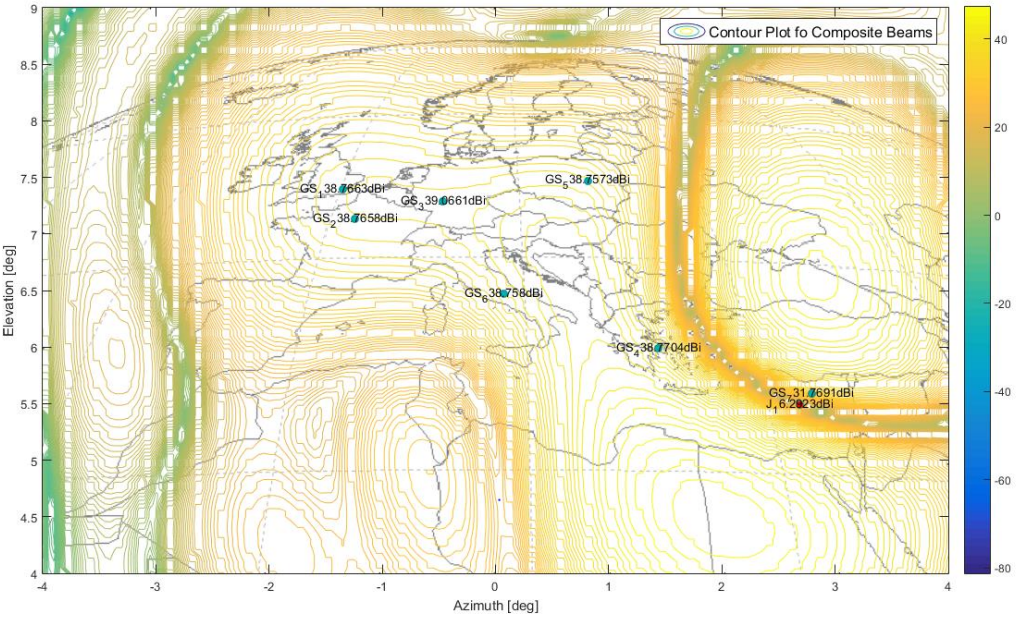

Fig. I-66 : Hot Case: Nulled Pattern with authorised station GS_7 and a 0.1 ° far interferer J_1

An angular separation of 0.1 ° (125,3 Km) does not allow to reach the required isolation level w.r.t. the interferer, a maximum of 18.8 dB of isolation is provided.

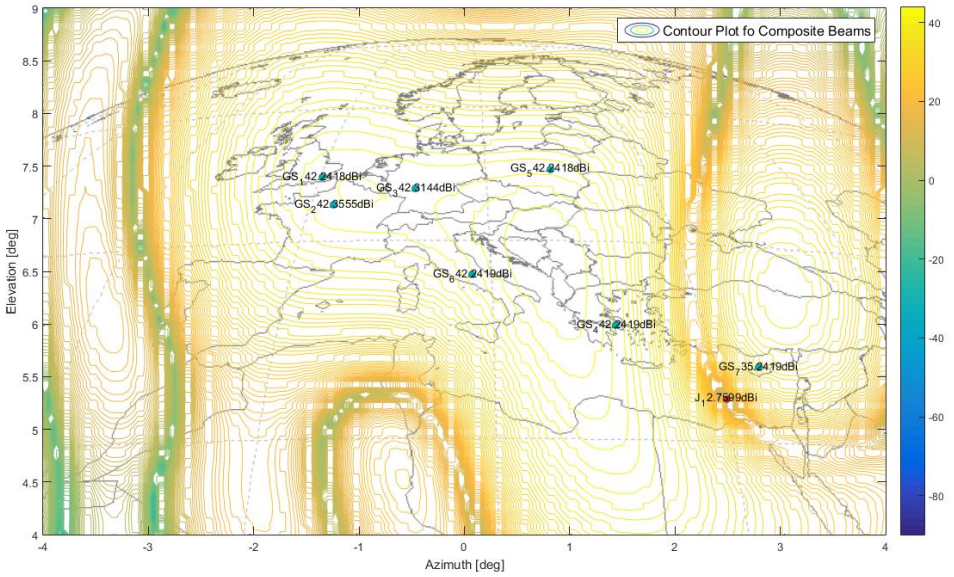

Fig. I-67 : Hot Case: Nulled Pattern with authorised station GS_7 and a 0.3 ° far interferer J_1

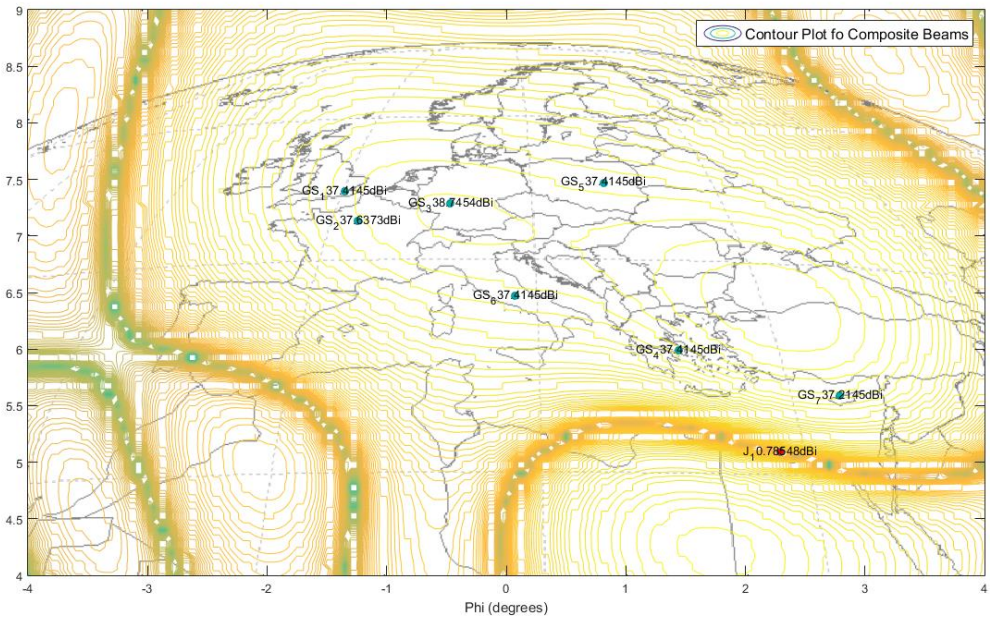

Fig. I-68 : Hot Case: Nulled Pattern with authorised station GS_7 and a 0.5 ° far interferer J_1

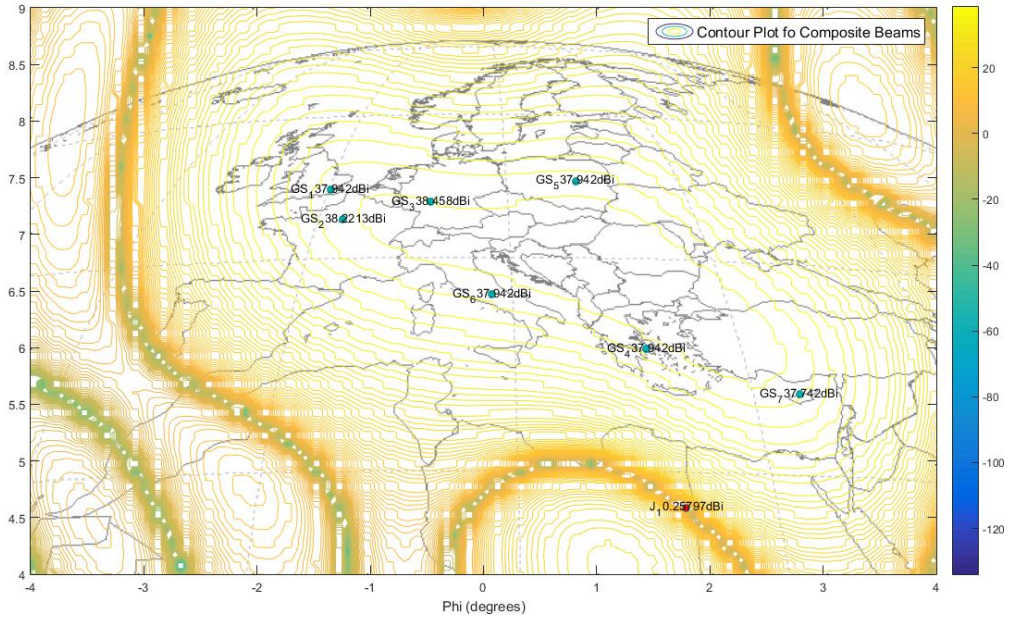

Fig. I-69 : Hot Case: Nulled Pattern with authorised station GS_7 and a 1 ° far interferer J_1

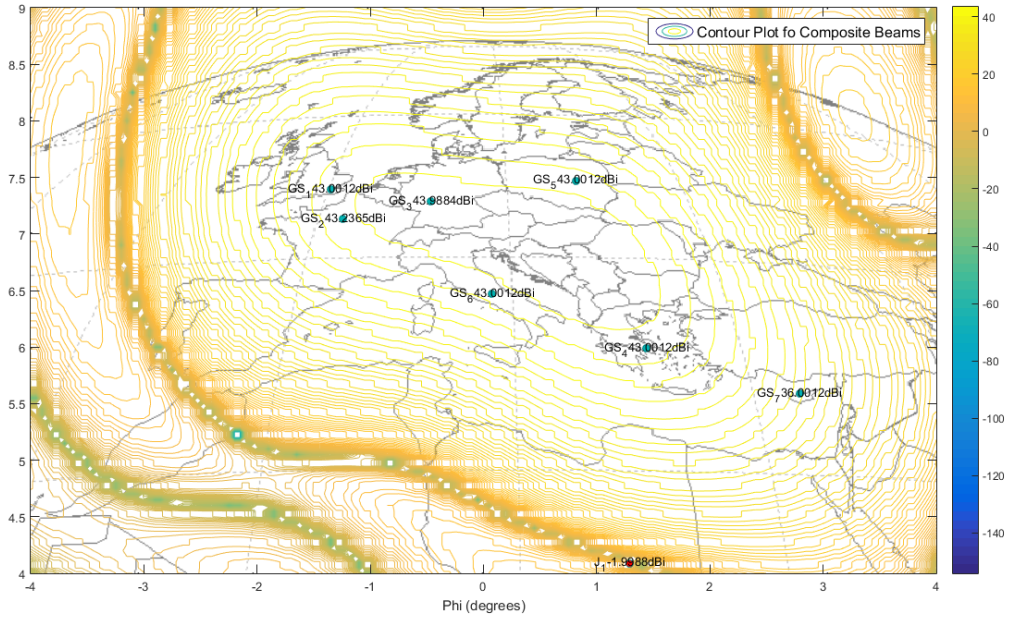

Fig. I-70 : Hot Case: Nulled Pattern with authorised station GS_7 and a 1.5 ° far interferer J_1

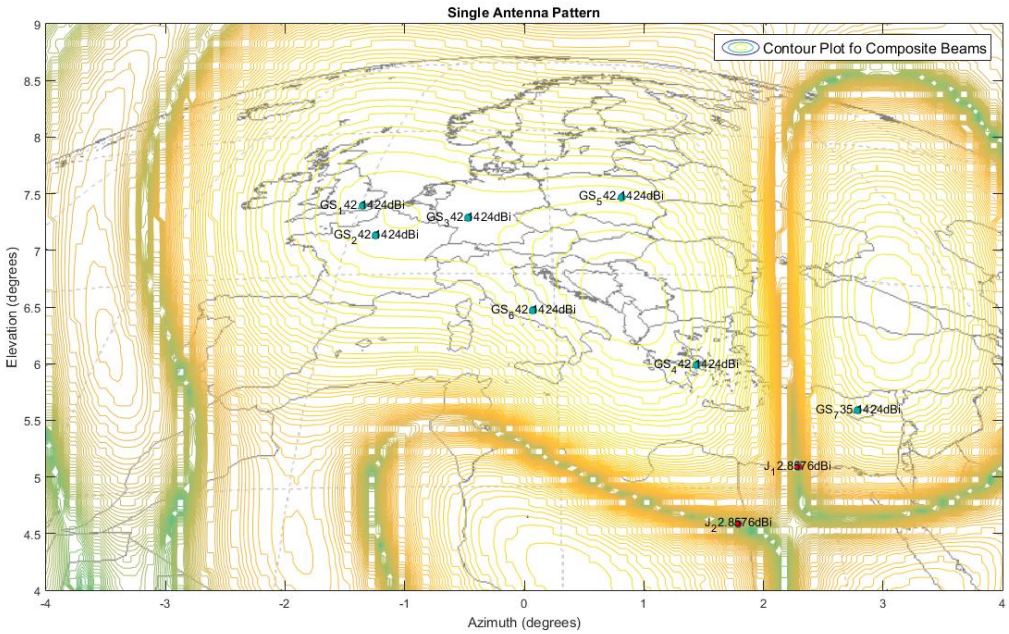

Fig. I-71 : Hot Case: Nulled Pattern with authorised station GS_7 and 3 interferers: a near J_1 (0.5 $^\circ$) and a far J_2 (1 $^\circ$) interferer

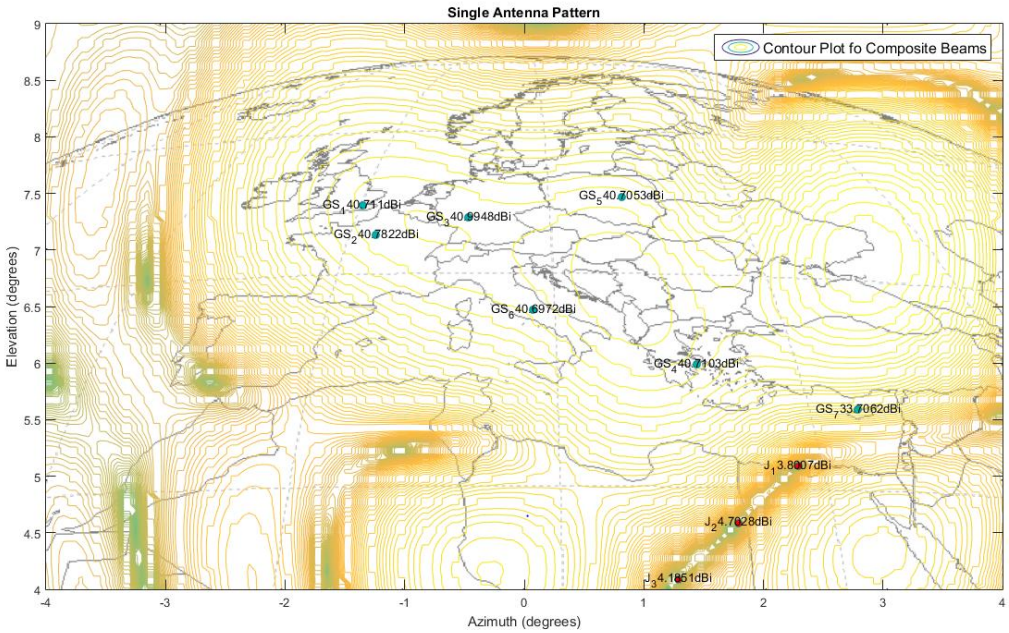

Fig. I-72 : Hot Case: Nulled Pattern with authorised station GS_7 and 3 interferers: a near J_1 (0.5 $^\circ$) and a far J_2 (1 $^\circ$) and far out interferer J_3 (1.5 $^\circ$)

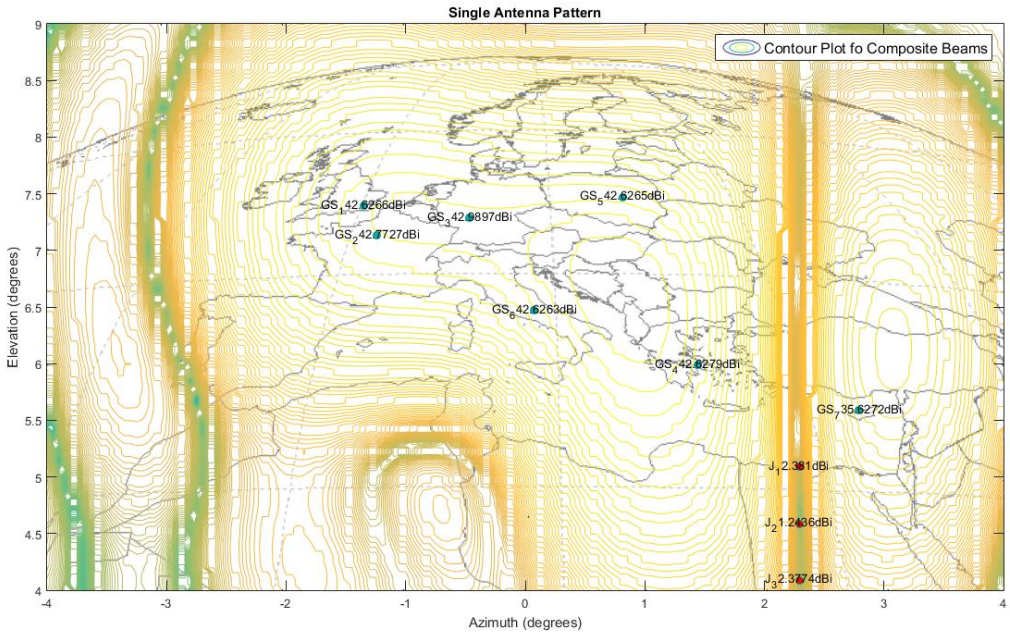

Fig. I-73 : Hot Case: Nulled Pattern with authorised station GS_7 and 3 interferers: a near J_1 (0.5 $^\circ$) and a far J_2 (1 $^\circ$) and far out interferer J_3 (1.5 $^\circ$)

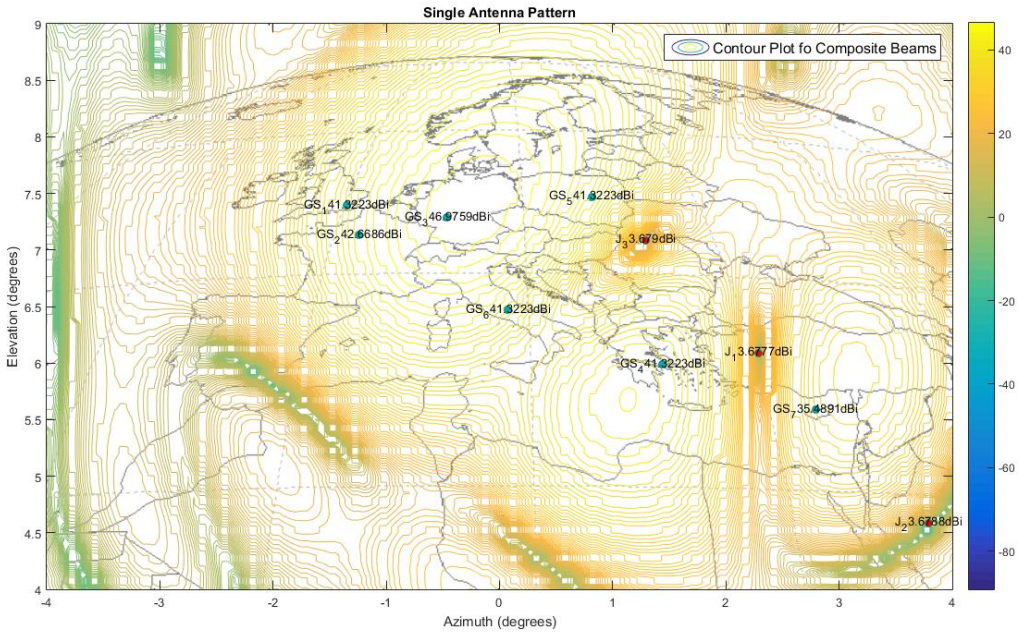

Fig. I-74 : Hot Case: Nulled Pattern with authorised station GS_7 and 3 interferers: a near J_1 (0.5 $^\circ$) and a far J_2 (1 $^\circ$) and far out interferer J_3 (1.5 $^\circ$)

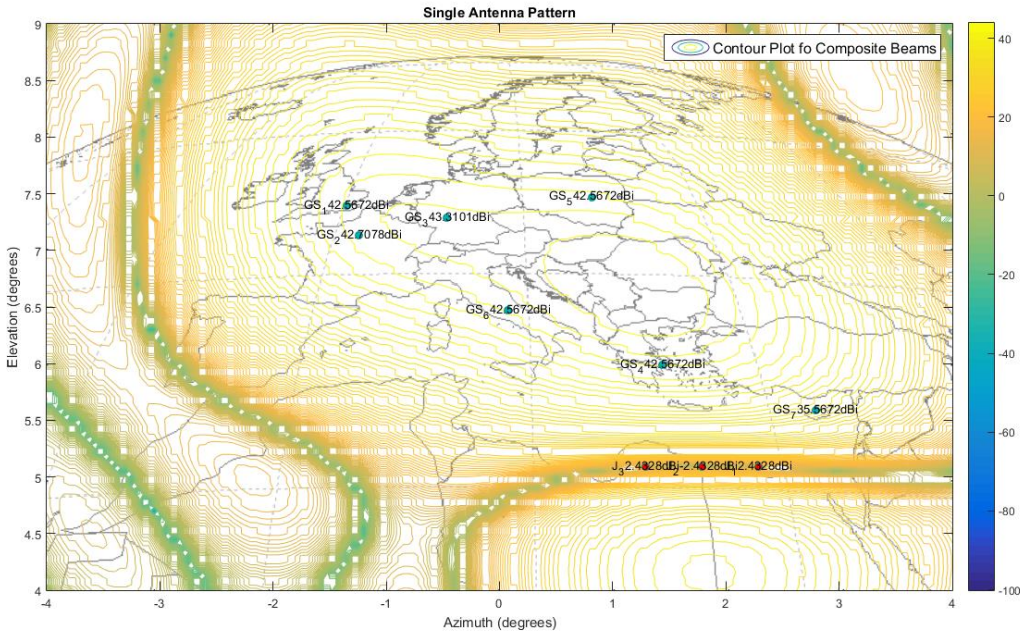

Fig. I-75 : Hot Case: Nulled Pattern with authorised station GS_7 and 3 interferers: a near J_1 (0.5 $^\circ$) and a far J_2 (1 $^\circ$) and far out interferer J_3 (1.5 $^\circ$)

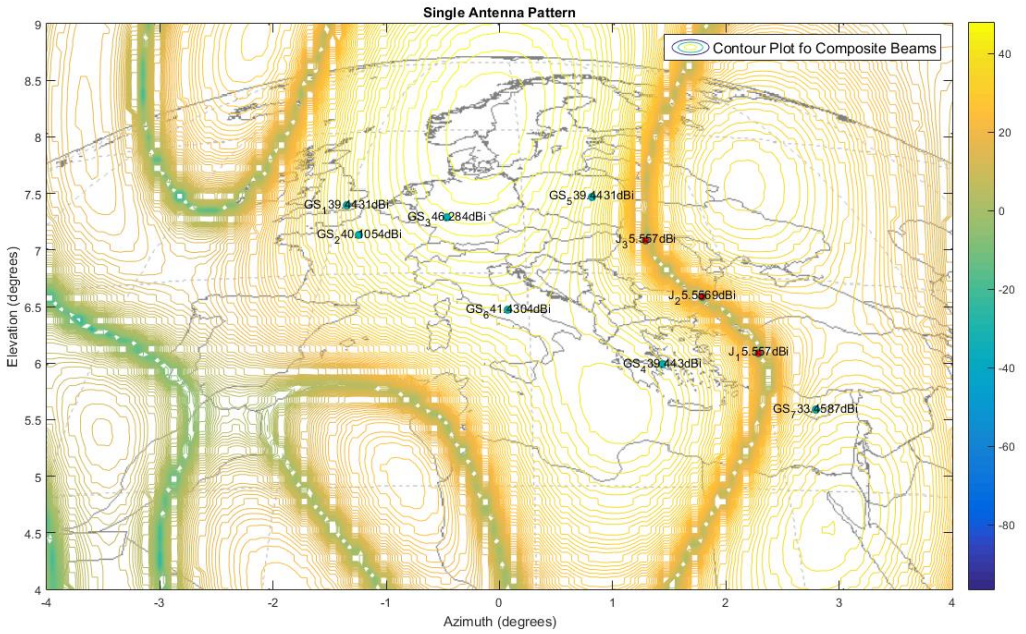

Fig. I-76 : Hot Case: Nulled Pattern with authorised station GS_7 and 3 interferers: a near J_1 (0.5 $^\circ$) and a far J_2 (1 $^\circ$) and far out interferer J_3 (1.5 $^\circ$)

A synoptic table will summarize the achieved isolation performances for each of the presented scenario.

J_3	J_2	J_1	Minimum Directivity User [dBi]	Maximum Directivity Jammer [dBi]	Achieved isolation [dBi]	Isolation Req. [dBi]	Delta Isolation [dBi]
		0.05	27,96	10,04	17,92	25	-7,08
		0.1	31,77	6,3	25,47	25	0,47
		0.3	35,24	2,76	32,48	25	7,48
		0.5	37,22	0,79	36,43	25	11,43
	1		37,74	0,26	37,48	25	12,48
1,5			36,001	-1,9	37,901	25	12,901
	1	0,5	35,14	2,85	32,29	25	7,29
1,5	1	0,5	33,7	4,18	29,52	25	4,52
1,5	1	0,5	35,62	2,43	33,19	25	8,19
1,5	1	0,5	35,489	3,67	31,819	25	6,819
1,5	1	0,5	35,56	2,4	33,16	25	8,16
1,5	1	0,5	33,45	5,56	27,89	25	2,89

Tab. I-9: MBA 47 λ performance table

It is worth noting that whenever the requested isolation is not achieved only toward the ground Station nearest to the interferer the receiving Satellite antenna shows a C/I ratio below the requested value and loose the link towards the satellite. The rest of the ground station keep the connection.

I.8.5 DRA Antenna Nulling Analyses

According to Tab. I-7the requested minimum antenna directivity to correctly use the satellite channel is 26.1 dB for DRA.

In the following coverage plots are reported the impact on the whole footprint of the nulling. A focus parameter which affects antenna nulling maximum achievable performance in the beam pointing error (BPE). The BPE is inner related to the precision which the position of the interferer or the authorised station is known with. All the analyses presented in the following take as reference a BPE of 0.05 ° . In order to set which is the minimum distance can be effectively nulled by the antenna system, a progressive sweep analysis is performed. Taking as reference a Ground Station on the Cyprus Island (GS_7) which is the nearest to the most probable interferer origin geographical location. Thus, it will be verified the performance of the nulling system by evaluating the capability to mitigate interferer located from 0.05 ° to 0.4 ° from the authorised station to establish the minimum nullable distance. That notwithstanding after a preliminary analysis, it can be seen that 0.3 ° of angular separation between the intended station and the interferer already introduce an impairment in the directivity of the authorised station which is 2dB over the minimum required directivity Fig. I-78.

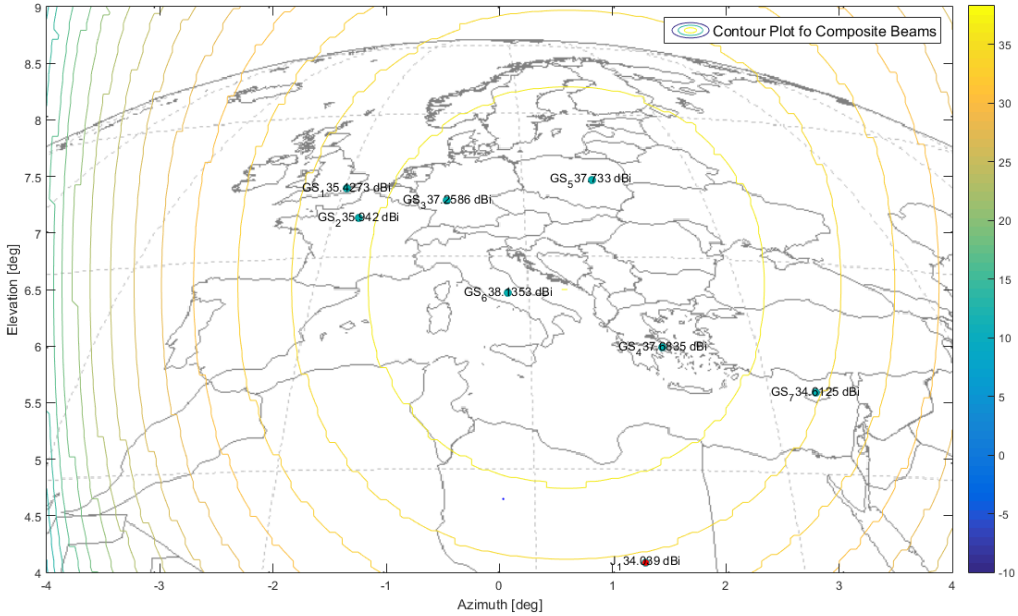

Fig. I-77 : Cold Case Coverage: No nulling sub-system is activated. It represents nominal coverage.

In the following plots are reported the coverage produced by a 23 λ DRA antenna in different nulling scenario. In order to set which is the minimum distance can be effectively nulled by the antenna system, a progressive sweep analysis is performed. Taking as reference a Ground Station on the Cyprus Island (GS_7) which is the nearest to the most probable interferer origin geographical location. Thus, it will be verified the performance of the nulling system by evaluating the capability to mitigate interferer located from 0.05 ° to 0.4 ° from the authorised station to establish the minimum nullable distance.

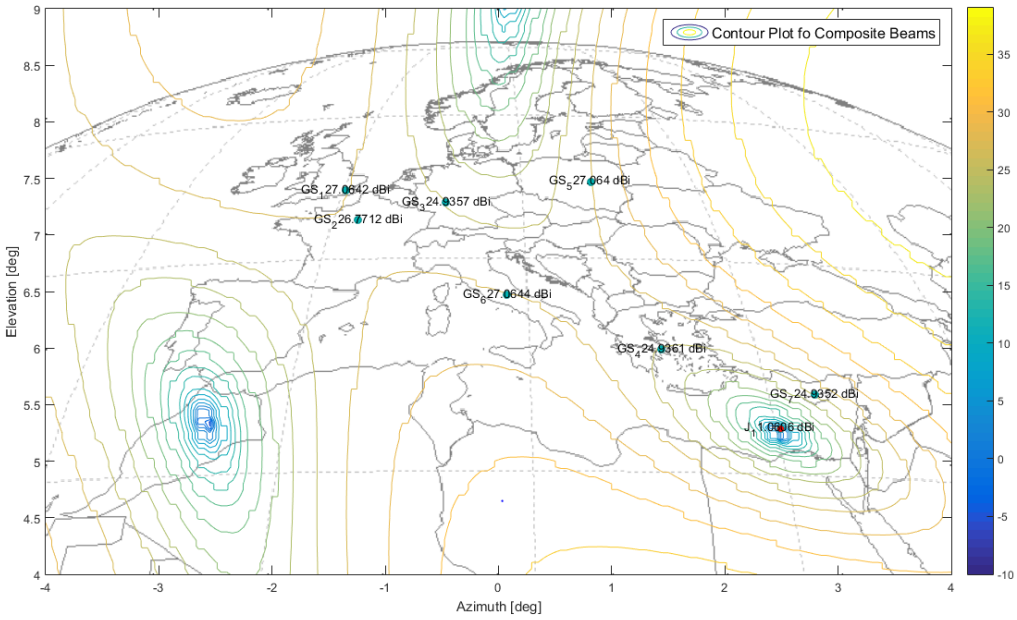

Fig. I-78 : Hot Case: Nulled Pattern with authorised station GS_7 and a 0.3 ° far interferer J_1

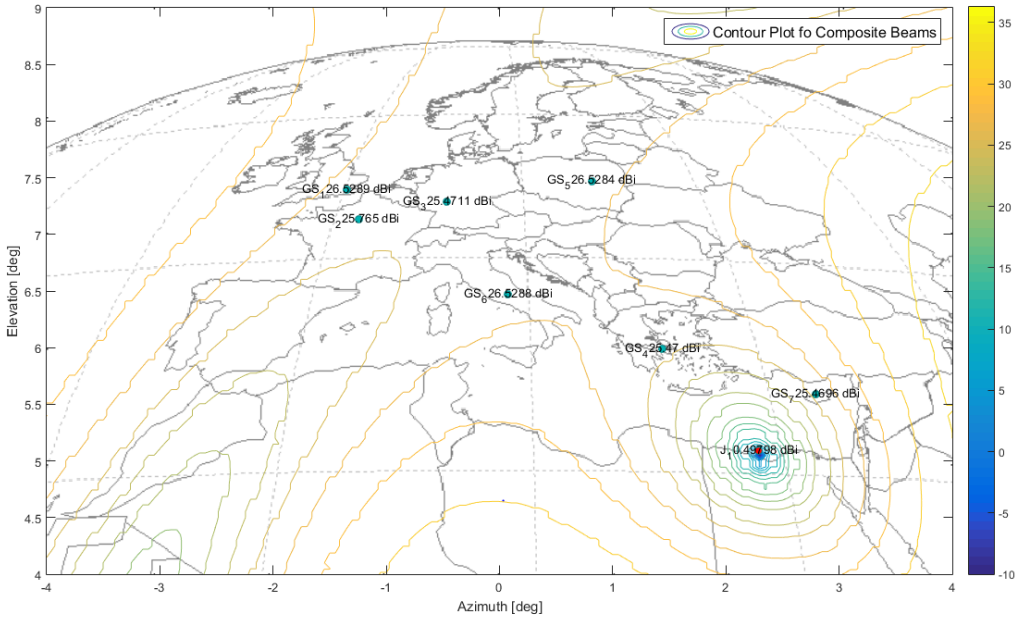

Fig. I-79 : Hot Case: Nulled Pattern with authorised station GS_7 and a 0.5 ° far interferer J_1

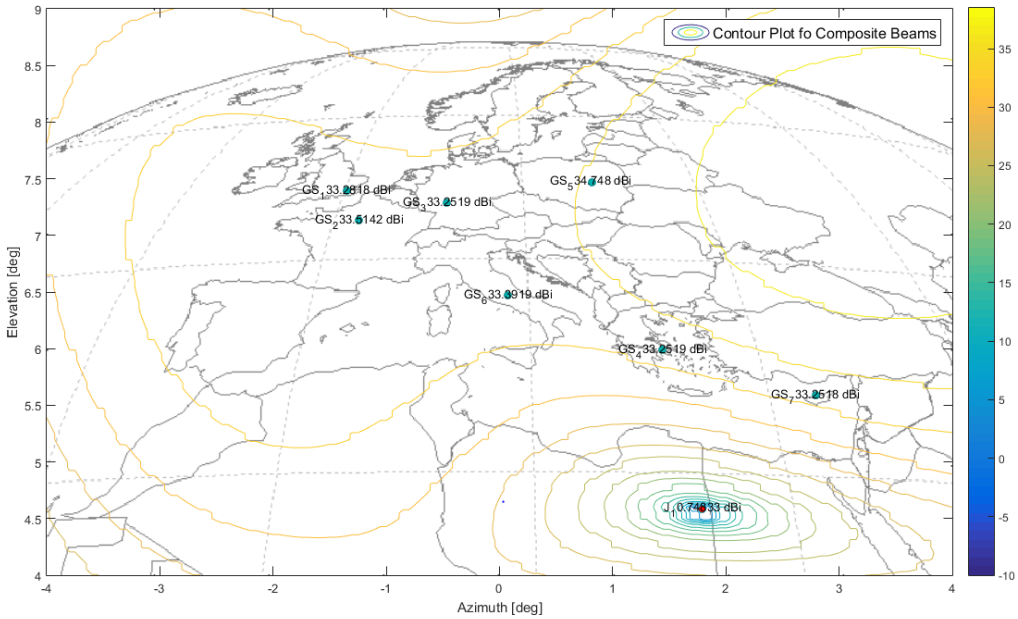

Fig. I-80 : Hot Case: Nulled Pattern with authorised station GS_7 and a 1 ° far interferer J_1

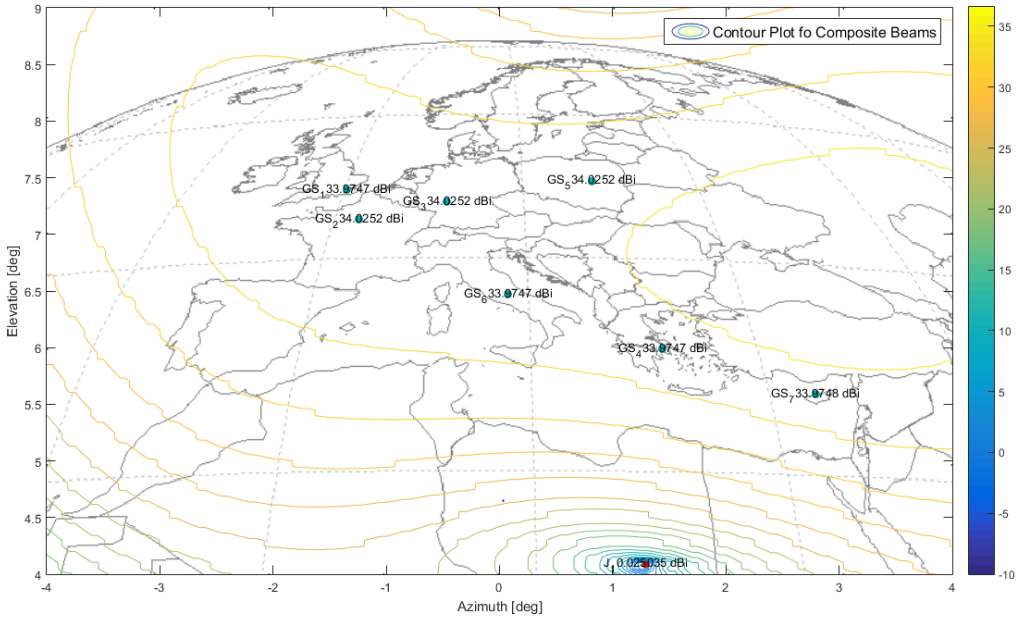

Fig. I-81 : Hot Case: Nulled Pattern with authorised station GS_7 and a 1.5 ° far interferer J_1

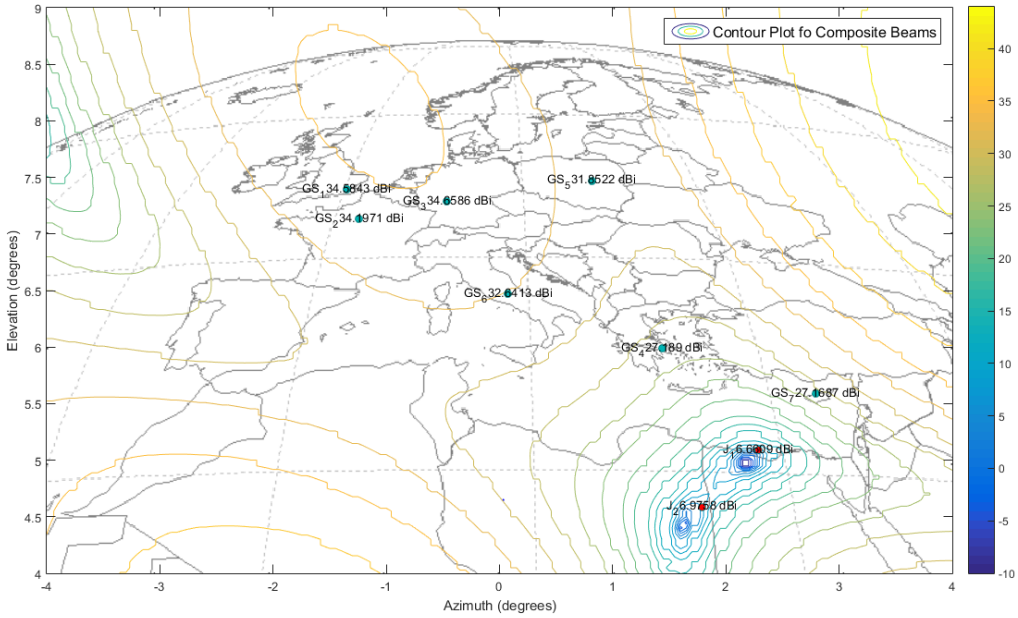

Fig. I-82 : Hot Case: Nulled Pattern with authorised station GS_7 and 2 interferers: a near J_1 (0.5 °) and a far interferer J_2 (1 °)

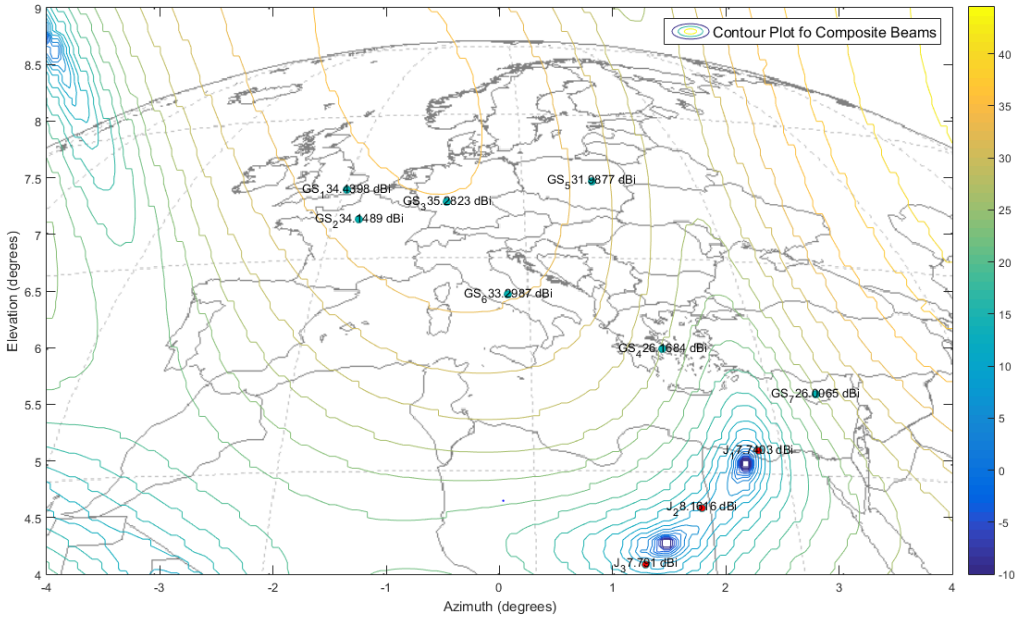

Fig. I-83 : Hot Case: Nulled Pattern with authorised station GS_7 and 3 interferers: a near J_1 (0.5 °) and a far J_2 (1 °) and far out interferer J_3 (1.5 °)

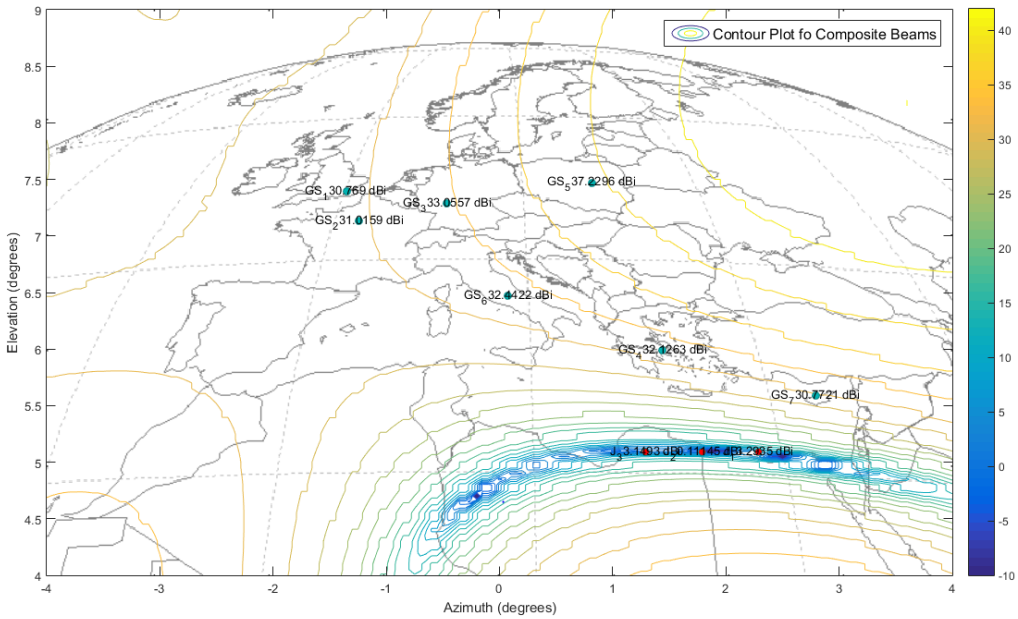

Fig. I-84 : Hot Case: Nulled Pattern with authorised station GS7 and 3 interferers: a near J_1 (0.5 °) and a far J_2 (1 °) and far out interferer J_3 (1.5 °)

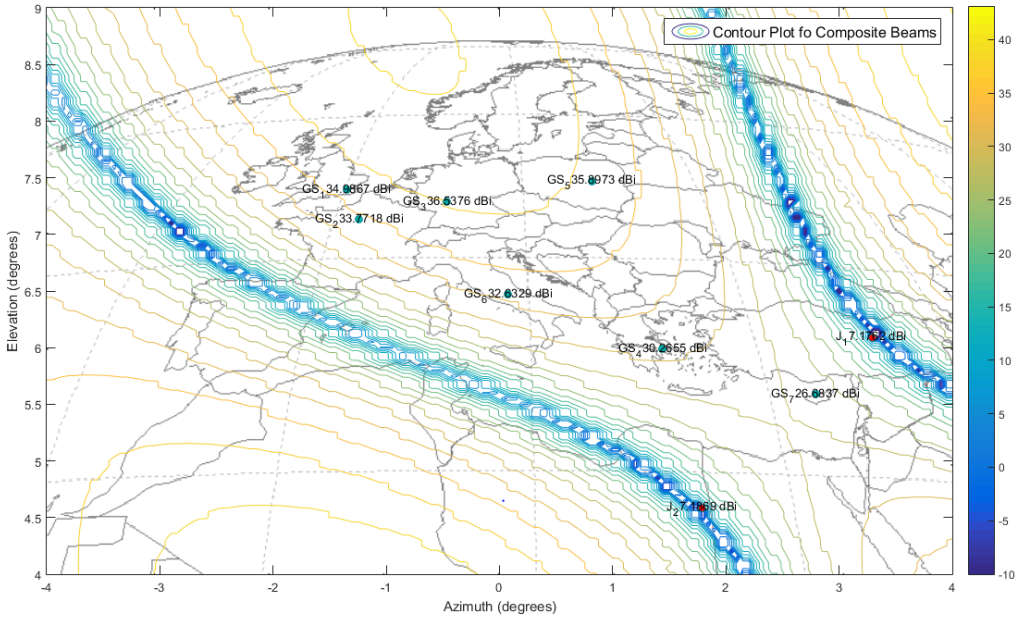

Fig. I-85 : Hot Case: Nulled Pattern with authorised station GS_7 and 2 interferers: a near J_1 (0.5 °) and a far interferer J_2 (1 °)

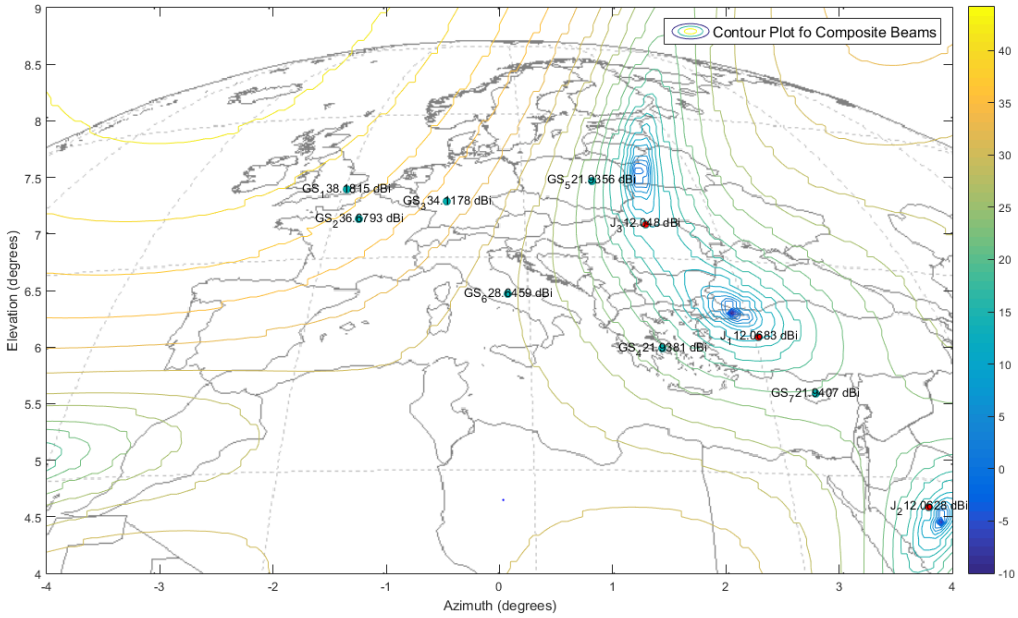

Fig. I-86 : Hot Case: Nulled Pattern with authorised station GS7 and 3 interferers: a near J_1 (0.5 °) and a far J_2 (1 °) and far out interferer J_3 (1.5 °)

A synoptic table will summarize the achieved isolation performances for each of the presented scenario.

J_3	J_2	J_1	Minimum Directivity User [dBi]	Maximum Directivity Jammer [dBi]	Achieved isolation [dBi]	Isolation Req. [dBi]	Delta Isolation [dBi]
		0,3	24,93	1,06	23,87	25	-1,13
		0,5	25,5	0,50	25,00	25	0,00
		1	33,25	0,70	32,55	25	7,55
		1,5	33,97	0,02	33,95	25	8,95
	1	0,5	27,16	6,66	20,51	25	-4,49
1,5	1	0,5	26,00	8,10	17,90	25	-7,10
1,5	1	0,5	30,77	3,30	27,47	25	2,47
	1	0,5	26,68	7,18	19,50	25	-5,50
1,5	1	0,5	21,92	12,06	9,86	25	-15,14

Tab. I-10: DRA 24 λ performance table

It is worth noting that whenever the requested isolation is not achieved, in some operative scenario, like the last one, not only the nearest ground Station to the interferer towards the receiving Satellite antenna shows a C/I ratio below the requested value and loose the link towards the satellite. Other two station are involved and thus losing the link with the requested performance and cannot keep operating properly.

I.9 CONCLUSIONS AND FUTURE WORKS

A robust overview of the interference phenomena that affect commercial satellite system where analysed. After a deep analysis and quantification of the interference phenomena considering also the main revenues' losses by the Operator, following defining suitable qualitative and quantitative criteria to analyse and trading-off the proposed

techniques in term of performance, operativeness and cost/benefit, the candidate techniques have been selected and described, performing on them a suitable trade-off analysis more conditioned by the effectiveness of them also in term of technological heritage as already available at Satellite industrial level and technology readiness level (TRL). To support the analysis phase, a satellite payload simulator has been developed to assess the impairment introduced by the interferer into the satellite communication system at physical level [R. 41]. The simulator has been tested and certified by using actual laboratory test and measurement systems already available at Thales Alenia Space-Italia and grouped under the facility labelled Satellite Network Certification Testbed (SNCT) where dedicated SAT-Link emulators and measurement instrumentations are available. After an extensive overview of the anti-interference techniques technologically implementable at both at RF and Antenna level on the satellite payload, Beam-shaping techniques at antenna level were selected as the most effective.

To mitigate such interference phenomena, antenna system based on phased array with nulling capabilities has been proposed and evaluated in terms of performance with respect to a commercial communication satellite scenario. The analytical formulation of the problem has been developed and studied, afterward with a trade-off analysis two benchmark configurations for both selected antennas has been defined.

A beam-forming algorithm has been implemented with a wide range of antenna simulation tools to prove theoretical assumption and to evaluate nulling performance of the two antenna technologies. As conclusion of the Study, at antenna level, antenna multi spot coverage configuration implemented through a MBA technique provided of Antenna Nulling Technique (ANT) seems to be a more robust and effective solution [R. 40R. 42 R. 43].

By comparison the simulated value, it can be seen in the first place that MBA can mitigate even very near interferer (0.3° w.r.t. 32 λ

reflector and 0.1° w.r.t. 45 λ reflector) respect to the equivalent DRA which became effective only for interferer farther then 0.5°.In terms of multiple nulling point, DRA seems to have limited performance w.r.t. MBA thus notwithstanding as can be seen in reported pattern, DRA allows a very precise beam nulling in space, which is better than the one provided by the MBA. But since MBA shows a narrower beam-width w.r.t. DRA (1.7° vs. 2.3°) and provided that the nulling performance are deeply related to the single analytic beam-width of the component antenna [R. 32,R. 33,R. 34], thus a larger radiating aperture would be necessary to fulfil the selected interference scenario requirements.

Beside, DRA turns out to have the following points of strength to respect the MBA: its uniform aperture distribution tapering needs about 20% narrower aperture to respect reflector MBA, due to the fact that it has an larger number of element an high quality theoretical beams can be implemented linearly controlling the phase of radiating aperture array elements and for the same reason an higher coverage flexibility w.r.t. MBA can be implemented, because increasing the number of elements used for sampling the aperture, the control of the pattern shaping increases. Moreover a DRA can be easily accommodated on the earth deck if the radiating aperture is of the order of the satellite earth deck dimension (around 1.5 m) with active element directly inside the spacebus. On the other hand, MBA presents an easier accommodation on spacecraft thanks to the fact that part of the reflector can be allocated outside the spacecraft body and the number of the radiant chains is considerably less than DRA's. The reduction of the number of active RF chains of a MBA in fact, can be close to a minimum w.r.t. a DRA, because MBA does not require sub-arraying for avoiding "grating lobes "; In the end a frequency insensitive in more easily achievable with MBA which intrinsically less sensitive to frequency variation while the DRA requires true time delays lines to avoid null mispointing in function of frequency.

Provided the above considerations and the performance results, MBA solution appears to be a better candidate w.r.t. the DRA for what concerns a an inti interference solution with a low impact on the commercial satellite in terms of costs. MBA is a good compromise between nulling performances and embark-ability on board payload comply, into a suitable range, with “low cost “requirement at the end this can guarantee to a possible Customer (Operator) a suitable AI/AJ solution with a convenient final cost both financially and for what concern the operative behaviour.

It is worth noting that w.r.t. to the implemented footprint, DRA shows a very good control of the radiation pattern, as increase the number of element. Thus, DRA is the candidate technique if besides the nulling system, a flexible and reconfigurable coverage wants to be implemented.

Antenna Nulling approach for communication satellite network is an effective and innovative way to approach the soaring problem of interference mitigation in such network [R. 44].

To these days, array antennas have been employed on commercial satellites from few years, however as technology from the military sector, in which it is used for protecting just one transponder, makes itself commercially available and attractive, as shown in the commercial analyses performed even in this work, it is foreseen an evolution of the role of the array as they respond to ever increasing demands from satellite operators. Not only they provide the effective ability of interference mitigation, as showed by this work. Besides improved volume footprints that aid accommodation of multi-band payloads, reduction in hardware for additional beams, flexibility in coverage definition are all key aspects that have seen an increasing demand for array antennas, and phased arrays on-board commercial telecommunication satellites.

Now the problem formulation and the trade-off analysis to select the more effective antenna technology has been developed and supported by a wide range of analyses for a typical commercial satellite scenario taking into account coverage and link budget analyses and antenna nulling capabilities by this work. This work has provided a very detailed overview over the anti-interference techniques based on nulling antenna system which could be implemented to counteract especially deliberate interferences for commercial satellites and it has represented a solid contribution to feasibility analyses and to definition of requirements of the next generation satellite systems. The focus of this study is on the mitigation of interferences at the satellite up-link level and the target time frame for a first implementation and in orbit introduction of the solution proposed shall be 2017, in accordance to the its development forecasts and the its technology readiness level [R. 66].

II. CHAPTER II

Inhomogeneous Wave Generation for Deep Penetration In Lossy Media

II.1 Introduction

During the last phase of my doctorate, I focused my research activity on a study of feasibility of a novel kind of antenna, which could generate an inhomogeneous wave in a lossless medium with a different approach from the well-known leaky wave antenna techniques. The aim of the activity was to prove how such waves can be also easily generated from the transmission of a homogeneous wave through a dissipative solid. Considering a dissipative triangular prism immersed in the free space, with the first interface illuminated by a homogeneous wave, an inhomogeneous wave is generated at the second interface. The results of the study represent a concrete and innovative approach to generate inhomogeneous waves which can find applications for the deep penetration of lossy materials.

II.1.1 Structure of The Work

In development of the research activity is structured in different phases which are briefly summarised, as follows:

In the first place a theoretical analysis of the antenna system was performed in the approximation of geometrical optics in order to define

a first level design and to prove the concept. By the mean of ad-hoc built software routines, parametric analysis of the phase $\underline{\beta}_3$ and attenuation $\underline{\alpha}_3$ vectors has been carried out with respect to different lossy material, χ prism angle and ξ_i incident angle of the plane wave. These ad hoc routines can easy allow to predict all the relevant parameters of the antenna.

The Optics of the system has been designed: a feed which fed the polarizer prism has been chosen as target antenna architecture. After a trade-off analysis the feed model has been assumed as an aperture antenna. A sensitivity analysis of the variation of characteristic antenna parameters as pointing angle and radiation pattern after the interaction with the prism have been predicted based on theoretical formulas by an ad-hoc developed software tool to create a theoretical baseline to be compared with the simulated one.

An ad –Hoc optimizer has been developed in order to varying the four characteristic parameters of the system (χ, ξ_{1i}, ε' and tgδ), which fully control the system, in order to maximize the derived parameters such, the phase vector of the leaky wave emerging from the prism. These design parameters can be employed to force the condition of deep penetration in lossy material in order to reduce wave attenuation towards the propagation phase direction.

To validate the theoretical assumption, and the effectiveness of such antenna in generating an inhomogeneous wave a full wave Frequency domain FEM model has been set. A WR90 interface Pyramidal Horn antenna in Ku-band has been designed to feed the prism with a homogenous plane wave. The distance between the horn and the prism has been initially set major than Fraunhofer distance so that only radiative Fairfield field has been considered.

Full Wave Simulated results were analysed with respect to the theoretical ones and conclusions were carried out.

In conclusion, a practical trade-off analysis for antenna parameter choice is presented. The aim of the analysis is to set antenna design parameters in order to generate a leaky wave radiation pattern to implement the deep penetration condition in lossy media.

II.2 Electromagnetic Waves penetration into lossy media

II.2.1 Theoretical background

Let us consider an electromagnetic plane wave incident, as in its most generic form. The propagation vector . $\underline{\boldsymbol{k}}$ is a complex vector $\underline{\boldsymbol{k}}=\underline{\boldsymbol{\beta}} - j\,\underline{\boldsymbol{\alpha}}$.. The incident phase vector $\underline{\boldsymbol{\beta}}$ and the attenuation vector $\underline{\boldsymbol{\alpha}}$ are the real and the imaginary part of the propagation vector respectively. The most general relation between these vectors with frequency is related to the Dispersion equation:

$$\underline{\boldsymbol{k}} \cdot \underline{\boldsymbol{k}} = k_0{}^2 \mu\varepsilon \quad with \quad \underline{\boldsymbol{k}}=\underline{\boldsymbol{\beta}} - j\,\underline{\boldsymbol{\alpha}} \tag{II.1}$$

We suppose the wave propagates in a lossy medium, whose characteristic conductivity is $\sigma \neq 0$. In such media, can be generated both homogenous and inhomogeneous waves.

$$Homogenous\ Waves \rightarrow \begin{cases} \boldsymbol{\alpha} \neq \mathbf{0} \\ \underline{\boldsymbol{\beta}} \cdot \underline{\boldsymbol{\alpha}} = \boldsymbol{\alpha\beta} \end{cases} \tag{II.2}$$

$$Inhomogenous\ Waves \rightarrow \begin{cases} \boldsymbol{\alpha} \neq \mathbf{0} \\ \underline{\boldsymbol{\beta}} \cdot \underline{\boldsymbol{\alpha}} = \boldsymbol{\alpha\beta cos(\eta)} \end{cases} \tag{II.3}$$

Where η represents the angle between $\underline{\boldsymbol{\alpha}}$ and $\underline{\boldsymbol{\beta}}$, also called inhomogeneity angle. It is worth noting that the properties of the general inhomogeneous wave which is generated in a lossy medium are defined by the material properties according to:

$$\begin{cases} \boldsymbol{\beta}^2 - \boldsymbol{\alpha}^2 = \boldsymbol{k_0}^2 \boldsymbol{\varepsilon}' \\ 2\boldsymbol{\beta}\boldsymbol{\alpha}\cos\boldsymbol{\eta} = \boldsymbol{k_0}^2 \boldsymbol{\varepsilon}'' \end{cases} \tag{II.4}$$

In a lossless medium, whose characteristic conductivity is $\sigma=0$. Thus, the general solution of the Maxwell Equations due to the material properties is a homogeneous wave ($\boldsymbol{\alpha}=0$). Inhomogeneous waves can be generated in lossless media too. The condition to generates such waves is:

$$\begin{cases} \boldsymbol{\alpha} \neq \mathbf{0} \\ \underline{\boldsymbol{\beta}} \cdot \underline{\boldsymbol{\alpha}} = \mathbf{0} \end{cases} \tag{II.5}$$

Such $\underline{\boldsymbol{\beta}}$ and $\underline{\boldsymbol{\alpha}}$, which fulfil this condition are related not to material properties but to antenna boundary conditions. Antennas which can generates such waves is called Leaky Wave Antennas and the emerging waves are called leaky waves.

Let us consider an interface between two lossy media, medium 1 and medium 2. If we suppose a media interface parallel to the y-z plane so x is the normal direction to the interface according to the next figure.

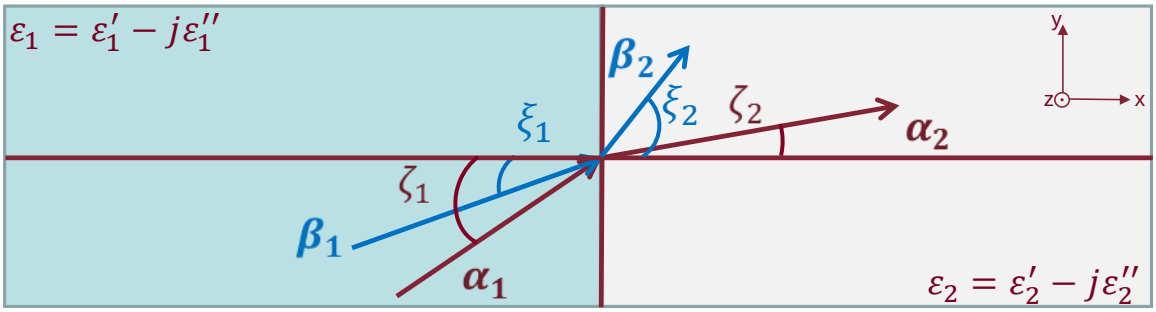

Fig. II-1 Geometry of the Problem.

Assume an electromagnetic plane wave coming from medium 1 with expression $e^{j(\underline{\boldsymbol{k_1}}\cdot\underline{\boldsymbol{r}}-\boldsymbol{\omega t})\cdot}$, where the propagation vector is a complex vector: $\underline{\boldsymbol{k_1}}=\underline{\boldsymbol{\beta_1}} - j\,\underline{\boldsymbol{\alpha_1}}$.The incident phase,$\underline{\boldsymbol{\beta_1}}$, and attenuation,$\underline{\boldsymbol{\alpha_1}}$, vectors form the angles ξ_1 and ζ_1, respectively, with the normal to the interface. The angle between the two vectors is $\eta_1 = \zeta_1 - \xi_1$. Similarly, the transmitted wave vector, $\underline{\boldsymbol{k_2}}$, has phase and attenuation vectors forming angles ξ_2, ζ_2, as shown in, and $\eta_2 = \zeta_2 - \xi_2$. Let us define the wavenumbers $\boldsymbol{k_0}$, $\boldsymbol{k_1}$, and $\boldsymbol{k_2}$, associated to vacuum, medium 1, and medium 2, respectively.

It is worth noting that the of the absolute values of vectors $\underline{\boldsymbol{\beta_1}}$, and attenuation,$\underline{\boldsymbol{\alpha_1}}$. Are uniquely defined by material properties in accordance to:

$$\beta_1 = k_0\sqrt{\frac{\epsilon_1'}{2}}\sqrt{1+\sqrt{1+\left[\frac{tan(\delta_e)}{\cos(\eta_1)}\right]^2}} \qquad \text{(II.6)}$$

$$\alpha_1 = k_0\sqrt{\frac{\epsilon_1'}{2}}\sqrt{1-\sqrt{1+\left[\frac{tan(\delta_e)}{\cos(\eta_1)}\right]^2}}$$

With $\eta_1 = \zeta_1 - \xi_1$ and $tan(\delta_e) = \frac{\epsilon_1''}{\epsilon_1'}$

The reflected and transmitted wave can be easily computed with well-known relations. By the means of the generalized Snell condition:

$$\begin{cases} \beta_1 sin\,\xi_1 = \beta_2\, sin\,\xi_2 \\ \alpha_2 sin\,\zeta_1 = \alpha_2\, sin\,\zeta_2 \end{cases} \tag{II.7}$$

And the dispersion equation:

$$\begin{cases} \beta^2 - \alpha^2 = {k_0}^2 \varepsilon' \\ 2\beta\alpha\, cos\ (\zeta_2 - \xi_2) = {k_0}^2 \varepsilon'' \end{cases} \tag{II.8}$$

The transmitted waves have a phase and attenuation vectors absolute value can be expressed as follows:

$$\beta_2 = \sqrt{\frac{\left|k_{1y}\right|^2 + Re\left({k_2}^2\right) + \left|{k_{1y}}^2 - {k_2}^2\right|}{2}} \tag{II.9}$$

$$\alpha_2 = \sqrt{\frac{\left|k_{1y}\right|^2 - Re\left({k_2}^2\right) + \left|{k_{1y}}^2 - {k_2}^2\right|}{2}}$$

The phase vector forms an angle ξ_2 with respect to the x-direction and the attenuation vector forms an angle ζ_2. By the Snell condition the behaviour of these two angles can be described, since:

$$\begin{cases} \frac{\beta_1}{\beta_2} sin\,\xi_1 = sin\,\xi_2 \\ \frac{\alpha_1}{\alpha_2} sin\,\zeta_1 = sin\,\zeta_2 \end{cases} \tag{II.10}$$

Thus, it can be evaluated the behaviour of these two angles with respect to the incident angle [R. 51]. A detailed description of the analytical solution for the Snell condition in this case of study can be found in literature [R. 48]. The solution can be calculated for and it is dependent on the ratio the losses of the two media: In the particular case of nonmagnetic media, the parameter, it reduces to the ratio of the imaginary parts of the relative permittivity. The solution presents the behaviour reported in Fig. II-2

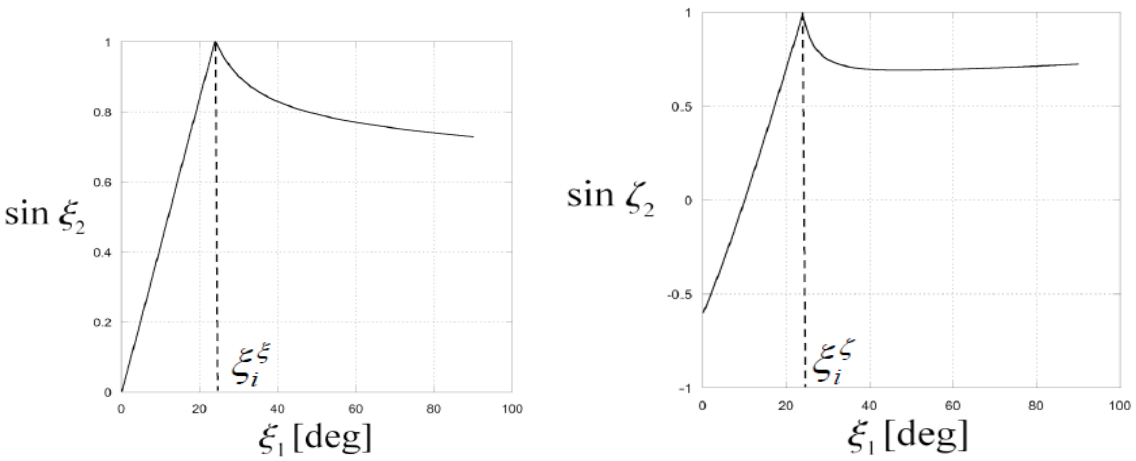

Fig. II-2 Transmitted Angles behaviour.

Two critical angles turn out by the solution: ξ_1^{ξ} and ξ_1^{ζ}. These two solution are related to a specific value of the transmitted angles:

$$\xi_i = \xi_1^{\xi} \Big| \xi_2 = \frac{\pi}{2} \tag{II.11}$$

$$\xi_i = \xi_1^{\zeta} \Big| \zeta_2 = \frac{\pi}{2}$$

As can be seen by inspection Fig. II-2 , the transmitted angles keep growing after these two angles of incidence. Now that the expressions

of ξ_1^{ξ} and ξ_1^{ζ} have been computed, let us try to get a physical interpretation of the

transmitted wave for these particular angles. When the incident wave, at a fixed η_1, has a phase vector with $\xi_i = \xi_1^{\xi}$ the transmitted phase vector is parallel to the interface, and the attenuation vector forms an angle ζ_2 with the normal to the interface. This wave has the constant phase planes orthogonal to the interface, and it's purely real power flow is orthogonal to α_2, if a TE wave is considered [R. 48]. Thus the transmitted wave is very similar to a surface wave which propagates along the y-direction over the y-z plane.

$$\xi_i = \xi_i^{\xi} \Big| \xi_2 = \frac{\pi}{2}$$

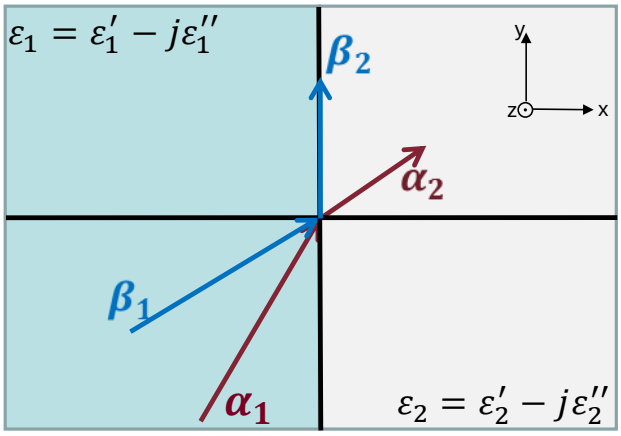

Fig. II-3 $\xi_i = \xi_1^{\xi}$ condition, constant-phase planes orthogonal to the interface.

More interesting is the other case, for a phase incident vector with $\xi_i = \xi_1^{\zeta}$.

The transmitted wave, in this case, has the constant amplitude plane orthogonal to the interface ($\zeta_2 = \frac{\pi}{2}$), and the phase vector with an angle ξ_2. That means the wave is not attenuated in the direction orthogonal to the interface, and it's purely real power flow, in the case of TE

polarization, is orthogonal to the interface, too. This result is surprising because it is achieved a transmitted wave in a lossy medium, which is not attenuated in the direction where the medium extends. This condition is defined "*Deep Penetration*".

$$\xi_i = \xi_i^{\zeta} \Big| \zeta_2 = \frac{\pi}{2}$$

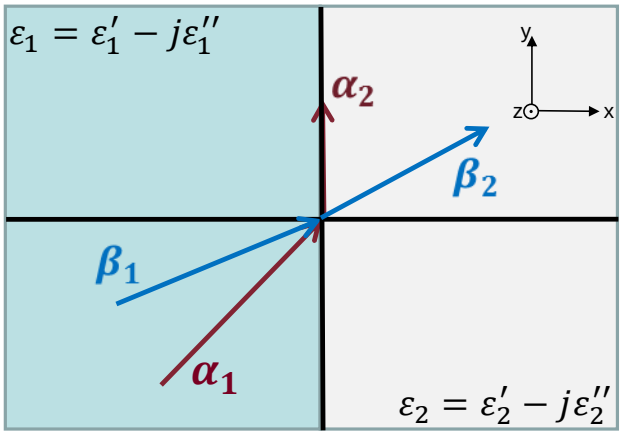

Fig. II-4 $\xi_i = \xi_1^{\zeta}$. condition, constant amplitude planes orthogonal to the interface.

Considering now an inhomogeneous wave generated in a lossless media, which shows an attenuation vector amplitude as $\alpha_1 \neq 0$ thus provided a $\underline{\boldsymbol{\beta}} \cdot \underline{\boldsymbol{\alpha}} = \mathbf{0}$, it results an inhomogeneity angles as $\eta_1 = \frac{\pi}{2}$.

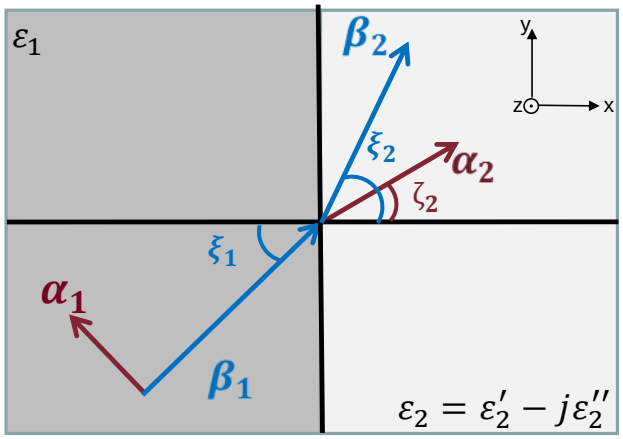

Fig. II-5 Leaky Wave incident over a lossy medium surface.

The transmitted wave is an inhomogeneous wave propagating in the lossy media and the deep penetration condition ($\xi_i = \xi_i^{\zeta} \left| \zeta_2 = \frac{\pi}{2}. \right.$) can be achieved for a determined angle of incidence which depends on the losses of the second medium ε_2'' and on the properties of the first medium $\beta_1 \cdot \alpha_1$:

$$\xi_{DPW} = \frac{1}{2} arcsin\left(\frac{k_0^2 \varepsilon_2''}{\beta_1 \alpha_1}\right) \tag{II.12}$$

Equation (12) makes sense when the argument of the inverse sine is less than 1. From this constraint, we can calculate the minimum value of β_1, which allows the effect. With some algebra, we found the following condition [R. 48]:

$$\beta_1 \geq \frac{k_1}{\sqrt{2}} \sqrt{1 + \sqrt{1 + \left[\frac{2Im(k_2^2)}{k_1^2}\right]^2}} \tag{II.13}$$

In order to trigger the effect of deep penetration a moderate value of phase vector amplitude is required β_1. In conventional Leaky -Wave Antenna, relative low phase vector amplitude is achievable. Increasing the amplitude of the phase vector, the aperture beam-width increases so that the wave cannot be approximated as a plane wave anymore. This consideration leads to the research of an alternative way to generate inhomogeneous waves in lossless media.

The generation of leaky wave is widely studied in the literature, and it is possible with the so-called leaky-wave antennas. Such antennas are traveling-wave antennas: open guiding structures designed to make the radiating mode (leaky mode) the dominant one [R. 49]. However, in recent studies has been pointed out that an inhomogeneous wave can

be obtained by irradiating with a homogeneous wave a dissipative prism, i.e., a two-dimensional lossy dielectric structure with two non-parallel interfaces [R. 50]. In the present paper, we consider the theoretical model of a lossy prism illuminated by a plane wave, and make some considerations on the properties of the transmitted inhomogeneous wave. It is important to emphasize that for the purpose of the study, it has been considered a finite-beam and treated in optical approximation in order to neglect the interaction with the wedge of the prism, which has been considered as a second order effect.

II.3 Lossy Prism Leaky Wave Antenna

The generation of inhomogeneous electromagnetic waves in a lossless medium is generally associated to leaky-wave antennas. In the present chapter it is shown how such waves can be also easily generated by the transmission of a homogeneous wave through a dissipative dielectric layer. A dissipative triangular prism in the free space, whose first interface is fed by a homogeneous wave can be employed to generate an inhomogeneous wave emerging at the second interface. The phase and attenuation vectors obtained are evaluated against the geometry and the material of the prism. The results illustrate a novel approach in generating inhomogeneous waves in lossless media which finds applications for the deep penetration of lossy materials.

II.3.1 Analytic problem formulation

Inhomogeneous waves are typical solutions of the Maxwell equations at the interface between two semi-infinite media [R.46], [R.47]. Inhomogeneous waves can be generated in lossless media by means of appropriate radiative structures, in which the field shows a complex wave number. These field solutions are also known as leaky

waves. In fact, their generation is generally made possible by introducing some leakage effect in the travelling-wave path, like opening the guiding structure, creating the so-called leaky-wave antennas. Such antennas are traveling-wave antennas: designed in order to make a radiating mode (leaky mode) the dominant one [R.48]. Nevertheless, in recent studies, it has been pointed out that an inhomogeneous wave can also be obtained by illuminating with a homogeneous wave a dissipative dielectric [4]. Let us consider a lossy two-dimensional triangular prism immersed in the free space as a dissipative dielectric with two non-parallel interfaces, forming an angle c, as shown in Fig. 1. We consider a quasi-plane wave incident at an angle x1i on the left side (vertical side) of the prism. We suppose that, using a geometrical-optics approximation, given the characteristics of a quasi-plane wave, the wave does not interact with the prism's wedges. In other words, a finite beam is considered impinging on the prism. The described system is considered to work at X-band (10.6 GHz) aiming at reducing the dimensions for the prism and at investigating the viability of generating an inhomogeneous wave for the deep penetration through lossy media at such frequencies, as never done before in the literature [R. 46].

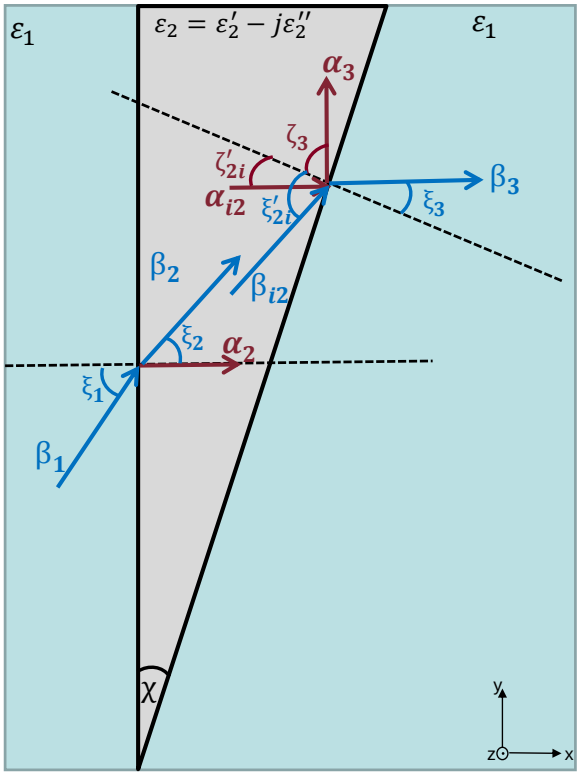

Fig. II-6 Leaky Wave incident over a lossy medium Prism – Reference Geometry.

The reflected and transmitted waves in the system, can be easily computed at both interfaces with well-known relations [R. 51]. While the incident vector has a null attenuation vector (lossless medium), the wave transmitted after each interface has both non-null attenuation and phase vectors. At the first interface (vertical side) of the prism, the phase vector forms an angle ξ_1 with respect to the z-axis, while the attenuation vector must be perpendicular to the interface. The wave impinges then on the second interface (oblique side) of the prism with an angle of the phase vector equal to ($\boldsymbol{\xi'_{2i} = \xi_2 + \chi}$) with respect to the normal direction to the interface. The attenuation vector impinges on the second interface with an angle $\boldsymbol{\chi}$ with respect to the normal direction to the interface ($\boldsymbol{\zeta'_{2i} = \chi}$).

The reflected and transmitted waves at the second interface can be computed using the results presented in [R. 52]–[R. 54]. The transmitted waves phase and attenuation vectors amplitude can be expressed as follows:

$$\beta_3 = \sqrt{\frac{\left|k_{i2y}\right|^2 + Re\left(k_3{}^2\right) + \left|k_{i2y}{}^2 - k_3{}^2\right|}{2}} \tag{II.14}$$

$$\alpha_3 = \sqrt{\frac{\left|k_{i2y}\right|^2 - Re\left(k_3{}^2\right) + \left|k_{i2y}{}^2 - k_3{}^2\right|}{2}}$$

Where k_{i2y} represents the amplitude of the imaginary part of the tangential component of the propagation vector, in the lossy material, the prism is made of.

On the other hand, the angles which attenuation and phase vectors define with respect to the normal direction of the prism can be calculated as:

$$\zeta_3 = arcsin\left(\frac{\alpha_2}{\alpha_3} sin\, \zeta'_{\mathbf{2i}}\right) \tag{II.15}$$

$$\xi_3 = arcsin\left(\frac{\beta_2}{\beta_3} sin\, \xi'_{\mathbf{2i}}\right)$$

In particular, transmitted wave results as an inhomogeneous wave. In fact, in lossless medium (the free space), the attenuation vector and the phase vector computed after the second interface result orthogonal, meaning that the equi-phase planes and the equi-amplitude planes are perpendicular to each other :

$$\zeta_3 - \xi_3 = \pm\frac{\pi}{2} \tag{II.16}$$

It is worth noting that the amplitude of the phase vector β_3 , in accordance to II.14, can be expressed as:

$$\beta_3 = f(\chi, \xi_1, \epsilon_2', tan\,\delta) \tag{II.17}$$

Thus, it results that β_3 can be controlled:

- by changing the material properties of the dissipative prism, its permittivity ϵ_2', or its loss tangent $tan\,\delta$,
- by modifying the incident angle of the feeding wave ξ_1
- by varying the angle of oblique prism interface χ

Once a lossy material to be penetrated by an electromagnetic wave is selected, this particular solution to generates inhomogeneous wave in a lossless medium provide additional degrees of freedom to set properties of the wave emerging from the prism in order to match the condition of deep penetration (II.13).

II.3.2 Antenna Design Parameters: Performance and Results

This innovative type of antenna has been developed to provide an easier way to generate inhomogeneous wave in lossless media in order to implement the deep penetration condition. As anticipated by varying the four characteristic parameters of the system $\chi, \xi_1, \epsilon_2', tan\,\delta$, relevant numerical results can be obtained. In particular, it will be highlighted how the angle of incidence ξ_1 appears paramount in defining characteristics of the system. For this reason, all the figures reported depends on such quantity. All the analytical results here

presented have been carried out by numerical simulation of the model in the approximation of geometrical optics. The reference scenario has been selected in X-Band (10.6 GHz) and where is not differently specified the dielectric prism material selected is the FR4 ($\boldsymbol{\epsilon_2' = 4.3}$ and $\boldsymbol{tan\,\delta = 0.025}$ at X-band.

As first results the normalised phase and attenuation vector amplitudes are reported.

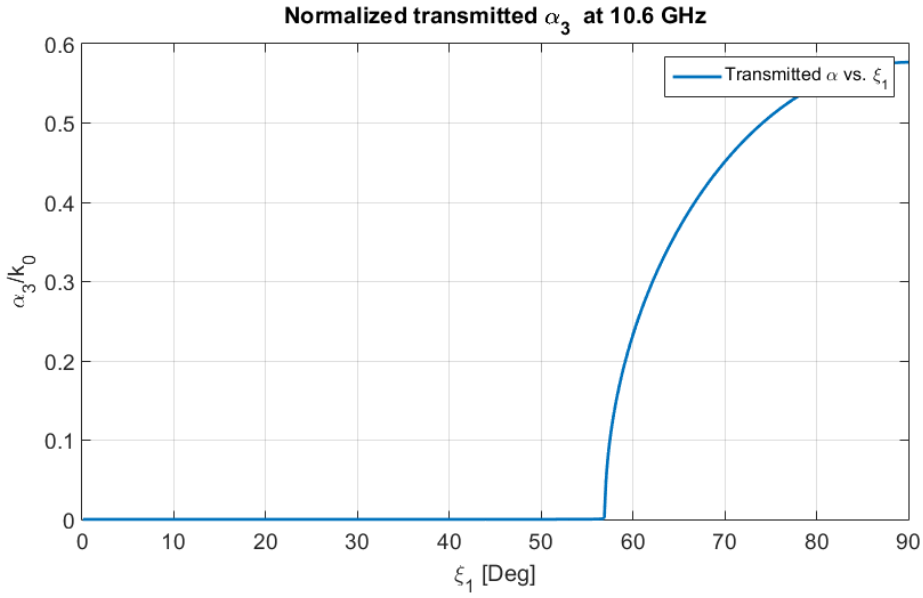

Fig. II-7 Attenuation vector amplitude behaviour.

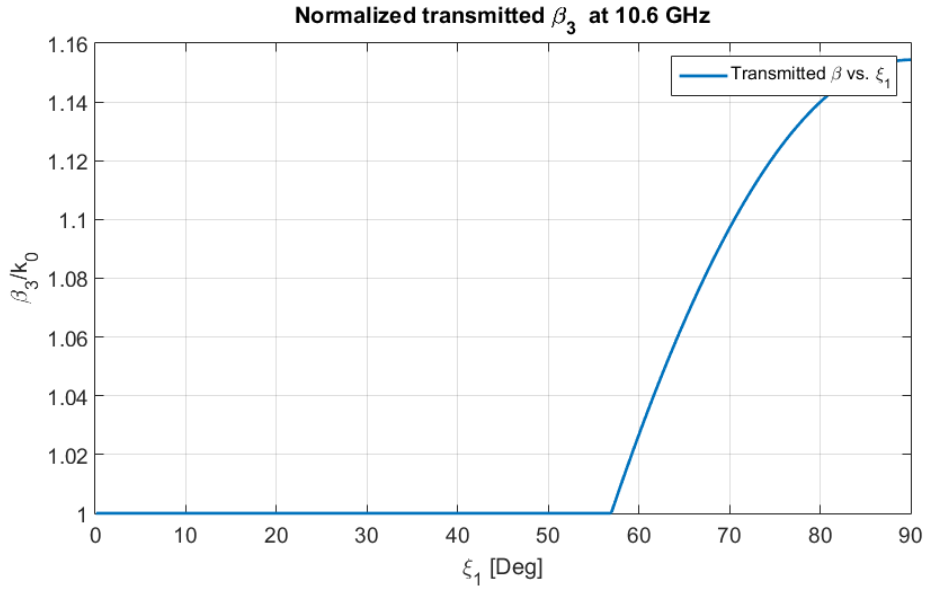

Fig. II-8 Phase vector amplitude behaviour.

In Fig. II-7 and Fig. II-8 the magnitudes of the attenuation and phase vectors are shown, respectively, functions of the angle of incidence and of the angle of the prism considering FR4 dielectric as lossy material. A step-behaviour of the magnitudes can be noted. The vectors' magnitudes are approximately constant, and equal to 0 and k_0 respectively, for a wide spectrum of the incident angles, but, the magnitude of both starts to increase for values greater than a specific critical angle. This behaviour is of extreme interest for the purpose of this study since it shows how the wave number of the transmitted field changes, by varying the incident angle. Moreover, the behaviour can be understood recalling the total internal reflection at the interface between two lossless media: in this case, after the critical angle, the transmitted wave is a surface wave with high magnitude of the phase vector. Here, we find the same behaviour. However, when lossy media are considered, we cannot talk about total reflection, because the reflection coefficient cannot be exactly equal to 1. Then, we can say that the critical angle in Fig- 7-8 is very close to the critical angle of the total reflection, we should call it angle of quasi-total reflection. As can be noted, transmitted wave turns into inhomogeneous wave for proper incident angles and its attenuation and phase vectors absolute values are higher than the threshold which allows the deep penetration condition in lossy materials [R. 48]. This notable result can be of interest in several applications. We must emphasize that the ratio of the attenuation vector magnitude with respect to the wave number is never zero before the critical angle, but it is considerably smaller than one, as typical for inhomogeneous waves generated by leaky wave antennas.

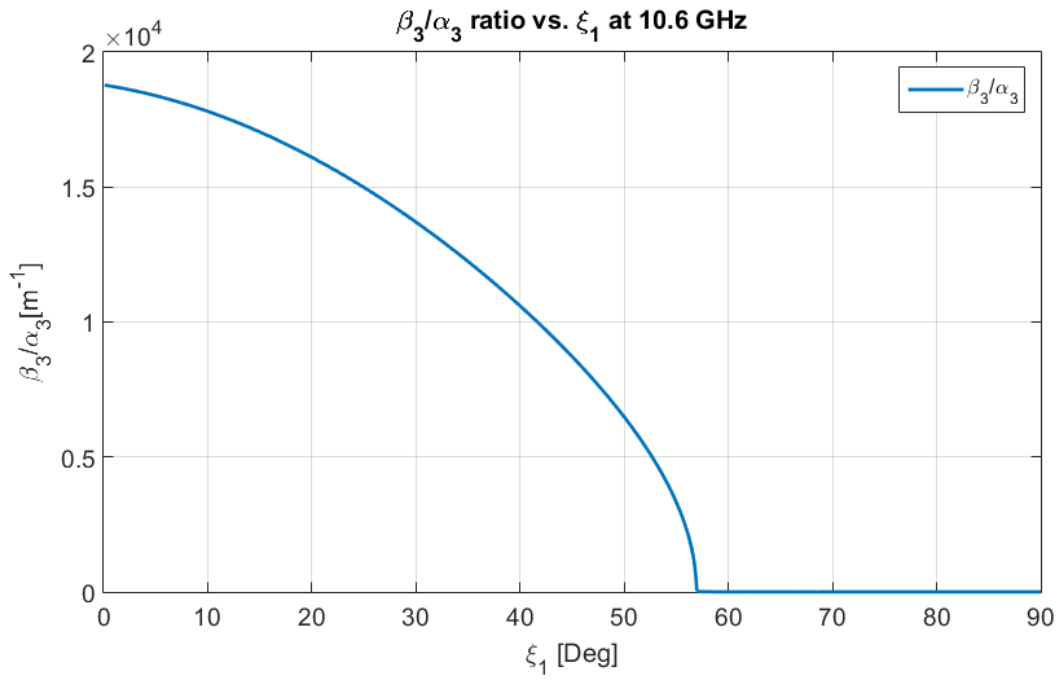

Fig. II-9 Phase vs Attenuation vector amplitude ratio behaviour.

The ratio $\frac{\beta}{\alpha}$ gives a hint on the purity of the leaky wave that can be generated by the structure. A large value of β is requested to fulfil the deep penetration condition, on the other hand a low value of α is desired to have a focused beam. Remarkable ratio can be obtained in the selected study case.

It is worth noting that when $\boldsymbol{\xi_1}$ approaches the 57.24 ° both β_3 and α_3 increases. By comparing these results with the transmitted field angles with respect to the normal to the prism surface, the predicted behaviour in case of surface wave can be recognized.

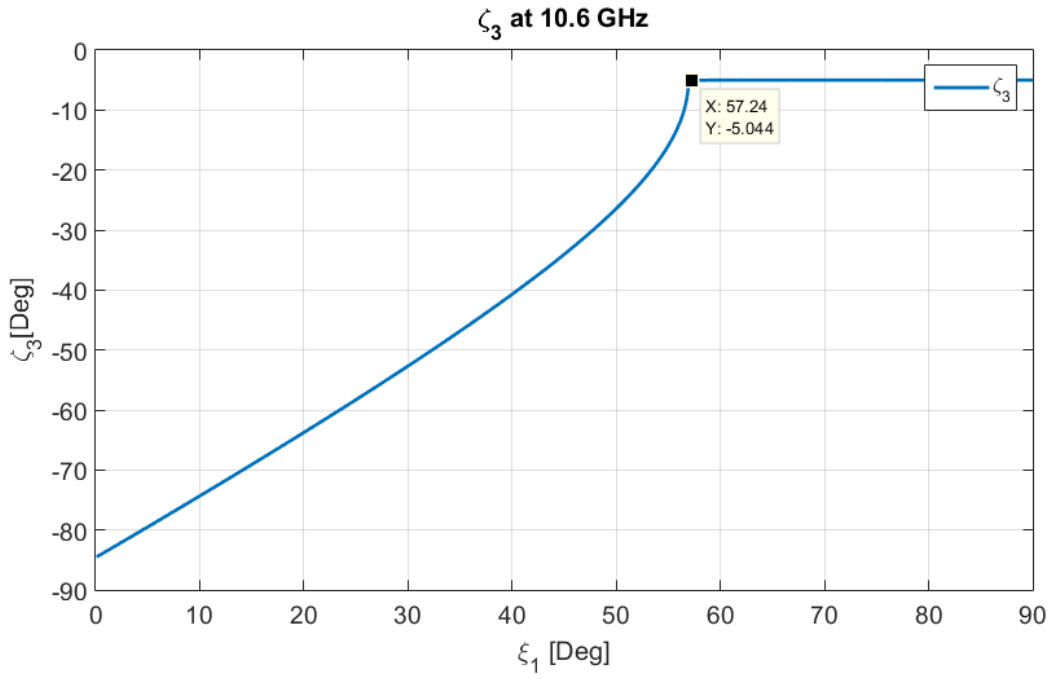

Fig. II-10 Attenuation vector angle behaviour.

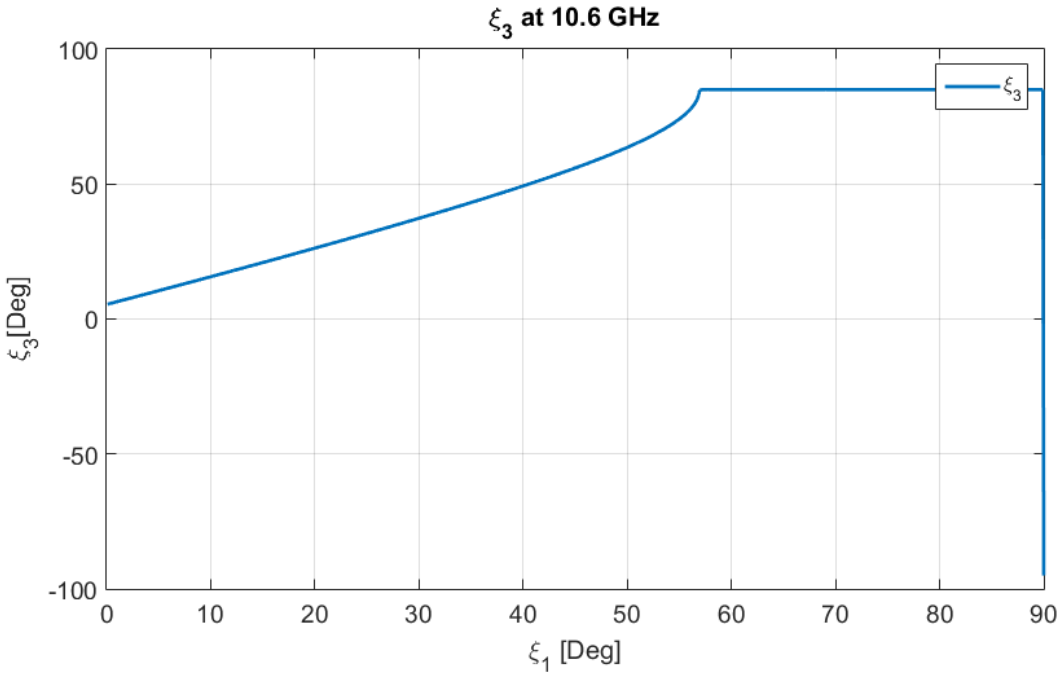

Fig. II-11 Propagation vector angle behaviour.

With respect to Fig. II-10 Attenuation vector angle behaviour.and Fig. II-11 Propagation vector angle behaviour. the pointing direction of

both attenuation an phase vector is reported in Fig. II-2. Angles keep increasing in value until they reach a critical angle for which propagation of the transmitted wave degenerates into a surface wave form along the prism interface. It must be underlined that $\boldsymbol{\zeta_3}$ and $\boldsymbol{\xi_3}$ keep a constant phase difference of $\frac{\boldsymbol{\pi}}{\boldsymbol{2}}$ throughout the variation span of $\boldsymbol{\xi_1}$. The peculiar step behaviour is very similar to the one expected, a span of some critical angles corresponding to each defined case of $\boldsymbol{\chi}$. In this regard, the plot of the ratio $\frac{\beta}{\alpha}$ (see Fig. 4) is very handy.

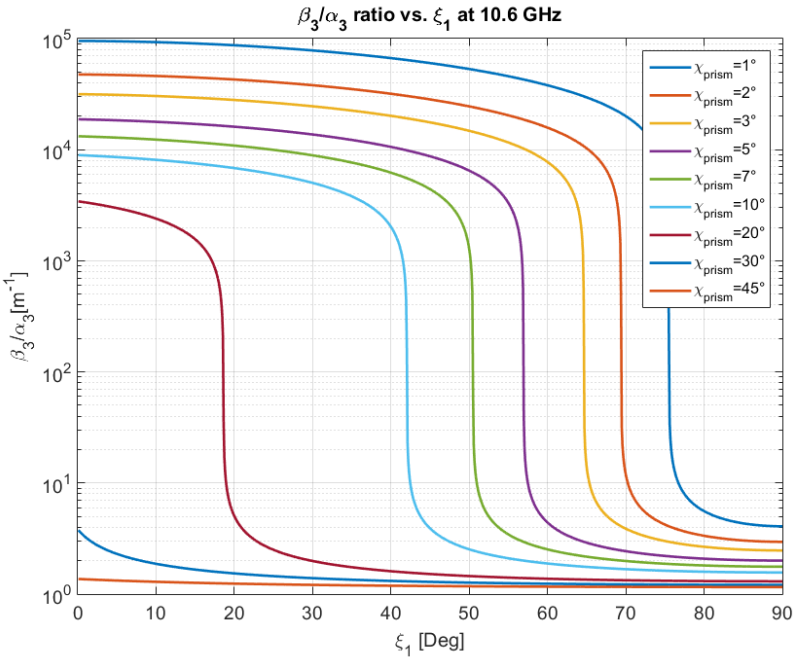

Fig. II-12 Phase vs Attenuation vector amplitude ratio behaviour w.r.t. χ.variation

Furthermore, it gives a comprehensive sign of the step behaviour individuated by the present analysis, with respect to the characteristic parameters. Fig. II-12 shows a strong dependability of the ratio $\frac{\beta}{\alpha}$ and of the critical angle on the angle of the prism. Increasing the angle of the triangular prism, reduces the possibility of having a high β, which are a favourable condition for deep penetration and the range of the

incident angles for which the transmitted wave is a usable wave according to Fig. 5 and 6.

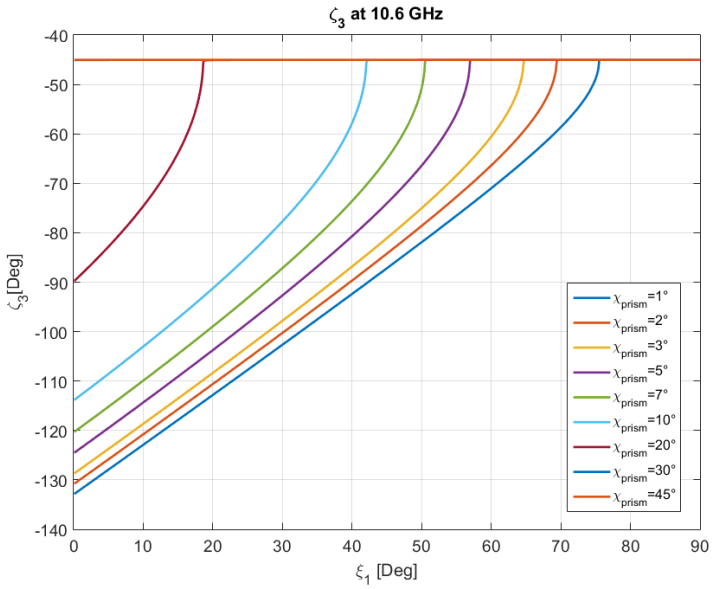

Fig. II-13 Attenuation vector angle behaviour w.r.t. χ.variation

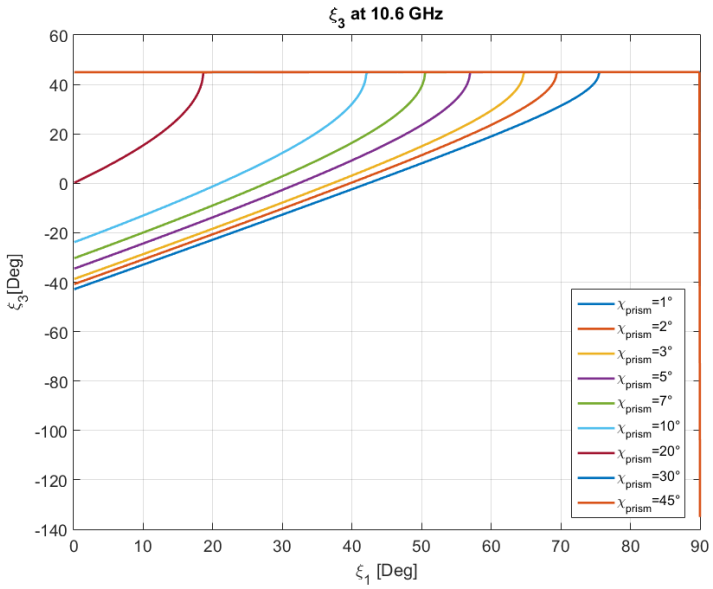

Fig. II-14 Phase vector angle behaviour w.r.t. χ.variation

In these figures, the transmitted angles of the attenuation and phase vectors are respectively shown as a function of the incident angle and the prism angle. A similar step behaviour is noted. The attenuation vectors angle grows with the initial incident angle and reaches a direction almost perpendicular to the oblique interface starting from the

critical angle. Similarly, the phase-vector becomes quasi-parallel to the oblique interface starting from a critical initial angle of incidence. In other words, after a critical angle the transmitted wave behaves like a surface wave.

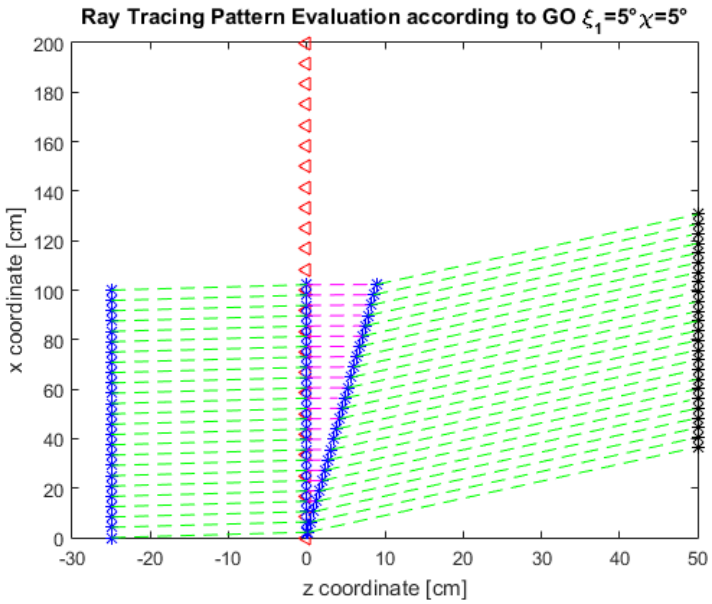

Fig. II-15 Incident electric field behaviour in Geometrical optics

Fig. II-15 depicts this condition assuming a pure geometrical optics approximation of the system and confirms that the wave is not exactly parallel to the prism side, then it is not a bounded wave, but it is able to propagate in free space. As expected, the phase vector of the transmitted wave is in general deflected from the initial direction, being this deflection higher with bigger prism's angles. In conclusion, the material of the prism is varied as well.

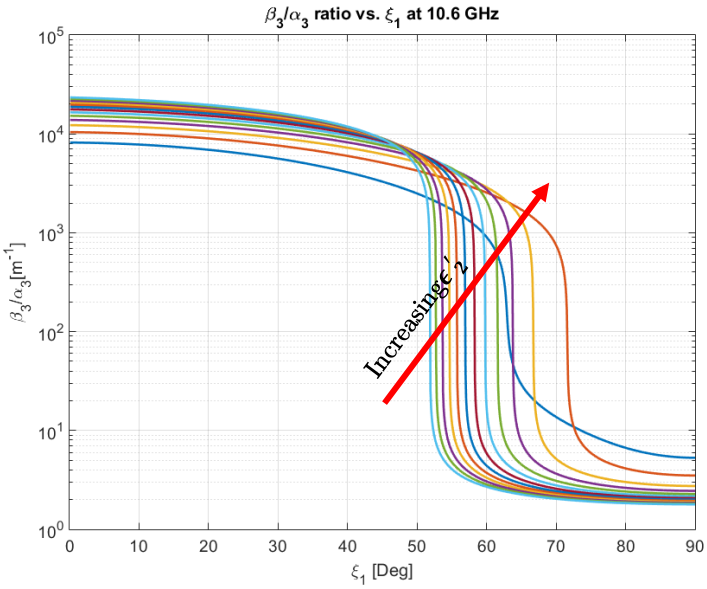

Fig. II-16 Phase vs Attenuation vector amplitude ratio behaviour w.r.t. ϵ_2' over a span cantered in reference FR4 $\epsilon_2' = 4.3$, with 0.5 step

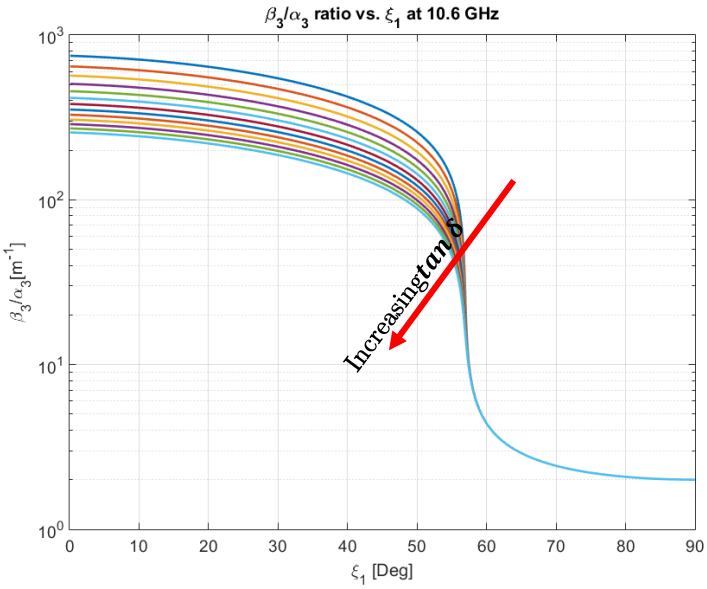

Fig. II-17 Phase vs Attenuation vector amplitude ratio behaviour w.r.t. $tan\,\delta$ over a span cantered in reference FR4 $tan\,\delta = 0.025$, with 0.01 step

The analysis showing the variation of the ratio $\frac{\beta}{\alpha}$ depending on the relative permittivity and on the loss tangent, respectively, with a $\boldsymbol{\chi}$ =

5°. An increase and saturation of the ratio $\frac{\beta}{\alpha}$ with the increase of $\boldsymbol{\epsilon_2'}$ and a marked dependence of the critical angle on $\boldsymbol{\epsilon_2'}$ can be noted. On the contrary, the increase of $\boldsymbol{tan\,\delta}$ causes a decrease of the ratio $\frac{\beta}{\alpha}$, while the critical angle results not affected. A theoretical trade-off analysis of the lead antenna solution developed has been carried out. According to geometric optics even the multiple reflections inside the prism has been analysed by defining an analytical expression of the optic path of the ray between the first and second internal reflections. In order to take into account even multipath effects into the prism structure, diffraction effects due interaction between the prism and the electromagnetic source which feed it and the finite angular dimension of the real beam-width full wave analysis of the structure has been performed. A realistic case of study has been considered. An electromagnetic wave generated by a aperture antenna (horn) antenna and illuminating a lossy prism. Most relevant results of the transmitted inhomogeneous field and some comparisons with the theoretical prediction are shown in the following paragraph.

II.3.3 Full Wave analyses and Results

As described, we considered a system composed by the polarizer prism and a field source.

The feed of the system is a Ku band rectangular tapered horn with a WR90 input, working in linear polarization. Operative bandwidth is centred in 10.6 GHz. Horn centre of phase is placed at an adequate distance from the prism to provide a finite section quasi-plane wave radiated field at the prism interface.

II.3.3.1 System Feed

A typical Tapered Ku-band horn has been designed for feeding the prism polarizer. The horn is provided with a WR90 waveguide port. Its operative bandwidth centre frequency is 10.6 GHz. Such pyramidal horn has been excited by an uniform TE_{10} mode at the input port.

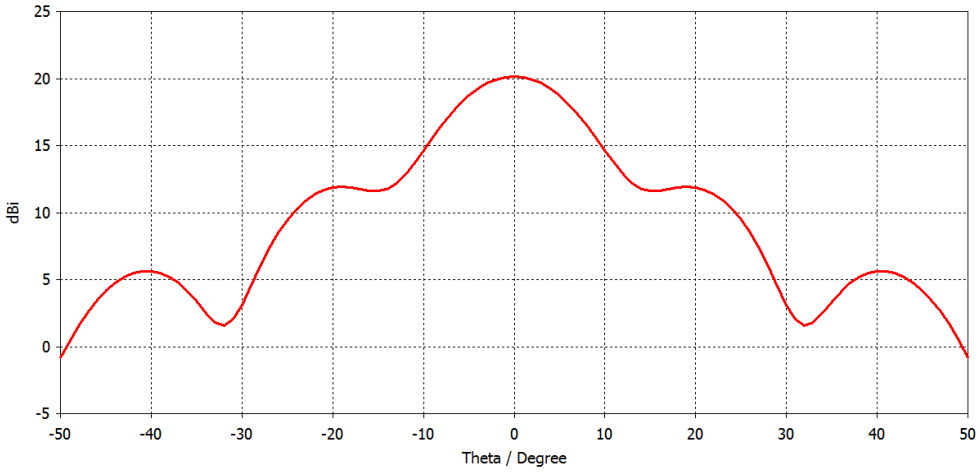

Fig. II-18 : Horn Directivity pattern [dBi], in red ϕ=0,90.

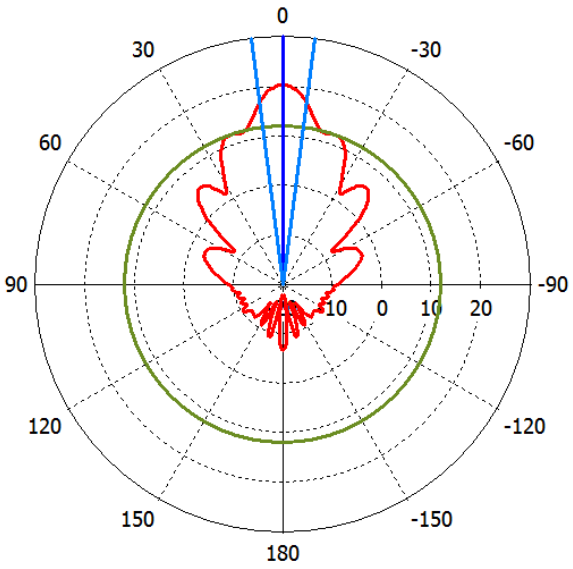

Fig. II-19 : Horn Polar Directivity pattern [dBi], in red ϕ=0,90.

The single horn shows a maximum directivity at boresight of 21.1 dBi and a 3dB beamwidth of Θ_{3dB}=14.5 deg. Both the horn in stand-alone configuration and the system horn+prism have been simulated with the commercial software CST Microwave Studio.

II.3.3.2 Assembly

The system is composed by the prism polarizer and the feed horn is shown in the following figure.

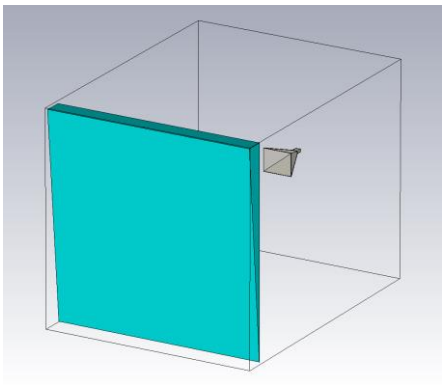

Fig. II-20 : Full Wave Simulator model of the assembly Horn+Prism.

Distance between prism and horn is a critical system parameters. For the purpose of this work has been chosen to decouple full-wave analysis from the study of resonant effects due to near field interaction between the two objects. Thus distance between feed and prism has set to be greater than the Fraunhofer distance ($FF_d = \frac{2D^2}{\lambda}$) at $L_m = FF_d + L_{ph}$, where L_{ph} take into account the phase path between phase centre and horn aperture placed in order to provide a finite quasi-plane wave radiated field at the prism interface. We considered a prism with squared transverse section, $\chi = 5^\circ$ and made of FR4 material. In order to minimize the diffraction effects due to the interaction with the vertex of the prism, the vertical side is 556.9 mm long, computed as the horn HPBW footprint at a distance L_m plus a margin evaluated as $FF_d/2$, being FF_d the far field distance of the horn antenna, equal to 1013 mm at the working frequency (10.6 GHz).

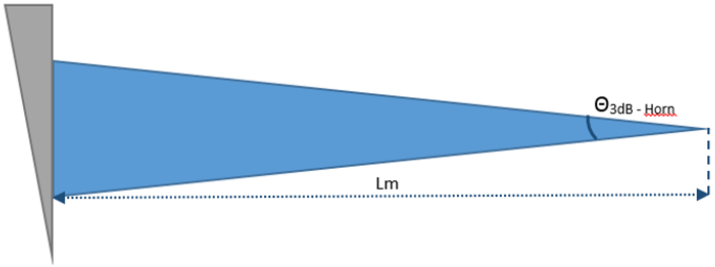

Fig. II-21 : Horn and Prism structure, geometrical layout.

II.3.3.3 Results

Most relevant results of the full-wave simulation have been reported as follows. The structure has been simulated with a Finite Element Method solver. The two components have been supposed to be in vacuum.

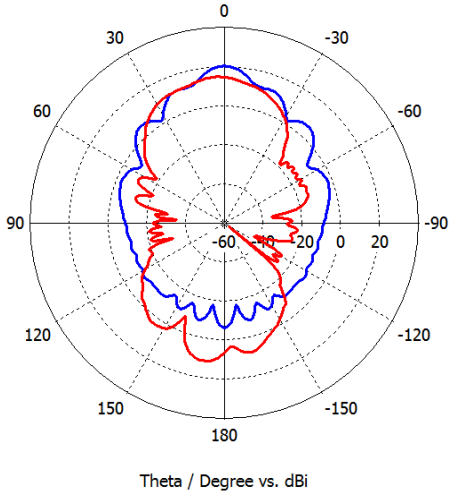

Fig. II-22 : CST pattern single tapered horn (blue) and system horn+prism (red).

The radiation patterns depicted in, blue-lined for the single horn, red-lined for the system show the impact of the dielectric prism in the radiating characteristics of the source used for the boresight case. As expected, the dielectric prism substantially affects the radiating

performances. In **Tab. II-1** , the cases of interest, where the impinging $\boldsymbol{\xi_1}$ angle is non-null are added. Fig. II-23 and Fig. II-24 show the electric field propagated in the y-z plane for the single horn and the system with $\boldsymbol{\xi_1} = 5^\circ$, respectively.

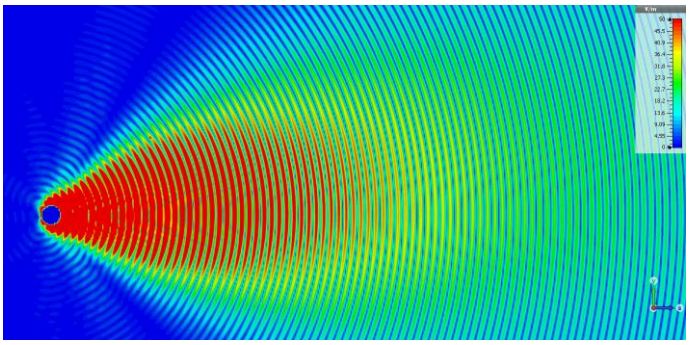

Fig. II-23 :Electric field along the propagation y-z plane of the single tepared horn modeled for angle $\boldsymbol{\xi_1} = 5^\circ$ with respect to the z-axis.

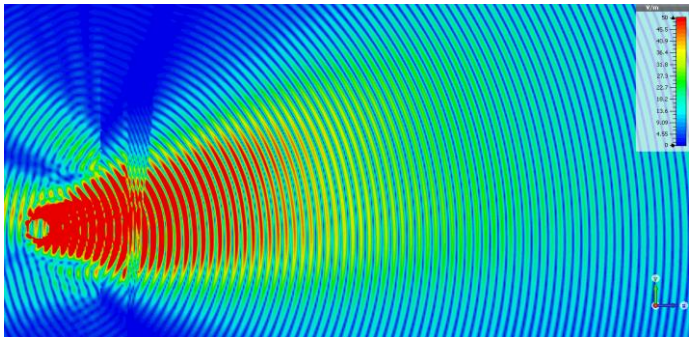

Fig. II-24 :Electric field along the propagation y-z plane with dielectric FR4 prism and incidence $\boldsymbol{\xi_1} = 5^\circ$

As can be noted, even by the visual inspection of the electric field along the propagation y-z plane, part of the incident wave is reflected by the interaction with the prism. This reflected field, which is the lead cause of the increasing of the antenna back lobes is generated by the multiple reflections which take place in the prism body. In Geometrical Optics, no secondary internal reflection in the prism were considered as can be seen in Fig. II-15. By examining the tangential electric Field on dielectric FR4 prism surface a secondary lobe can be noticed. Regarding

Fig. II-25 the first plot shows the electric field distribution over the straight surface which is directly fed by the horn, the second plot shows the electric field distribution over the oblique surface, which the transmitted field emerging from

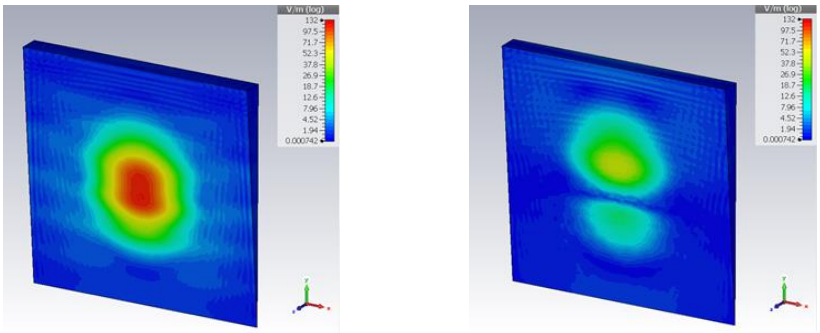

Fig. II-25 Electric field on dielectric FR4 prism surface tangential and normal at incidence ξ_1.

By considering that the first reflection on the oblique side forms an angle $\xi_3 + \chi$ with the normal direction to the interface. Then the reflected rays impinge the vertical side at an angle $\xi_3 + 2\chi$, thus the path followed by the ray from the first transmission into the prism and the first reflection, and the path between the first and the second reflection can easily be computed by geometric considerations and can be written as functions of the angle of the prism and the height at which the considered ray impinges on the prism [R. 45].

Main radiated characteristics of the single horn compared to the horn+prism system for various cases of incidence. As expected, simulated results shows a depointing in line with the theoretical analyses performed in GO. An increased back-lobe pattern of the radiation pattern of the assembly w.r.t. the one of the horn in standalone configuration is also reported. In the following table, a summary of some of the most relevant results of the full-wave simulation has been reported. The three leading parameters that has been considered are:

- Directivity Value in the pointing direction;
- Main Lobe Direction;
- Half-beamwidth aperture angle.

By comparison main-lobe directivity with the achieved assembly directivity is possible to evaluate the losses in terms of beam tapering due to the interaction with the prism towards the pointing direction. The Main lobe direction gives a hint of the additional depointing introduced by prism on the feeding pattern with respect to the inner depointing already foreseen at design level originated by the prism only. Thus by comparison the physical depointing as resulted by the FEM simulation and the value of $\boldsymbol{\xi_3}$ as foreseen by the geometrical optics theoretical evaluation, it is possible to evaluate the accuracy of the theoretical model that has been developed for the analysis of this kind of antenna.

Target	**Single Horn**	**Horn+prism** $\boldsymbol{\xi_1} = 0^\circ$	**Horn+prism** $\boldsymbol{\xi_1} = 5^\circ$	**Horn+prism** $\boldsymbol{\xi_1} = 45^\circ$
Mainlobe magnitude [dBi]	20.1	14.8	14.4	15.2
Main lobe direction (ϕ=0) [deg]	0.0	3	6	57
HPBW [deg]	14.3	29.2	37.8	31.1

Tab. II-1: Main radiated characteristics of the single horn compared to the horn+prism system for various cases of incidence

In order to prove the accuracy of the adopted theoretical model, full wave simulated transmitted angles samples have been compared compared with the theoretical results coming from the geometrical optics analyses, as reported in the following.

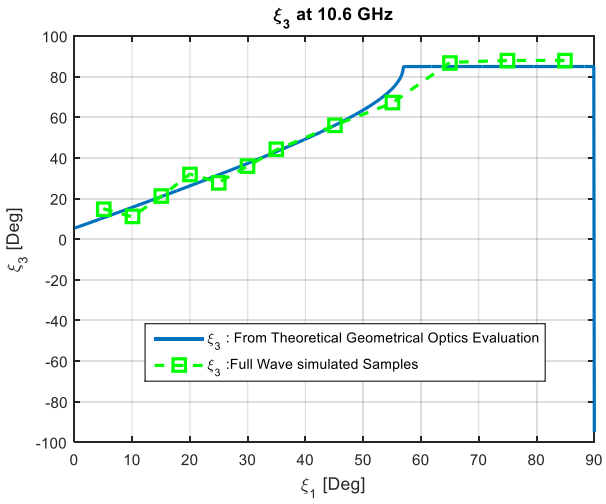

Fig. II-26 Transmitted phase vector ξ_3 from dielectric FR4 prism surface ($\chi = 5°$), theoretical vs simulated comparison.

Simulated and Theoretical results has been compared for a transmitted phase vector direction angle in a FR4 prism with a $\chi = 5°$. Results show very good accordance with theoretical values as can be seen by the curves in Fig. II-26 Transmitted phase vector ξ_3 from dielectric FR4 prism surface ($\chi = 5°$), theoretical vs simulated comparison.

II.4 Conclusion

In the last part of the work, a novel approach for inhomogeneous waves generation in lossless media based on the illumination of a dissipative triangular prism by a homogeneous wave has been studied and characterised. A theoretical analysis of the problem has been carried. As expected, the behaviour of the magnitudes and angles of the

transmitted attenuation and phase vectors showed a dual behaviour defined by a critical incident angle. Below such incident angle, the inhomogeneous wave which emerges from the prism is not a surface wave and presents magnitudes typical of the leaky waves; therefore, usable for the deep penetration of lossy media. It has been proved that magnitudes and angles of this inhomogeneous wave can be tuned by the choice of the prism's geometry (angle of aperture) and material. The incident critical angle is defined as well by the prism's properties. In particular, it is primarily dependant on the angle of aperture of the prism and secondarily on its relative permittivity, while independent of the loss tangent of the material. Finally, a more realistic model of this antenna has been developed to perform full-wave analysis of the structure. A rectangular tapered horn antenna illuminating a lossy prism of FR4 material has been considered to evaluate the accuracy of the theoretical model developed and to assess all the impairment in terms of antenna parameters. Results shows a very good accordance with theoretical values and prove that the beam depointing is very well controlled at design level. Antenna directivity shows an impairment due to the interaction with the prism which never exceeds 5.6 dB. In any case, one of the driver of the development was the maximization of the transmitted $\frac{\beta}{\alpha}$, in order to creates favourable condition to meet the deep penetration condition. A proper optimization of the matching between horn and prism has not been performed yet but at design and theoretical point of view there will be no issue in including the matching constraints in the definition of $\boldsymbol{\xi_1}$ so that incident field is below the critical angle but very near to the Brewster angle.

In conclusion, by considering a dissipative triangular prism immersed in the free space, with the first interface illuminated by a homogeneous wave, an inhomogeneous wave is generated at the second interface. More degrees of freedom introduced by the dielectric- prism feature in the design so that it is easier to generate an inhomogeneous

wave which could meet the deep penetration conditions for propagation in lossy media.

The results of the study represents a concrete and innovative approach to generate inhomogeneous waves which can find applications for the deep penetration of lossy materials [R. 45 R. 46].

For future application, an optimizer has been developed to find the suitable set of parameters ($\boldsymbol{\chi}, \boldsymbol{\xi_1}, \boldsymbol{\epsilon_2'}, \boldsymbol{tan\,\delta}$), which can provide a solid deep penetration behaviour over a lossy media, like the water. Some preliminary test has already been performed over fresh water, sea water and polar ice. The challenge is to meet the correct set of parameters to fulfil: the deep penetration condition over the beta value for the selected material; to avoid the quasi superficial wave condition, which is the typical step behaviour shows by this kind of structure, to have a large ratio beta/alpha for the amplitudes of the vectors of the wave generated by the prism and to match the Brewster incident angle to minimize the power losses due to the incidence with the prism.

REFERENCES

R. 1 MARAL G., B. M. Satellite Communication Systems: Systems, techniques and technology. [S.l.]: John Wiley & Sons Ltd, 2009.

R. 2 QINGXIONG, H. Nulling Algorithm for a Seven Element GPS Array. [S.l.]. 2010.

R. 3 STEINBERGER, J. A. A Survey of Satellite Communications System. Ohio. 2008.

R. 4 EUTELSAT COMMUNICATION. HOT BIRD™ 6 : 13fl EAST. Eutelsat Communication. Disponivel em: ¡http://www.eutelsat.com/satellites/13ehb6.html¿.

R. 5 ELECTRONIC Warfare. Wikipedia. Disponivel em: ¡http://en.wikipedia.org/wiki/Electronic˙warfare¿.

R. 6 10% of all sat-interference is deliberate. advanced-television.com. Disponivel em: ¡http://advanced-television.com/index.php/2012/03/16/10-of-all-sat-interference-is-deliberate/¿.

R. 7 ALISON BROWN, D. R. C. D. R. M. S. S. Jammer and Interference Location System - Design and Initial Test Results. Proceedings, Nashville, 1999.

R. 8 H, R. Jamming commercial Satellite communications during wartime an empirical study. [S.l.]. 2006.

R. 9 WENYUAN XU, W. T. Y. Z. A. T. W. The Feasibility of Launching and Detecting Jamming Attacks in Wireless Networks. [S.l.].

R. 10 PRASAD, S. IEEE 802.11g,n Multi-Network Jamming Attacks - A Cognitive Radio Based Approach, Raleigh, North Carolina, 2012.

R. 11 ETSI. [S.l.]. (EN 302 307 v1.2.1 (2009-08)). Digital Video Broadcasting (DVB); “Second generation framing structure, channel coding and modulation systems for Broadcasting, Interactive Services, News Gathering and

other Broadband satellite applications".Available at: http://www.etsi.org.

R. 12 E. Casini, R. De Gaudenzi, A. Ginesi; "DVB-S2 modem algorithms design and performance over typical satellite channels"; International Journal of Satellite Communications and Networking; Int. J. Satellite Communication Networks; 2004; 22:281–318 (DOI: 10.1002/sat.791).

R. 13 ITU Implores Iran To Help Stop Jamming. Spacenews, 26 March 2010. Disponivel em: ¡http://www.spacenews.com/policy/100326-itu-implores-iran-help-stop-jamming.html¿.

R. 14 THURAYA Accuses Libya of Jamming Satellite Signals. Spacenews, 25 February 2011. Disponivel em: ¡http://www.spacenews.com/satellite˙telecom/110225-thuraya-accuses-libya-jamming.html¿.

R. 15 F.S. MARZANO, N. P. Fondamenti di Antenna. 5.0. ed. Roma: [s.n.], 2008-2009.

R. 16 LINK Budget. Disponivel em: ¡http://www.google.it/url?sa=t&rct=j&q=&esrc=s&source=web&cd=2&ved=0CFcQFjAB&url=http%3A%2F%2Felectronica.udea.edu.co%2Fcursos%2Fsistemasc%2FLINK%2520BUDGET.ppt&ei=nf3hT-OjKdHLsga07vFy&usg=AFQjCNHijjXl7zJvTb46HAFwXgGwAAHdMw&sig2=NJQhFgnSeicb4Rfx6VdYIA¿.

R. 17 NERI, M. Advanced Countermeasures for Interference , Distorsion and Fading in Satellite Communication Systems, Bologna, 2006.

R. 18 SALEH, A. A. M. Frequency-Independent and Frequency-Dependent Nonlinear Models of TWT Amplifiers. IEEE, November 1981.

R. 19 SHEIKHAN, A. G. A. M. The Effect Of Solid State Power Amplifiers (SSPAs) Nonlinearities On MPSK And M-QAM Signal Transmission. *University o f Amirkabir (Tehran Polytechnic). Tehran Jran, p. 193 - 197.

R. 20 HOME Vision, 2007. Disponivel em: ¡http://www.01net.it/01NET/Photo˙Library/3/HomeVision˙pdf.pdf¿.

R. 21 LIBYA Caught Jamming Sat-Phones. Wired, 09 April 2007. Disponivel em: ¡http://www.wired.com/dangerroom/2007/04/if˙youre˙travel/¿.

R. 22 LIBYA Accused of Jamming Satellite Signals. Space, 1 March 2011. Disponivel em: ¡http://www.space.com/11000-libya-satellite-jamming-accusations.html¿.

R. 23 PROTEST to Libya after satellites jammed. The Guardian, 3 December 2005. Disponivel em: ¡http://www.guardian.co.uk/uk/2005/dec/03/politics.libya¿.

R. 24 TV Broadcasts Bound for Iran Intentionally Jammed. Spacenews, 8 September 2010. Disponivel em: ¡http://www.spacenews.com/satellite˙telecom/broadcasts-bound-for-iran-jammed.html¿.

R. 25 MEACONING, Intrusion, Jamming, Interference (MIJI). Disponivel em: ¡http://informationtechniciantraining.tpub.com/14222/css/14222˙88.htm¿.

R. 26 SEN, C. Digital Communications Jamming, Monterey, California, 2000.

R. 27 MODERN Electronic Countermeasures. Disponivel em: ¡http://www.vectorsite.net/ttradar˙5.html¿.

R. 28 RAO, S.et Alii Multiple Beam Antenna Technology for Satellite Communications Payloads , ACES JOURNAL, VOL. 21, NO. 3, NOVEMBER 2006

R. 29 March 1st, 2010, Via Satellite, Giovanni Verlini, "New Efforts to Mitigate Satellite Interference"

R. 30 M. Coleman; "*Satellite Interference! ……the Carrier ID Process*"; satellite Interference Reduction Group (IRG) formerly Satellite Users Interference Reduction Group (SUIRG); WBU-ISOG, Zagreb, Croatia; October 24-25, 2011.

R. 31 H. Fenech, E. Lance and A. Tomatis, "*Satellite Broadband On The First Full Ka-Band Eutelsat Infrastructure*", 14th KaConf, 2008.

R. 32 Mayhan, J. (1976). Nulling limitations for a multiple-beam antenna. IEEE Transactions on Antennas and Propagation, 24(6), 769–779. doi:10.1109/TAP.1976.1141441

R. 33 8 : J.T. Mayhan – *Area Coverage Adaptive Nulling from Geosynchronous Satellites: Phased Arrays Versus Multiple-Beam Antennas.* – IEEE Trans. On Antennas and Propagation. Vol. AP34, no. 3, march 1986.

R. 34 10 : J.T. Mayhan, L.J. Ricardi – *Physical Limitations on Interference Reduction by Antenna Pattern Shaping.* – IEEE Trans. On Antennas and Propagation. Vol. AP23, no. 5, september 1975.

R. 35 1 : R.E. Collin – *Antennas and Radiowave Propagation*. Mc Graw Hill, 1985.

R. 36 L.J. Ricardi – *Multiple Beam Antennas* – Antenna Engineering Handbook, R.C. Johnson, H. Jasik, Cap. 6, Mc Graw Hill, 1984.

R. 37 Yu, K. (1996). Adaptive beam-forming for satellite communication with selective earth coverage and jammer nulling capability. IEEE Transactions on Signal Processing, 44(12), 3162–3166. doi:10.1109/78.553494

R. 38 Milligan, T. (2005). Modern Antenna Design. Hoboken, NJ, USA: John Wiley&Sons, Inc. doi:10.1002/0471720615

R. 39 Guenad,B., Meriah,S.M., Bendimerad, T.,F., Multibeam Antennas Array Pattern Synthesis Using a Variational Method, RADIOENGINEERING, VOL. 16, NO. 2, JUNE 2007.

R. 40 V. Schena, G. Losquadro, V. Pascale; "Low Cost Anti Interference Techniques and Performance for Commercial TLC SatCom Missions"; 18th Ka and Broadband Communications, Navigation and Earth Observation Conference Proceedings; September 24-27, 2012; Ottawa (Canada), pages 459-466.

R. 41 G. Losquadro, V. Schena, J. Capolicchio, V. Pascale, "End-to-End Anti-Interference SATCOM System

Architecture: a Simulation Approach", 19th Ka and Broadband Communications, Navigation and Earth Observation Conference Proceedings 31th AIAA International Communications satellite systems conference, Firenze, Italia, October 14-17,2013.

R. 42 G. Losquadro, V. Schena, F. Spongetta, V. Pascale, "New Generation TLC Anti Interference Satellite Systems: Technical Solutions for Commercial Satellites", 19th Ka and Broadband Communications, Navigation and Earth Observation Conference Proceedings 31th AIAA International Communications satellite systems conference, Firenze, Italia, October 14-17,2013.

R. 43 A. Pisano, V. Schena, F. Spongetta, V. Pascale, "Interference Mitigation on Commercial Satellite System: Perimeter and Ideas", 19th Ka and Broadband Communications, Navigation and Earth Observation Conference Proceedings 31th AIAA International Communications satellite systems conference, Firenze, Italia, October 14-17,2013.

R. 44 G. Losquadro, V. Schena, V. Pascale, "Anti-Interference/Anti-Jamming Technique based on Multi-Beam Antenna Approach: A Preliminary Study for the Application in Commercial SATCOMs", 20th Ka and Broadband Communications, Navigation and Earth Observation Conference Proceedings 32th AIAA International Communications satellite systems conference, Salerno, Italia, October 1-3,2013.

R. 45 N.Tedeschi,V.Pascale,F.Pelorossi,F.Frezza,"Electromagnetic inhomogeneous waves generation by a lossy prism", URSI Commission B International Symposium on Electromagnetic Theory, Espoo, Finland, August 14-18 2016 -Pages: 838 - 841, DOI: 10.1109/URSI-EMTS.2016.7571534

R. 46 V.Pascale, F.Pelorossi, N.Tedeschi F.Frezza,"Inhomogeneous waves generation for the electromagnetic deep penetration into lossy media", XXI RiNEM Riunione Nazionale di Elettromagnetismo, Parma, Italia, September 12 -14, 2016. -

R. 47 T. Tamir, "Inhomogeneous waves types at planar structures: III. Leaky waves," Optik, Vol. 38, No. 3, pp. 269-297, 1973.

R. 48 F. Frezza and N. Tedeschi, "Electromagnetic inhomogeneous waves at planar boundaries," J. Opt. Soc. Am. A, vol. 32, no. 8, pp. 1485-1501, 2015.

R. 49 D.R. Jackson and A.A. Oliner, "Leaky-Wave Antennas", Ch. 7, Modern

R. 50 Antenna Handbook, Edited by C.A. Balanis, Wiley, 2008.

R. 51 N. Tedeschi and F. Frezza, "An analysis of the inhomogeneous wave interaction with plane interfaces," in Proc. URSI GASS'14, 2014, paper BP1.25, p. 109.

R. 52 J.A. Stratton, Electromagnetic Theory, McGraw-Hill, New York, 1941.

R. 53 J.E. Roy, "New results for the effective propagation constants of nonuniform plane waves at the planar interface of two lossy media," IEEE Trans. Antennas Propag., vol. 51, pp. 1206-1215, 2003.

R. 54 F. Frezza and N. Tedeschi, "Deeply penetrating waves in lossy media" Opt. Lett. vol. 37, pp. 2616-2618, 2012.

R. 55 F. Frezza and N. Tedeschi, "On the electromagnetic power transmission between two lossy media: discussion," J. Opt. Soc. Am. A, vol. 29, pp. 2281-2288, 2012.

R. 56 J.Capolicchio, , "Development of a Satellite System Simulator for the Study of Intentional/Unintentional Interference Effect Analysis", MSc Thesis, 2012.

R. 57 https://artes.esa.int/projects/low-cost-anti-interference-techniques-satcom-commercial-satellites

R. 58 http://www.cytaglobal.com/cytaglobal/userfiles/description-of-makarios-teleport-site-and-its-capabilities.pdf

R. 59 http://www.worldteleport.org/?Teleports

R. 60 ITU-R.PN618-7." -Propagation data and prediction methods required for the design of Earth-Space telecommunication systems"

R. 61 ITU-R.P676." Attenuation by atmospheric gases"

R. 62 ITU-R.P838." Specific attenuation model for rain for use in prediction methods"

R. 63 ITU-R.PN840." Attenuation due to clouds and fog"

R. 64 ITU-R.PN834. "Effects of tropospheric refraction on radiowave propagation"

R. 65 ITU-R.SM.2021." Production and mitigation of intermodulation products in the transmitter"

R. 66 H.Fenech, S.Amos, T.Waterfield. "The role of array antennas in commercial telecommunication satellites". Conference: 2016 10th European Conference on Antennas and Propagation (EuCAP), DOI: 10.1109/EuCAP.2016.7481857.

R. 67 Shin, C., Ju, J., Kang, D., Choi, S., Lee, C., Cheong, C., ... Salazar-Palma, M. (2013). Implementation of an antenna array for satellite communications with the capability of canceling jammers. IEEE Antennas and Propagation Magazine, 55(1), 32-48. [6474483]. DOI: 10.1109/MAP.2013.6474483

ACRONYM LIST

AGC	Automatic Gain Controller
ADC	Analog Digital Converter
AWGN	Additive White Gaussian Noise
BER	Bit Error Rate
BSS	Broadcasting Satellite Service
BCH	Bose Chaudhuri Hocquenghem
BNJ	Broadband Noise Jamming
CCTV	China Central TV
CDMA	Code Division Multiple Access
CW	Continuous Wave
DSP	Digital Signal Processing
DRA	Direct Radiating Array
DVB-S	Digital Video Broadcasting-Satellite
DVB-S2	Digital Video Broadcasting-Satellite 2
DOA	Direction Of Arrival
EIRP	Equivalent Isotropic Radiated Power
ESA	European Space Agency
ES	Electronic warfare Support
EA	Electronic Attack
ETSI	European Telecommunication Standard Institute

ECCM	Electronic Counter Countermeasures Mode
FSS	Fixed Satellite Service
FEC	Forward Error Correction
FFT	Fast Fourier Transform
FISSS	Frequency Independent Strong Signal Suppressor
HPA	High Power Amplifier
IM	InterModulation
ISI	Inter-Symbol Interference
ITU	International Telecommunication Union
ICCPR	International Covenant on Civil and Political Rights
IBO	Input Back Off
LNA	Low Noise Amplifier
LDPC	Low Density Parity Check
LLR	Log-Likelihood Ratio
MBA	Multi Beam Antenna
MSS	Mobile Satellite Service
NNJ	Narrow-band Noise Jamming
OBO	Output Back Off
PSK	Phase Shifting Keying
PER	Package Error Rate
PSD	Power Spectral Density

PNJ	Partial-band Noise Jamming
PM	Phase Modulation
QPSK	Quadrature Phase Shifting Keying
QEF	Quasi Error Free
RF	Radio Frequency
SNR	Signal Noise Ratio
S-PCNS	Satellite-Personal Communication Network Satellite
SUIRG	Satellite Users Interference Reduction Group
SSPA	Solid State Power Amplifier
TWTA	Traveling Wave Tube Amplifier
TEM	Transverse ElectroMagnetic
TVRO	TeleVision Receive Only
TLC	TeLeCommunication
UAT	User Acceptance Test
VSAT	Very Small Aperture Terminal
W.r.t.	With respect to
WBS	Work Breakdown Structure
XPD	Cross Polarization Discrimination